Genetic intervention and biochemical analysis of antioxidant enzyme function and their post-translational modifications in yeast

Dorival Martins Jr

A Thesis

in

The Department of

Chemistry and Biochemistry

Presented in Partial Fulfillment of the Requirements

for the Degree of Doctorate in Chemistry at

Concordia University

Montreal, Quebec, Canada

April 2014

Examiners:

Dr. Ann M. English _____

Dr. Paul Joyce _____

Dr. Vladimir Titorenko _____

Dr. Malcolm Whiteway _____

Dr. Dao Nguyen _____

Abstract

Genetic intervention and biochemical analysis of antioxidant enzyme function and their post-translational modifications in yeast

Dorival Martins Jr, PhD

Concordia University, 2014

Antioxidant enzymes play a critical role in stress response and cell viability by controlling intracellular levels of reactive oxygen species (ROS). While at low concentrations they trigger stress response and extend chronological lifespan, high ROS levels are toxic since they damage DNA, lipids and proteins. Thus, cells must rapidly sense changes in ROS levels and synchronize the activities of antioxidant enzymes to prevent harmful oxidative modifications of cellular components. This thesis reports on how genetic manipulation of the mitochondrial antioxidant enzyme cytochrome c peroxidase (Ccp1) alters the synchronization of the activity of antioxidant enzymes during the chronological aging of yeast. Ccp1 is identified as a mitochondrial H_2O_2 sensor that prevents mitohormesis and lifespan extension by increasing catalase A (Cta1) activity and attenuating the H_2O_2-dependent stress response during aging. On the other hand, Ccp1 signaling protects cells against acute H_2O_2 stress by increasing peroxiredoxin and catalase activity. The latter activity was found to be a critical defense against exogenous H_2O_2, since blocking the induction of catalase activity by genetic intervention or low nutrient availability impairs adaptation on H_2O_2 challenge. The critical antioxidant enzyme copper-zinc superoxide dismutase (Sod1) from 7-day, stationary phase yeast cells was observed to be oxidized, which induced the formation of soluble high-molecular weight Sod1-containing aggregates. These species resemble the non-amyloid aggregates seen in neurodegenerative diseases such as Amyotrophic Lateral Sclerosis (ALS). Combined, the presented work provides

molecular insights into how antioxidant defenses are synchronized and modified during acute stress and during aging. Such synchronization modulates ROS levels, stress response and longevity, which in yeast was found to correlate with oxidative damage to mitochondrial proteins.

To my family, friends and my love

Acknowledgements

I would like to thank my supervisor Dr. Ann M. English for her insightful ideas and discussions, for her motivation, patience, constructive criticisms, support and exemplary guidance through all the steps of my PhD.

Thanks to my committee members Dr. Vladimir I. Titorenko and Dr. Paul Joyce for their insightful suggestions and critical evaluation of my work.

Thanks to my external thesis examiners Dr. Dao Nguyen and Dr. Malcom Whiteway for reading this thesis and providing insightful comments.

Thanks to my lab colleagues Marc, Meena, Maria, Samaneh and Vinod for their support, exchange of ideas, experiences and good moments during my time at Concordia.

Thanks to Dr. Pamela Hanic-Joyce for constructing the strain *ccp1*^{W191F}, which was of critical importance to accomplish the work reported in Chapters 3, 4 and 5.

Thanks to Dr. François Dragon and Denis Flipo (Centre Toxen, Université du Québec à Montréal) for giving me access to the Flow Cytometry Facility, which allowed me to accomplish a very important part of my thesis.

Thanks to Dr. Philip Hieter, Dr. Shingo Izawa and Dr. Christopher Brett for providing the yeast strains that were critical to accomplish the work in Chapters 6 and 7, respectively.

Thanks to the funding agencies FQR_NT, NSERC, PROTEO and Concordia University for the financial support during my PhD.

List of abbreviations

2-HE: 2-hydroxyethidine
Aco1: yeast aconitate hydratase or aconitase
ATP: adenosine triphosphate
BSA: bovine serum albumin
Ccp1: yeast cytochrome c peroxidase
ccp1^{W191F}: yeast strain producing the Ccp1^{W191F} protein variant with the W191F mutation
*ccp1*Δ: yeast strain deleted for the *CCP1*gene
cfu: colony forming units
CmpdI: Compound I, the two-electron oxidized form of Ccp1
CmpdII: Compound II, the one-electron oxidized form of Ccp1
CTA1: yeast gene encoding yeast peroxisomal/mitochondrial catalase A (Cta1)
CTT1: yeast gene encoding yeast cytosolic catalase T (Ctt1)
Cyc1$^{II/III}$: ferro/ferricytochrome c
DHE: dihydroethidine
DHR: dihydrorhodamine 123
DNPH: 2,4-dinitrophenylhydrazine
DTNB: 5,5'-dithiobis-(2-nitrobenzoic acid)
DTT: dithiothreitol
EDTA: ethylenediaminetetraacetic acid
FACS: fluorescence activated cell sorting
Ferrozine: 3-(2-pyridyl)-5,6-diphenyl-1,2,4-triazine-p,p′-disulfonic acid
GFP: green fluorescent protein
Gpx3: yeast glutathione peroxidase 3
GSH: reduced glutathione
GSSG: oxidized glutathione
GSX: GSH+GSSG
Hap1-5: heme activator protein 1-5
HPF: 3'-(*p*-hydroxyphenyl) fluorescein
HRP: horseradish peroxidase
ICP-MS: inductively coupled plasma mass spectrometry
LB: Luria broth
NAD^+/NADH: oxidized and reduced forms of nicotinamide adenine dinucleotide
$NADP^+$/NADPH: oxidized and reduced forms of nicotinamide adenine dinucleotide phosphate
NBT: nitroblue tetrazolium
ORF: open reading frame
P10: mitochondria enriched pellet from subcellular fractionation
Paraquat: 1,1'dimethyl-4,4'-bipyridinium dichloride
PBS: phosphate buffered saline
PMSF: phenylmethylsulfonyl fluoride
Prx: peroxiredoxin
PTM: post-translational modification
Rhod123: rhodamine 123
ROS: reactive oxygen species
RFU: relative fluorescence units

S2: denucleated lysate from subcellular fractionation
S10: mitochondria-depleted supernatant from subcellular fractionation
SCD: synthetic complete medium with dextrose
SEC: size-exclusion chromatography
Ras: Superfamily of rat sarcoma proteins
Sch9: serine/threonine kinase Sch9
Skn7: Suppressor of kre null 7 transcription factor
Sod1: yeast superoxide dismutase 1 or copper-zinc superoxide dismutase
Sod2: yeast superoxide dismutase 2 or manganese superoxide dismutase
TEMED: Tetramethylethylenediamine
TSA1: gene encoding thioredoxin peroxidase 1 (Tsa1)
TOR: target of rapamycin
Tris: t*ris*(hydroxymethyl)aminomethane
4-VP: 4-vinyl pyridine
Yap1: yeast activator protein 1or AP-1-like transcription factor
Ybp1: Yap1-binding protein 1
YPD: yeast extract peptone dextrose (medium)
$\Delta\psi$: mitochondrial membrane potential

Contents

List of tables

List of figures

Chapter 1: General introduction

1.1) Reactive oxygen species and antioxidant defenses

Aerobic respiration is an efficient process to extract energy from organic compounds using the flux of electrons in the electron transport chain from nicotinamide adenine dinucleotide (NADH) to dioxygen (O_2) to generate ATP [1, 2]. Although aerobic respiration is much more efficient than fermentation in generating ATP, it also produces partially reduced forms of O_2, also known as reactive oxygen species (ROS) [3]. The one-electron reduction of O_2 generates the superoxide radical anion ($O_2^{\bullet-}$), which can be dismutated to hydrogen peroxide (H_2O_2) by gaining a second electron and two protons [3, 4]. Finally, the reductive cleavage of H_2O_2 by ferrous iron (Fe^{2+}) via Fenton chemistry generates hydroxyl radical ($^{\bullet}OH$), a short-lived and indiscriminating oxidizing species [3, 5, 6].

Previously, ROS were viewed solely as harmful molecules that promote cellular damage by reacting with proteins, lipids and DNA [6-9]. Also, the increased generation of ROS is associated with aging and age-related diseases such as cancer, diabetes and neurodegenerative disorders [3, 4, 6-14]. However, low ROS levels are required to induce stress responses, expression of antioxidant defenses, and to promote lifespan extension, the so-called mitohormesis effect [15-20]. Thus, ROS concentrations have to be tightly regulated and cells have developed antioxidant non-enzymatic and enzymatic systems to fulfill this role [4]. Glutathione (GSH) is the predominant non-enzymatic ROS scavenger in eukaryotic cells. This thiol containing tripeptide is present in millimolar (2-10 mM) levels in the cytosol of yeast and mammalian cells [21] and scavenges species with unpaired electrons such as $^{\bullet}OH$ [22, 23]. Enzymatic defenses are present to scavenge $O_2^{\bullet-}$ and H_2O_2 at very fast rates [4, 24-26]. For

example, superoxide dismutases (SOD) use a redox active metal such as copper or manganese to detoxify $O_2^{\bullet-}$ at diffusion-controlled rates (k~ 10^9 M^{-1} s^{-1}) in a first-order reaction [25]. Yeast has two SOD enzyme isoforms, a 32 kDa homodimeric copper-zinc superoxide dismutase (Sod1) and a 84 kDa homotetrameric manganese superoxide dismutase (Sod2). Yeast also possesses peroxidases [4, 26] and catalases [27-29] to react with H_2O_2 at rates of 10^6-10^8 M^{-1} s^{-1}. Several classes of peroxidases are present in yeast, including the thiol- and heme-containing peroxidases. These enzymes couple the two-electron reduction of H_2O_2 with the one-electron oxidation of a reducing substrate (X in Table 1. 1). Peroxiredoxins (five isoforms) [30-32] and glutathione peroxidases (two isoforms) [21, 33] rely on activated thiols to metabolize H_2O_2 and use thioredoxin or GSH as reducing co-factors, respectively. Cytochrome c peroxidase (Ccp1) is a monomeric heme-enzyme that couples the two-electron reduction of H_2O_2 with two sequential one-electron oxidations of ferrocytochrome c ($cyc1^{II}$), which acts as a reducing substrate for the enzyme [34]. Yeast has two catalases, which are tetrameric heme-containing enzymes that catalyze the disproportionation of H_2O_2 to H_2O and O_2 [27, 28]. The main features, cellular localization and isoforms of these enzymes present in yeast are summarized in Table 1. 1. A full description of all properties of these enzymes is beyond the scope of this introduction, but the catalytic and structural details relevant to this work will be presented in the introduction of the pertinent chapters.

1.2) Antioxidant enzymes in stress response and cell aging

Antioxidant enzymes are critical for cell viability and fitness [3, 4, 35-37]. They have been studied broadly in stress response and aging. Numerous studies involving overexpression or deletion of antioxidant enzymes reveal their critical roles in adaptation [38-41] and in defense against oxidative stress [42-45] and heat shock [46, 47]. In yeast, more than 40 proteins have

their levels increased after H_2O_2 challenge including Ccp1, catalase T (Ctt1), the peroxiredoxin Tsa1, Sod1 and Sod2 [42].

Table 1. 1 *Antioxidant enzymes present in yeast*.

Enzyme class	Reaction catalyzed	Isoforms	Localization[a]
Superoxide dismutases (SOD)	$2O_2^{\bullet-} + 2H^+ \rightleftharpoons H_2O_2 + O_2$	Copper-zinc SOD (Sod1) Manganese SOD (Sod2)	C, N, M (IMS) and P M (matrix)
Peroxidases	$H_2O_2 + 2X^b \rightleftharpoons H_2O + 2X^+$	Cytochrome c peroxidase (Ccp1) Thioredoxin peroxidases (Peroxiredoxins) Glutathione peroxidases	M (IMS) C, N and M C and M
Catalases	$2H_2O_2 \rightleftharpoons 2H_2O + O_2$	Catalase T (Ctt1) Catalase A (Cta1)	C P and M (matrix)

[a] C = cytosol; N = nucleus; M (IMS) = mitochondrial intermembrane space; M (matrix) = mitochondrial matrix; P = peroxisomes.

[b] X = reducing substrate and X^+ = oxidized form of the reducing substrate

Some antioxidant enzymes, viewed as ROS scavengers, can also act as ROS sensors. A well-characterized example is the peroxiredoxin Gpx3 or Orp1, which functions as a redox switch that is controlled by thiol exchange following oxidation by H_2O_2 [48, 49]. The oxidized form of this protein can convey a redox signal to the transcription factor Yap1, which increases the expression of antioxidant enzymes such as Sod1, Sod2, Ccp1, Ctt1 and the peroxiredoxin Tsa1, and thereby resistance to H_2O_2 [42, 43, 48, 49]. These observations indicate that an antioxidant enzyme can participate in the stress response to control H_2O_2 levels and deletion or overexpression of these enzymes and sensors can modulate stress response and chronological lifespan.

Contrary to expectation, overexpression of an antioxidant enzyme does not always extend lifespan. In fact, overexpression of most antioxidant enzymes has either a questionable or no effect on longevity in different model organisms [50]. Only a few interventions, such as

overexpression of mitochondrially-targeted catalase, have a clear lifespan-increasing effect [51, 52]. Furthermore, deletion of an antioxidant enzyme does not necessarily shorten lifespan. For example, deletion of either or both catalases (Table 1. 1) in yeast does not result in H_2O_2 hypersensitivity in exponentially growing cells [38] but actually extends yeast chronological lifespan [19]. In contrast, deletion of SODs in yeast compromises their survival in stationary phase [35]. However, deletion of the five isoforms of SODs in worms has no effect on lifespan [53], whereas *Sod-2* knockout mice are not viable [54]. Importantly, most of these studies did not address how the knockout or overexpression of the specific antioxidant defense influences the levels of ROS and the activity of other components of stress response. A certain ROS balance is necessary to trigger the stress response and prevent ROS accumulation to toxic levels [4, 19]. Thus, careful analyses of how genetic interventions alter the ROS balance are necessary to achieve an accurate view of how antioxidant enzymes participate in modulating aging and stress response.

1.3) Antioxidant enzymes and neurodegenerative diseases

Mutations in protein-encoding genes and post-translational modifications in proteins, including antioxidant enzymes, can promote promote misfolding and the formation of soluble protein aggregates [10]. For example, over 170 mutations in *Sod1* are associated with Sod1 misfolding and oligomerization in neurodegenerative disorders such as Amyotrophic Lateral Sclerosis (ALS) [10, 55-57]. Although not all mutations promote loss of Sod1 activity, they all decrease the melting temperature of the apo-enzyme from 52 to 40 °C [58]. The result is a gain of toxic function involving the generation of Sod1 aggregates that promote toxicity to motor neurons by a mechanism that is not yet fully understood, but increased mitochondrial damage is implicated [59, 60]. Notably, soluble Sod1 oligomers are linked with the death of neurons

observed in late-onset diseases [10, 55, 58]. *In vitro* data suggest that misfolded species can be formed on oxidizing native Sod1 with H_2O_2 [61, 62]. Oxidative post-translational modifications to Sod1 also have been reported in brains of patients with Parkinson's and Alzheimer's diseases [63]. Importantly, global protein oxidation increases as cells age [64] and may be a causative factor in the 90% of ALS cases [10, 55] that do not exhibit a genetic component. Previously, oxidized Sod1 has been isolated from Parkinson's and Alzheimer's brains [63], but interestingly no oxidized forms were isolated from the liver cells of aging rats [65]. We will discuss the limitations of these studies in Chapter 6, but to date it remains a matter of debate as to whether the oxidation of Sod1 during aging is a trigger for the development of neurodenegerative diseases.

1.4) Yeast as a model for studying redox homeostasis and aging

Studies on the yeast *Saccharomyces cerevisiae*, in particular, have provided important insights regarding mitochondrial function, ROS generation and metabolism, and aging. Yeast antioxidant enzymes display high sequence homology (>75%) with those from other eukaryotes [66] and genetic circuits that influence aging (Tor and sirtuins) also are present in humans and other mammals [67]. From yeast studies, it is possible to extrapolate some conclusions on ROS biology and aging in other eukaryotes. Since the lifespan of yeast is much shorter than that of mammals [68], insights into the aging process can be obtained in a very short time. Yeast cells possess great metabolic versatility and can grow on different carbon sources and under various levels of aeration [35, 37, 68, 69], which allows wide manipulation of their ROS generation and aging under different metabolic states. Furthermore, the yeast genome has been fully sequenced and there is extensive information regarding its proteome. Knockouts, affinity purification and fluorescent protein tags are available for all yeast open-reading frames (ORFs). This combination

of available tools for yeast manipulation and its conserved redox and aging pathways with other eukaryotes make yeast a robust and powerful model system to study the aging process.

1.5) Scope of this thesis

The narrow view of ROS as detrimental molecules is challenged nowadays [3, 15, 16]. The mechanisms by which these molecules are sensed and metabolized continue to be a topic of intense investigation due to their implication in stress response [42, 43, 70], aging [4, 50] and age-related diseases such as Parkinson's, Alzheimer's, ALS and cancer [4, 50]. ROS effects on cells are intriguing and inconsistent results have been reported for different model organisms [50]. Notably, most studies concerning the deletion of antioxidant enzymes have not analyzed the impact of these deletions on the activity of other antioxidant defenses and ROS levels [50]. Thus, a systematic study analyzing how the activities of antioxidant enzymes are coordinated to balance ROS needs to be carried out. Here, we uncover the role of cytochrome c peroxidase (Ccp1) as a mitochondrial sensor of H_2O_2 and peroxynitrite [OHOO(H)], as discussed in Chapters 2 and 3. We showed that the sensing role of Ccp1 influences the activity of other antioxidant enzymes and levels of H_2O_2, $O_2^{\bullet-}$ and $^{\bullet}OH$ to modulate aging and oxidative damage, as discussed in Chapter 4. Moreover, we suspect that the role of inducible antioxidant enzymes such as catalase isoforms may be underestimated since the lack of nutrients for *de novo* protein synthesis may have prevented cells from responding to exogenous stresses in some experiments [38, 71]. We sought to readress this issue in Chapter 5.

The actions of ROS in cells go beyond signaling and stress response, since they can also induce post-translational modifications (PTMs) in proteins. Notably, some of these PTMs can lead to loss of function and/or gain of toxic properties as reported for Sod1 [55, 56, 58]. Although mutations in the gene coding for this protein lead to familial ALS, these mutations

account for only 2-3% of the total cases of this disease [55, 58, 72]. ALS is a late-onset disease and we hypothesize that PTM-driven misfolding of Sod1 may be implicated in the development of sporadic ALS, which accounts for 90% of cases [55, 58]. Since oxidative PTMs in Sod1 are reported *in vitro* [61] and in Alzheimer's brains [63], we analyze PTMs in Sod1 from 7-day, stationary phase yeast cells to elucidate the biochemical mechanisms that lead to misfolding of this protein during aging of eukaryotes. The results of this study are reported in Chapter 6.

1.6) Objectives of this thesis

a) Characterize Ccp1 as a mitochondrial H_2O_2 sensor
b) Characterize the H_2O_2 and peroxynitrite signaling and sensing effects of Ccp1 in response to a bolus H_2O_2 and addition of a OHOO(H)-generator
c) Examine the role of Ccp1 H_2O_2 sensing in the lifespan of yeast cells
d) Examine the role of catalases in protecting yeast cells against challenge with H_2O_2
e) Examine post-translational modifications in Sod1 during aging of yeast

Note this overall introduction may appear somewhat brief. This is to avoid repetition since a comprehensive introduction is provided for the topics disussed in Chapters 2-6.

Chapter 2: Ccp1 as a mitochondrial H_2O_2 sensor

2.1) Preface

The work presented in this Chapter 2 was published in: Martins D. Kathiresan M, English AM (2013). **Cytochrome c peroxidase (Ccp1) is a mitochondrial heme-based H_2O_2 sensor that modulates antioxidant defense.** Free Radical Biology and Medicine. 65, 541-551. Meena Kathiresan contributed some of the datapoints for catalase activity, with helpful discussions and revisions of drafts of this paper. The production and interpretation of the other data, writing and revisions of the manuscript were performed by me. Dr. English contributed to discussions, data analysis and revisions of the paper. The content of this section was slightly modified from the published work to include a brief discussion on the technique to measure H_2O_2 release from intact mitochondria. The permission for using the manuscript's content in this thesis was granted by Mrs. Tiffany Hicks, journal manager of Free Radical Biology and Medicine (Elsevier).

2.2) Abstract of the manuscript

Hydrogen peroxide (H_2O_2) is a key signaling molecule that also induces apoptosis. Thus, cells must rapidly sense and tightly control H_2O_2 levels. Well-characterized cellular responses to exogenous H_2O_2 involve oxidation of specific cytosolic protein-based thiols, but sensing of H_2O_2 generated by mitochondrial respiration is less well described. Here we provide substantial biochemical evidence that the heme enzyme Ccp1 (cytochrome c peroxidase), which is targeted to the intermembrane space, functions primarily as a mitochondrial H_2O_2 sensing and signaling protein in *Saccharomyces cerevisiae*. Key evidence for a sensing role for Ccp1 is the significantly higher H_2O_2 accumulation in *ccp1*-null cells (*ccp1*Δ) vs *ccp1*^{W191F} cells producing the catalytically inactive Ccp1^{W191F} variant. In fact, intracellular H_2O_2 levels (*ccp1*Δ >wild-type

>*ccp1*^{W191F}) correlate inversely with the activity of the mitochondrial (and peroxisomal) heme catalase, Cta1 (*ccp1*Δ <wild-type <*ccp1*^{W191F}). Mitochondrial Sod2 activity also varies in the three strains (*ccp1*Δ >wild-type >*ccp1*^{W191F}) and *ccp1*Δ cells exhibit low superoxide levels. Notably, Ccp1^{W191F} is a more persistent H_2O_2 signaling protein than wild-type Ccp1, and this enhanced mitochondrial H_2O_2 signaling decreases the mitochondrial fitness of *ccp1*^{W191F} cells. However, these cells are fully protected from a bolus (0.4 mM) of exogenous H_2O_2 added after 12 h of growth whereas the viability of *ccp1*Δ cells drops below 20%, which additionally associates Ccp1 with Yap1-dependent H_2O_2 signaling. Combined, our results strongly implicate Ccp1, independently of its peroxidase activity, in mitochondrial H_2O_2 sensing and signaling to maintain reactive oxygen species (ROS) homeostasis.

2.3) Introduction

H_2O_2 is the product of the one-electron reduction of $O_2^{\bullet-}$ [4]. Although H_2O_2 is a powerful oxidant, its thermodynamic stability is much higher than that of its precursor, $O_2^{\bullet-}$ [73]. Because of its uncharged and non-polar nature, H_2O_2 can also diffuse through cell membranes and selectively react with activated thiols and heme moieties, which makes it the ideal ROS to fulfill a role of second messenger in cells [70]. In fact, it is now well established that H_2O_2 is not just a harmful oxidant but also a key signaling molecule that modulates diverse biological processes from cell differentiation to apoptosis [70]. Consistent with its potentially toxic nature, H_2O_2 signals are transmitted over short distances and cellular responses to H_2O_2 are both site- and concentration-dependent [70]. Thus, its signals must be sensed and transmitted at short distances from its site of generation and its levels are tightly controlled by the activity of H_2O_2-metabolizing enzymes. The focus on cellular defenses to exogenous H_2O_2 has provided significant insight into thiol-based cytosolic H_2O_2 sensors [42, 49]. For example, Orp1 or Gpx3,

a cytosolic thiol peroxidase, senses excess H_2O_2 through oxidation of its active-site cysteine and conveys this redox signal via disulfide exchange to the transcription factor Yap1 on exposure of *Saccharomyces cerevisiae* to nonlethal doses of H_2O_2 [48, 49]. Oxidized Yap1 is translocated to the nucleus [74] to regulate the transcription of several genes encoding antioxidant defenses such as *CTT1*, *TSA1*, *SOD1* and *SOD2* [43]. However, oxidative environments exist within eukaryotic cells but sensing of endogenously generated H_2O_2 or ROS within these regions is poorly documented. For example, mitochondria are the main sites of H_2O_2 production in respiring yeast [75] but to date only a single case of mitochondrial H_2O_2 sensing has been reported [76], although ROS sensing by mitochondria has been extensively discussed in the context of oxygen availability [77, 78].

Yeast switch from anaerobic to aerobic metabolism when a fermentable carbon source such as glucose becomes limiting. Since mitochondrial ROS spike during this diauxic shift [18], yeast cells must be prepared for an imminent spike in mitochondrial ROS. Given its chemical properties [79] and known signaling functions [70], H_2O_2 is likely a crucial messenger of changes in mitochondrial ROS. We and others demonstrated previously that Ccp1, a 34 kDa heme peroxidase targeted to the mitochondrial intermembrane space (IMS) [80, 81], protects yeast from challenge with a bolus of exogenous H_2O_2 [82-84]. This was not surprising given that *in vitro* Ccp1 serves as a highly efficient H_2O_2 scavenger in the presence of excess donor cyc^{II} (Fig. 2. 1) [34]. However, unexpectedly, we also found that *ccp1*^{W191F} cells producing the Ccp1^{W191F} variant with negligible cytochrome c peroxidase activity are *less* sensitive to H_2O_2 than wild-type cells. The added protective effect of Ccp1^{W191F} cannot be attributed to H_2O_2 scavenging since unlike the oxidized form of wild-type Ccp1 (CmpdI, Fig. 2. 1), CmpdI bearing the W191F mutation [85], is not reduced by cyc^{II} back to the resting ferric enzyme. Consistent

with our results, it has been demonstrated that both Ccp1 and its inactive variant Ccp1^{W191F} convey an oxidative stress signal to the nuclear transcription factor Skn7 [86], which regulates the expression of many antioxidant enzymes including Tsa1, a thiol peroxidase that protects cytosolic proteins against oxidative damage [87, 88].

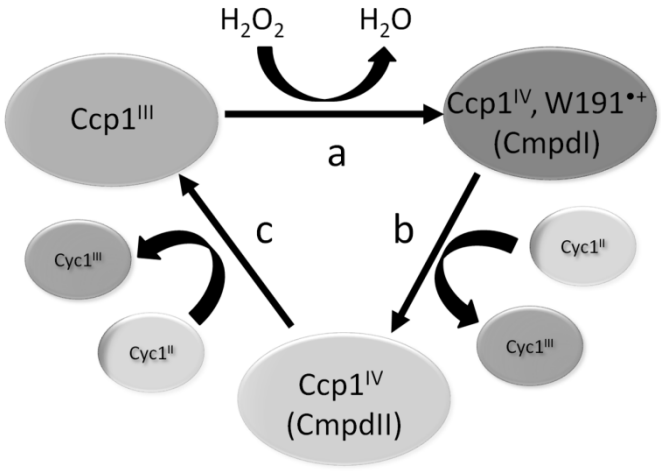

Fig. 2. 1 *Cytochrome c peroxidase catalysis.* Resting ferric (Fe^{III}) Ccp1^{III} is oxidized by H_2O_2 to compound I (CmpdI), which has a Fe^{IV} heme group and a cation radical on residue W191. CmpdI reacts with a ferrous (Fe^{II}) Cyc1^{II} to form compound II with a Fe^{IV} heme but no W191 radical [16]. Reaction with a second Cyc1^{II} reduces the Fe^{IV} heme to yield resting Ccp1^{III}. The Ccp1^{W191F} variant rapidly reacts with H_2O_2 (Step a) but is very slowly reduced by Cyc1^{II} (Steps b, c) such that it exhibits negligible Cyc1^{II}-oxidizing activity [85].

In the present work we report on the function of Ccp1 and its Ccp1^{W191F} variant in responding to endogenously produced H_2O_2. In support of independent H_2O_2 scavenging and H_2O_2 signaling roles for Ccp1, we find that respiring *ccp1*^{W191F} yeast cells accumulate *less* H_2O_2 than wild-type cells. To establish how *ccp1*^{W191F} cells suppress H_2O_2, we performed a detailed biochemical analysis of the enzyme activities involved in H_2O_2 breakdown (peroxidases and catalases) in the wild-type, *ccp1*Δ and *ccp1*^{W191F} strains. We additionally monitored accumulation of $O_2^{\bullet-}$, the direct chemical precursor to mitochondrial H_2O_2, as well as superoxide dismutase activity, which catalyzes $O_2^{\bullet-}$ dismutation to H_2O_2 and O_2.

Our findings clearly establish a role for Ccp1 as a heme-based mitochondrial H_2O_2 sensor and signaling protein. Like cytosolic Gpx3, Ccp1 reacts rapidly with H_2O_2 ($k_1 = 4.5 \times 10^7$ M^{-1} s^{-1}, [89]), which is a hallmark of sensor specificity in signaling pathways [79]. Another common feature of these peroxidases is their utilization of small electron-donor proteins as reducing substrates. Cyc^{II} reduces Ccp1 CmpdI (Fig. 2. 1) back to the resting ferric enzyme and thioredoxin reduces the sulfenic acid formed in Gpx3 back to the sulfhydryl. Thus, as is the case for Gpx3-thioredoxin [48, 49], H_2O_2 signaling by Ccp1 CmpdI is likely controlled by the availability of cyc^{II}. Furthermore, we provide evidence that Ccp1 signals via distinct pathways in response to a steady flux of H_2O_2 generated endogenously by the mitochondria vs challenge with a bolus of exogenous H_2O_2. We re-examined the effects of exogenous H_2O_2 on yeast in the BY4741 genetic background since the W303-1B strains we studied previously [83] exhibit impaired Yap1 signaling [90]. Yap1 is a master regulator of the response to H_2O_2 challenge [43], so the analysis of strains with functional Yap1 signaling is critical in understanding Ccp1's role in sensing both exogenous and endogenous H_2O_2.

2.4) Materials and methods

2.4.1) Yeast strains, media, and growth conditions

The BY4741 *Saccharomyces cerevisiae* strains used in this study are listed in Table 2. 1. Wild-type and *ccp1*Δ cells were purchased from the European *Saccharomyces cerevisiae* Archive for Functional Analysis (EUROSCARF, Frankfurt, Germany). The DNA template for catalytically inactive mature Ccp1 (m*ccp1*^{W191F}) was kindly provided by Professor Yi Lu (Department of Chemistry, University of Illinois, USA) and chromosomally integrated under control of the *CCP1* promoter by homologous recombination [91]. Briefly, the gene *URA3* was amplified by PCR from the plasmid pRS306-*URA3* using the primers *1f* and *1r* (Table 2. 1),

which also contain the homologous recombination sequences for genomic integration of the *URA3* gene in place of *CCP1* (underlined in Table 2. 1). The amplicon was used to transform wild-type BY4741 using the lithium acetate method [92]. Recombinants were selected in synthetic complete (SC) medium lacking uracil and the resulting strain was labelled as DC1-4 (Table 2. 1). Next, m*ccp1*^{W191F} was amplified by PCR using the primers *2f* and *2r* and this product was used to replace *URA3* in the strain DC1-4. After transformation, cells were incubated for 48 h in YPD (1% yeast extract, 2% peptone, and 2% glucose) liquid medium and spread on SC-agar medium containing 5 mM 5-fluoroorotic acid for selection of recombinants [93]. The sequence of m*ccp1*^{W191F} integrated in the chromosome of the recombinants was confirmed by sequencing the genomic DNA with the primers *3f* and *3r* (Table 2. 1).

Yeast cells were grown under high aeration in YPD liquid medium (1% yeast extract, 2% peptone, and 2% glucose) at a flask-to-medium volume ratio of ≥5. The cultures at initial OD_{600} of 0.01 were incubated at 30 °C with shaking at 225 rpm. YPD medium was chosen for the present studies since its pH of 7.2 is close to physiological pH. We previously used synthetic complete (SCD) medium [83], which has a pH ~3 [94], and as noted below the choice of medium strongly influences the results. Additionally, the spent YPD medium was replaced with 0.85% (w/v) NaCl solution after 72 h to extend culture viability [69] and avoid the accumulation of acetic acid, which may create a toxic environment [94].

2.4.2) Detection of intracellular reactive oxygen species (ROS)

The profluorescent dyes, dihydrorhodamine 123 (DHR) and dihydroethidine (DHE) (Molecular Probes), which become fluorescent on oxidation (Fig. S2. 1), were used to probe the relative H_2O_2 and superoxide ($O_2^{\bullet-}$) levels, respectively, in live cells. DHR is also oxidized to rhodamine 123 (Rhod123) by peroxynitrite [95] but since we detected negligible 3-nitrotyrosine,

a peroxynitrite marker [96], in mitochondria isolated from 2-day wild-type or *ccp1*Δ cells (data not shown), we conclude that DHR is oxidized mainly by H_2O_2 (Fig. S2. 1). DHE oxidation to 2-hydroxyethidine (2-HE) correlates with aconitase inactivation [97], which validates 2-HE fluorescence as readout of $O_2^{\bullet-}$ levels (Fig. S2. 1) [19, 98].

Cells were stained as described in [99] with slight modifications. Briefly, 10^7 cells were harvested by centrifugation at 2,000xg for 10 min, incubated at 30 ºC with 1 mL of 5 µM dye in PBS (10 mM sodium phosphate and 150 mM NaCl, pH 7.0) for 60 min (2-HE and DHE) or 120 min (Rhod123 and DHR), centrifuged, washed twice, and diluted to 10^6 cells/mL in PBS. To compare dye uptake by the strains, cells were stained with Rhod123 (Molecular Probes) and 2-HE (2-hydroxyethidine prepared by air oxidation of DHE) [100], the fluorescent oxidized forms of DHR and DHE, respectively (Fig. S2. 1). Dye stocks (5 mM) dissolved in ethanol (Rhod123 and DHR) or DMSO (2-HE and DHE) were stored at -20 ºC in the dark until use.

Flow cytometry (FACS) analysis was performed with a BD FACScan flow cytometer equipped with a 15 mW argon laser emitting at 488 nm (Becton Dickinson). The fluorescence of 10,000 stained cells and the autofluorescence of 10,000 unstained control cells were recorded at a flow rate of 1,000 cells/s using 530/30 (Rhod123 and DHR) and 580/45 (2-HE and DHE) nm bandpass filters. A minimum fluorescence-to-autofluorescence (signal-to-noise) ratio of 10 was obtained under these conditions, and signals were processed using FlowJo Software Version 7.5.5 (Tree Star). The fluorescence of the mutant strains plotted in Fig. 2. 2B, Fig. 2. 5B, Fig. S2. 3 and Fig. S2. 5 is normalized to wild-type cells to account for variation in the FACS instrumentation over 15 days.

DHR-stained cells were also visualized by fluorescence microscopy using a wide-field fluorescence microscope (Model BX 51, Olympus). An equal volume of 90% aqueous glycerol

was added to 10^4 cells/mL in PBS, 10-µL aliquots were spotted per slide, and samples were analyzed using a 50x objective with numerical aperture of 0.5. Cells were excited at 490 nm using a tungsten-halogen lamp and emission was collected using a 520 nm long-pass filter.

Table 2. 1 *S. cerevisiae strains, plasmids and primers*

Strain, plasmid or primer	Description	Reference
wild-type BY4741 strain	*MATa his3Δ1 leu2Δ0 met15Δ0 ura3Δ0*	EUROSCARF
*ccp1*Δ strain	*ccp1::KAN4MX*	EUROSCARF
pRS306-*URA3*	pRS306 plasmid encoding *URA3* which replaces *CCP1* (ORF YKR066C) in the first step of homologous recombination	[101]
DC1-4 strain	BY4741 cells with *ccp1::URA3*	This work
m*ccp1*^{W191F} gene	Ccp1(MI)W191F, I53T, G152D	[102]
pET17b-m*ccp1*^{W191F}	pET17b plasmid encoding m*ccp1*^{W191F}	[102]
ccp1^{W191F} strain	BY4741 cells with *ccp1::*m*ccp1*^{W191F}	This work
primer 1f	5'AAGCTGAGGGAAGATGACGAATATGACAACTAT ATAGGC TATGGGCCCTGTGCGTTTCACACCG – 3'	This work
primer 1r	5'TAAATGGACTGGGCGCGTCTTTAGGGAAAGTGA TACCGTTTTCCAACAGTAGATTGTACTGAGAGTGC AC-3'	This work
primer 2f	5' - CTACACCGCTCGTTCATGTC – 3'	This work
primer 2r	5' - CCTTGTTCCTCTAAAGTCTTGA – 3'	This work
primer 3f	5' – CATGGTCAGGCCCAGATTTG – 3'	This work
primer 3r	5' – CATAGACGTACCGTACAAACG – 3'	This work

2.4.3) H_2O_2 release assay from intact mitochondria

Intact mitochondria were isolated as described elsewhere [103]. Cells grown as described under "Yeast strains, media, and growth conditions" were harvested and washed twice with 100 mM KPi buffer (pH 7.0). The cell pellets were resuspended in 10 mL of pre-warmed 100 mM Tris-H_2SO_4 (pH 9.4) with 10 mM DTT, incubated for 10 min at 30 °C and 80 rpm, harvested, washed twice with 10 mL of 10 mM potassium phosphate buffer (pH 7.4) containing

1.2 M sorbitol, and treated with 3 mg of Zymolyase 20T per g of wet cells for 40 min at 30 ºC. The resulting spheroplasts were washed twice with 10 mL of the same buffer and resuspended in 5 mL of 10 mM Tris-HCl (pH 7.4) containing 0.6 M sorbitol, 1 mM EDTA and 1 mM PMSF. Spheroplasts at 4 ºC were disrupted by 15 strokes of a glass-Teflon homogenizer, the homogenates were centrifuged at 2,000xg and the supernatants (*i.e.,* denucleated lysates or S2 fractions) were collected. The S2 fractions were further centrifuged at 10,000xg for 15 min at 4 °C, and the mitochondria-depleted supernatants (S10 fractions) were separated from the mitochondria-enriched pellets (P10 fractions). P10 fractions were carefully resuspended into 250 mM sucrose, 1 mM EDTA and 10 mM MOPS-KOH (pH 7.2) and applied to a step gradient of 60/32/23/15% sucrose (w/v) in 1 mM EDTA and 10 mM MOPS-KOH (pH 7.2). The gradient was ultracentrifuged at 134,000xg for 1 h at 2 ºC and the highly purified mitochondrial fraction was collected between the 60/32% layer of the gradient.

Because of the increasing discussion on lack of specificity of DHR for monitoring intracellular H_2O_2 production [95], we also determined H_2O_2 release from intact mitochondrial suspensions using the Amplex® Red Hydrogen Peroxide/Peroxidase Assay Kit from Molecular Probes according to the manufacturer's instructions. Since Amplex® Red is a membrane-impervious dye [95], it will only be oxidized to resorufin by H_2O_2, which can permeate the mitochondrial membranes and be released to the assay mixture containing horseradish peroxidase (HRP; Appendix 2. 1)

An assay solution containing 100 μM Amplex Red and 2 U/mL HRP in 100 mM KPi buffer (pH 7.4) was prepared using the kit components. Mitochondria were resuspended at a protein concentration of 0.2-0.6 mg/mL in a 10 mM MOPS-KOH buffer (pH 7.2) with 250 mM sucrose and 1 mM EDTA. Following mixing of 50 μL of mitochondrial suspension with 50 μL

of assay solution, the HRP-catalyzed oxidation of Amplex Red by mitochondria-derived H_2O_2 was monitored at 22 °C in a fluorescence plate reader (Spectra Fluor) with 550/20 nm excitation and 590/30 nm emission bandpass filters. Rates of H_2O_2 released from mitochondria (pmol per min per mg of protein) were calculated using a linear calibration plot of fluorescence intensity vs 20-600 pmol of H_2O_2.

2.4.4) Preparation of soluble protein extracts and enzyme activity assays

The proteins soluble in aqueous buffer were extracted as described previously [83]. Briefly, cells were centrifuged at 2,000xg, washed twice with 100 mM KPi buffer (pH 7.0), resuspended in this buffer containing Complete^{TM} protease inhibitor cocktail (Roche) and mixed with an equal volume of acid-washed glass beads. Suspensions were subjected to four cycles of vortexing, 15 s each, and the cell debris was removed by centrifugation at 13,000xg for 10 min at 4 ºC. The total protein in the supernatants was determined by the Bradford assay with bovine serum albumin (BSA) as a standard [104], and enzyme activities were assayed at 22 °C using a diode-array UV-Vis spectrophotometer (Agilent) or a 96-well plate reader (SpectraFluor Plus)

To determine catalase activity, 5.0-20 µL aliquots of soluble protein extract were added to 1.0 mL of 20 mM H_2O_2 in 50 mM KPi buffer (pH 7.0). H_2O_2 decomposition was monitored at 240 nm (ε_{240}=43.6 M^{-1} cm^{-1}) [105], and 1 unit of catalase activity catalyzed the degradation of 1 µmol of H_2O_2 per min. Cta1 and Ctt1 activities were assayed separately following extract fractionation by native PAGE as described in [106] with slight modifications. Briefly, extracts containing 1.0-5.0 µg total protein were electrophoresed on a 4% stacking (10x4x0.1 cm) and 8% resolving (10x6x0.1 cm) gel at 50 mA for 3 h at 4 ºC. Importantly, we found that a long stacking gel was required to separate Cta1 and Ctt1. The gels were incubated for 10 min at 20 ºC in the dark with 10 mM H_2O_2 in 100 mM KPi buffer (pH 7.0), rinsed once with distilled water,

and stained with 60 mM $K_3[Fe(CN)_6]$ and 75 mM $FeCl_3$ for 5 min at 20 ºC. Active catalase creates a white band in the gel by degrading H_2O_2 and preventing $K_3[Fe(CN)_6]$ reduction to $K_2[Fe(CN)_6]$, which reacts with $FeCl_3$ to form a Prussian blue precipitate [106].

Sod1 and Sod2 in-gel activities also were assayed separately following native PAGE [106]. Extracts containing 0.75-2.0 µg total protein were electrophoresed on 12% resolving gels at 50 mA for 2 h at 4 ºC. The gels were incubated for 30 min at 20 ºC in the dark with the staining solution (0.17 mM NBT, 6.7 mM TEMED and 0.3 mM riboflavin in 100 mM KPi buffer, pH 7.2), rinsed twice with distilled water and exposed to white light from a 60 W mercury lamp for 60 min. Active enzyme inhibits reduction by $O_2^{\bullet-}$ (generated by excited-state riboflavin autoxidation) of NBT to blue formazan and gives white bands [36]. These were quantified on an AlphaImager (AlphaInnotec), and converted to units of SOD activity based on the calibration plot in Fig. S2. 2 prepared using purified human Sod1. Note that negative images of the gels (light areas appear dark and vice versa) are shown in Fig. 2. 6A, Fig. 2. 8A, Fig. S2. 2 and Fig. S2. 6A. To discriminate between Sod1 and Sod2, the resolved gels were incubated for 1 h prior to the staining with 5 mM KCN to specifically inhibit Sod1.

Human recombinant thioredoxin used in the Prx activity assays was kindly provided by Professor William Montfort (University of Arizona). Prx activity was determined by measuring NADPH oxidation at 340 nm (ε_{340}=6.22 mM^{-1} cm^{-1}) in a coupled thioredoxin/thioredoxin reductase assay [107]. Aliquots (10-50 µL) of soluble protein extract were added to 1.0 mL of Prx assay solution (90 µM H_2O_2, 6 µg/mL thioredoxin, 1 µg/mL thioredoxin-reductase and 250 µM NADPH in 50 mM HEPES-NaOH buffer, pH 7.0), and 1 unit of Prx activity catalyzed the oxidation by H_2O_2 of 1 µmol of NADPH/min. Gpx activity was assayed by monitoring NADPH oxidation in a coupled GSH/glutathione reductase assay [108]. Aliquots (5.0-10 µL) of soluble

protein extract were added to 100 µL of Gpx assay solution (2 mM GSH, 100 µM tBHP, 120 µM NADPH and 1 U/mL glutathione reductase in 50 mM Tris-HCl/0.1 mM EDTA buffer, pH 7.6), and 1 unit of Gpx activity catalyzed the oxidation of 1 µmol of NADPH by tBHP/min.

2.4.5) Expression and purification of recombinant human Sod1 (rhCuZnSOD)

The DNA template for rhCuZnSOD was kindly provided by Professor P. John Hart (University of Texas Health Science Center at San Antonio). The cDNA for human Sod1 was subcloned into the *Nco*I and *Hind*III (Fermentas Life Sciences) sites of the Novagen pET22b(+) vector (EMD Millipore), and *E. coli* BL21(DE3) cells were transformed with pET22b-hSod1. Cells were grown to an OD_{600} of 0.6 in LB medium with 100 µg mL^{-1} ampicillin at 37 ºC and 250 rpm. After this time, 1 mM IPTG was added to induce Sod1 overexpression and the culture was further incubated at 23 ºC and 250 rpm for 16 h. Cells were lysed at 75 °C in 50 mM Tris-HCl (pH 8.0) buffer with 100 mM NaCl, 0.1 mM EDTA and 5 mM DTT, centrifuged at 30,000xg for 15 min, and Sod1 in the supernatant was purified on a 2.6x10 cm Q-Sepharose anion-exchange column (GE Healthcare Life Sciences) at 20 °C using a linear 0.1-1 M NaCl gradient at a flow rate of 2 mL/min. The purified protein (49 mg/L culture) was incubated with 0.5 mM $CuCl_2$ and 0.5 mM $ZnCl_2$ in 0.5 M sodium acetate buffer (pH 5.5) at 4 °C for 20 h, desalted on a NAP-5 (Sephadex G-25; GE Healthcare Life Sciences) column, and analyzed for metal ion content on an Agilent 7500ce ICP-MS [72]. Sod1 was found to be 25% Cu- and Zn-loaded and the ng/well in Fig. S2. 2 is corrected for metal loading.

2.4.6) Ccp1 and Ccp1^{W191F} protein levels

Rabbit anti-Ccp1 serum was kindly provided by Prof. David Goodin (University of California, Davis). Immunoblots were used to determine the levels of the Ccp1 and Ccp1^{W191F} proteins in wild-type and *ccp1*^{W191F} cells, respectively. Soluble protein extracts were

electrophoresed under reducing conditions in 6% stacking and 12% resolving SDS-PAGE for 1 h at 150 V. Wet transfer of electrophoresed proteins to a polyvinylidene fluoride (PVDF, BioRad) membrane was carried out at 100 mA for 3 h at room temperature. After blocking for 1 h at room temperature with 5% (w/v) skim milk in TBST (50 mM Tris, 150 mM NaCl and 0.05% v/v Tween 20, pH 7.6), membranes were incubated with rabbit anti-Ccp1 serum (1:10,000 dilution) for 2 h, washed 3 times with TBST, and incubated with goat anti-rabbit HRP conjugated secondary antibody (1:20,000, Biorad) for 1.5 h at room temperature. Blots were visualized using the Super Signal West Pico Enhanced Chemiluminscence (ECL) kit from Thermo Fisher in an AlphaImager (Alpha Innotech). To generate loading controls, membranes were stained with Commassie (ICN Biomedicals) after immunodetection, and the integrated intensity of each anti-Ccp1 reactive band was normalized by the sum of the integrated intensity of all Commassie bands in the same lane [109]. Each lane contained 3 μg of total protein since the Ccp1 signal (2-min exposure) was linear over 0.5-4 μg total protein in 5-day cells, which exhibited the highest Ccp1 production.

2.4.7) Challenge of exponentially growing cells with a bolus of exogenous H_2O_2

Cells grown for 12 h (OD_{600} 0.5) in YPD medium were exposed to 0.4 mM H_2O_2. After a further 1.5 h incubation at 30 ºC and 225 rpm, the cultures were diluted 10-fold, plated on YPD-agar medium and colony forming units (cfu) were counted following incubation at 30 ºC for 2 days [18]. Aqueous 0.85% NaCl was added to the control cells. Catalase, Prx and SOD activities in the soluble protein extracts were determined as described above.

2.4.8) Statistical analyses

Three biological replicates (*i.e.*, three independent cultures) were analyzed in each experiment. Statistical significance between the mutant strains (*P <0.05) was determined by Student's t-test calculated using Origin 9.1 software (OriginLab).

2.5) Results

2.5.1) Independently of its peroxidase activity, Ccp1 senses H_2O_2 and regulates catalase activity

DHR-derived fluorescence, and hence H_2O_2 levels, spike in wild-type cells at day 2 (Fig. 2. 2A). This corresponds to the diauxic shift [18] when most cells are respiring and generating H_2O_2 in their mitochondria due to electron leakage from complex III of the respiratory chain to O_2 [5]. Wild-type cells quickly increase their antioxidant defenses since on day 3 their H_2O_2 level is dramatically lower (Fig. 2. 2A). Since they exhibit higher DHR-derived fluorescence (see DHR activation, Fig. S2. 1), *ccp1*Δ cells appear to respond more weakly to the spike in mitochondrial H_2O_2 relative to wild-type cells at day 3 (Fig. 2. 2B-D, Fig. S2. 3). An additional H_2O_2 spike is seen in the null mutant around day 7 when cells are in stationary phase, which is associated with increased oxidative stress [18]. This reflects again their sub wild-type H_2O_2 scavenging capacity. In contrast, *ccp1*^{W191F} fluorescence drops below that of wild-type cells at day 3 (Fig. 2. 2B-D; Fig. S2. 3), revealing that these cells mount a stronger defense than wild-type to elevated H_2O_2. Consistent with the intracellular results, mitochondria from 2- and 7-day *ccp1*Δ cells release more H_2O_2 than those from wild-type cells, whereas sub wild-type levels of H_2O_2 are released from mitochondria isolated from *ccp1*^{W191F} cells (Fig. 2. 2E).

If Ccp1 were to function solely as a mitochondrial H_2O_2 scavenger [75, 82, 83], production in cells of the catalytically inactive Ccp1^{W191F} variant should not depress H_2O_2 levels.

Thus, we hypothesized that Ccp1 might modulate the activities of other yeast H_2O_2-metabolizing enzymes such as Prx (thioredoxin peroxidase), Gpx or catalase. Wild-type and *ccp1*Δ cells possess comparable Prx activity but this is clearly depressed in *ccp1*^{W191F} cells (Fig. 2. 3A,B), which accumulate *less* H_2O_2 than wild-type cells (Fig. 2. 2B,E). Furthermore, Gpx activity is similar in the three strains (Fig. S2. 4). Thus, the lack of correlation between Prx or Gpx activity and mitochondrial H_2O_2 levels, especially in *ccp1*^{W191F} cells, suggests that H_2O_2 accumulation (Fig. 2. 2) is controlled by another enzymatic activity. Catalases effectively scavenge H_2O_2 by catalyzing its disproportionation with high efficiency [27]. The *ccp1*Δ cells display significantly lower catalase activity than *ccp1*^{W191F} cells (Fig. 2. 3C) notably around the diauxic shift (day 2) and in stationary phase (between days 5 and 10) when this activity peaks in wild-type cells (Fig. 2. 3C). Since yeast express Ctt1, a cytosolic catalase and Cta1 [110, 111] that is co-targeted to mitochondria and peroxisomes [112], we separately monitored the activity of each catalase isoform using in-gel assays. In agreement with previous report, Cta1 has a slower migration in native PAGE than Ctt1 despite its lower molecular weight (234 kDa for Cta1 versus 258 kDa for Ctt1) due to Cta1's less compact structure and lower net charge [113]. Fig. 2. 3D reveals that while Ctt1 activity is comparable in the three strains, Cta1 activity varies dramatically. Importantly, the high and low H_2O_2 levels in *ccp1*Δ and *ccp1*^{W191F} (Fig. 2. 2B,E) cells, can be associated with their low and high Cta1 activities, respectively (Fig. 2. 3D). This leads us to propose that respiration-derived H_2O_2 is removed principally by mitochondrial Cta1, which is regulated in a H_2O_2-dependent manner by Ccp1, defining a H_2O_2 sensing and signaling function for this peroxidase.

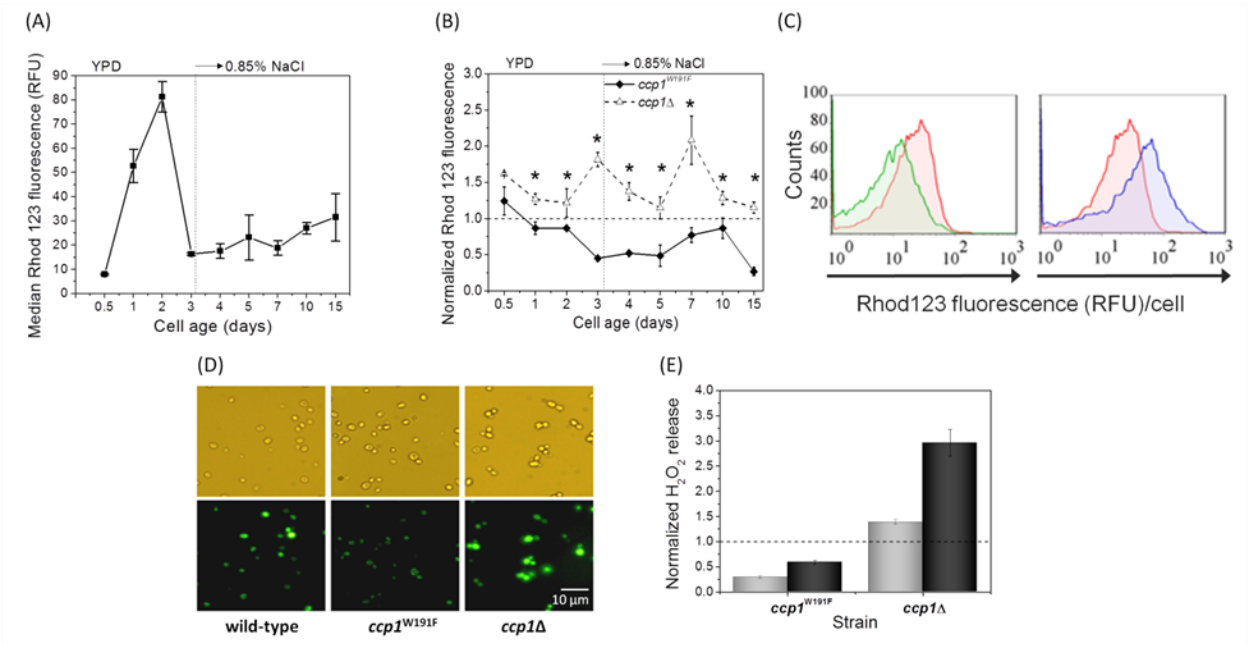

Fig. 2. 2 *H_2O_2 accumulates above wild-type levels in ccp1Δ but not in ccp1^{W191F} cells*. (A) FACS measurements of H_2O_2 in wild-type cells stained with dihydrorhodamine 123 (DHR). Data points are the median fluorescence/cell (RFU, relative fluorescence units) measured in 10,000 cells/sample for three separate cultures ± SD. (B) Median fluorescence/cell normalized to wild-type values in panel A for *ccp1*^{W191F} (solid diamonds) and *ccp1*Δ (open triangles). Yeast cells were grown at 30°C with 225 rpm stirring in YPD medium and changed to 0.85% NaCl at the vertical dotted line. Cells (10^7) were stained with 1 mL of 5 µM DHR for 2 h at 30 °C, diluted to 10^6 cells/mL with PBS (pH 7.0), and Rhod123 fluorescence was recorded using 488-nm laser excitation and a 530/30 nm emission filter. The statistical significance in panel B between *ccp1*^{W191F} and *ccp1*Δ cells (*P <0.05) was determined by Student's t-test and the lines between the data points in panels A and B are for visualization only. (C) Histograms of the FACS measurements of 3-day wild-type (red), *ccp1*^{W191F} (green) and *ccp1*Δ (blue) cells (counts = number of cells with a given RFU). (D) Photomicrographs of 3-day cultures (diluted to 10^4 cells/mL) showing intracellular H_2O_2 (bottom panels) and the corresponding bright-field images (top panels). Rhod123-positive cells were visualized by wide-field fluorescence microscopy with excitation at 490 nm (tungsten lamp; 220-ms exposure) and emission at 520 nm (long-pass filter). See *Materials and methods* for additional information. (E) Normalized rates of H_2O_2 release from intact mitochondria of 2-day (grey bars) and 7-day (black bars) *ccp1*^{W191F} and *ccp1*Δ cells measured by Amplex Red peroxidation in a fluorescence microplate reader with 550/20 nm excitation and 590/30 nm emission band-pass filters. Values are normalized to those of wild-type, and the average rates of H_2O_2 release by wild-type mitochondria were 51.97±5.84 and 16.00±1.12 pmol of H_2O_2/min/mg protein for 2- and 7-day cells,

respectively. Data points are the averages of three separate cultures ± SD. The final mitochondrial suspensions contained 0.1-0.3 mg/mL protein, 50 μM Amplex Red, 1 U/mL horseradish peroxidase (HRP) in 50 mM KPi buffer (pH 7.4). See *Materials and methods* for additional information.

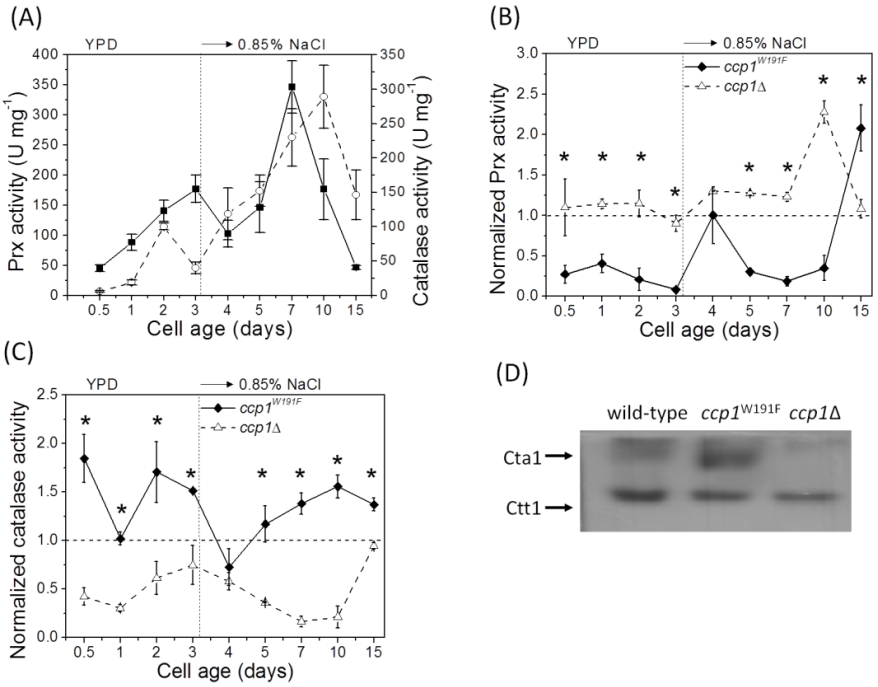

Fig. 2. 3 *Catalase activity is depressed in ccp1Δ cells and Prx activity is depressed in ccp1^{W191F} cells.* (A) Total Prx (solid squares) and total catalase activities (open circles) in the soluble protein extracts from wild-type cells vs cell age. (B) Prx and (C) catalase activities normalized to the corresponding wild-type values in panel A of ccp1^{W191F} (solid diamonds) and ccp1Δ (open triangles). Data points are the averages of three separate cultures ± SD. The statistical significance in panels B and C between ccp1^{W191F} and ccp1Δ cells (*P <0.05) was determined by Student's t-test and the lines between the data points were added for visualization only. (D) In-gel assay of Cta1 and Ctt1 catalase activities in the soluble protein extracts (2.5 μg protein/lane) from 7-day cells. See *Materials and methods* for additional information.

2.5.2) Ccp1^{W191F} is a more persistent H_2O_2 sensor protein than wild-type Ccp1

The elevated Cta1 activity (Fig. 2. 3D) suggests that H_2O_2 signaling is more persistent in *ccp1*^{W191F} cells. Persistent H_2O_2 signaling by oxidized or activated Ccp1^{W191F} is likely since its reduction or deactivation by cyc^{II} (Steps b,c in Fig. 2. 1) is very slow relative to wild-type Ccp1 deactivation [85]. Notably, increased Ccp1^{W191F} protein production does not contribute to

enhanced H_2O_2 signaling because Ccp1^{W191F} and Ccp1 levels are comparable in their respective strains (Fig. 2. 4).

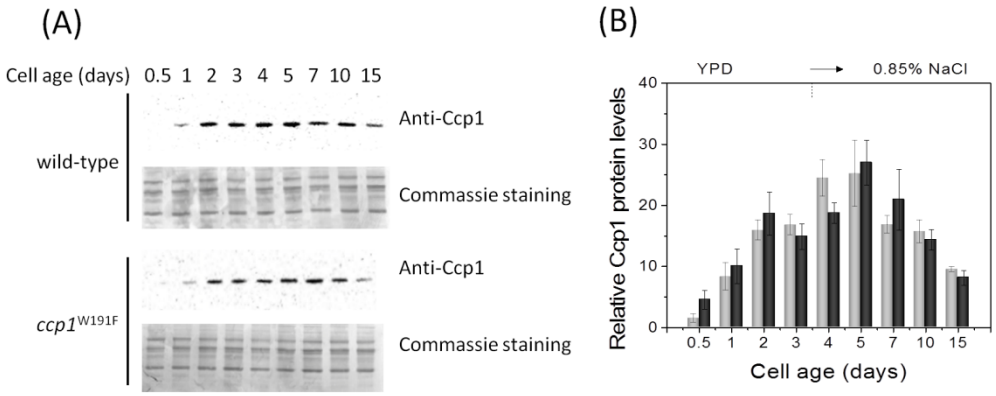

Fig. 2. 4 *Ccp1 and Ccp1^{W19F} production is comparable in wild-type and ccp1^{W191F} strains.* (A) Western blotting of Ccp1 and Ccp1^{W191F} from wild-type (upper panel) and *ccp1*^{W191F} (lower panel) cells over 0.5 to 15 days. Extracts of total soluble protein (3 µg/lane) were separated under reducing conditions by SDS-PAGE, transferred to PVDF membranes over 3 h at room temperature, the membranes were blocked for 1 h in 5% milk-TBST, and probed with rabbit anti-Ccp1 for 2 h followed by a HRP-conjugated anti-rabbit antibody for 1.5 h. The anti-Ccp1 reactive bands were detected by enhanced chemiluminescence (ECL). (B) Intensities of the anti-Ccp1 reactive bands in wild-type (grey bars) and *ccp1*^{W191F} cells (black bars) corrected for loading. The membranes were stained with Commassie after probing for Ccp1 and the sum of Commassie band intensities in each lane serve as a loading control [109]. Data points are the averages of three separate cultures ± SD.

2.5.3) Ccp1 H_2O_2 sensing/signaling regulates Sod2 activity to control superoxide levels

H_2O_2 in respiring yeast cells is derived mainly from the dismutation of superoxide ($O_2^{\bullet-}$) generated by one-electron reduction of O_2 in the electron-transport chain. Although $O_2^{\bullet-}$ spontaneously dismutates to H_2O_2 and O_2 ($k\sim10^5–10^6$ $M^{-1}s^{-1}$), its level in cells is controlled by SODs that catalyze this reaction ($k\sim10^9$ $M^{-1}s^{-1}$) [79]. Yeast possess two SODs, an abundant and largely cytosolic Sod1, which is additionally present in the mitochondrial intermembrane space [114], and Sod2 localized in the mitochondrial matrix [115]. DHE staining reveals that at all time

points, *ccp1*Δ cells have lower $O_2^{\bullet-}$ levels than the Ccp1 producing strains (Fig. 2. 5A,B; Fig. S2. 5), consistent with the enhanced SOD activity of the null mutant (Fig. 2. 6; Fig. S2. 6). However, $O_2^{\bullet-}$ levels in *ccp1*Δ cells drop significantly below wild-type levels (Fig. 2. 5B) only when Sod2 activity spikes at day 3 (Fig. 2. 6A, C). For Sod2 activity to control its accumulation, the $O_2^{\bullet-}$ flux from the electron transport chain must be directed largely to the matrix [5] and trapped there because its charge impedes diffusion across membranes [96].

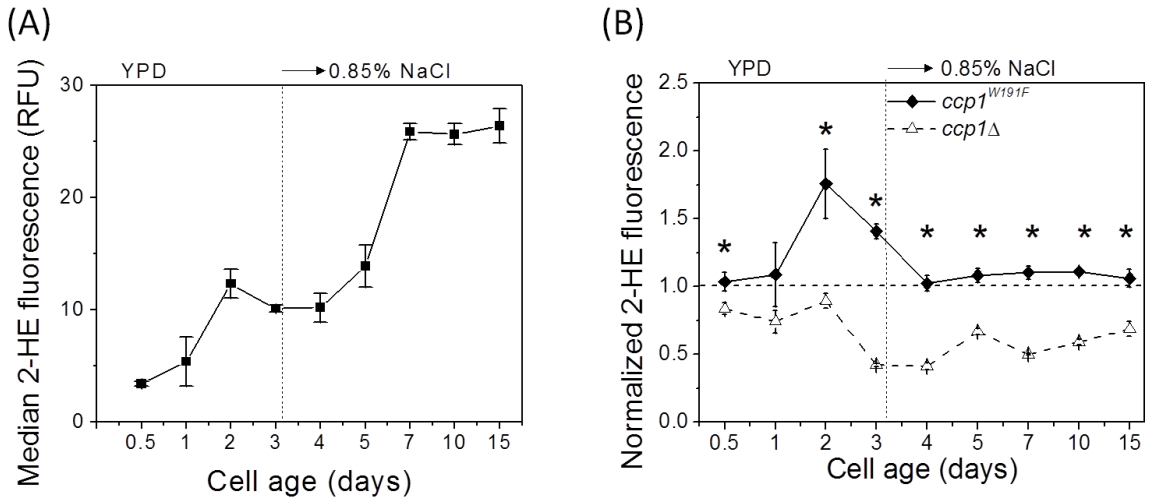

Fig. 2. 5 *Superoxide ($O_2^{\bullet-}$) accumulates above wild-type levels in ccp1^{W191F} but not in ccp1Δ cells.* (A) FACS measurements of $O_2^{\bullet-}$ in wild-type cells stained with dihydroethidine (DHE). Data points are the median fluorescence/cell (RFU) measured in 10,000 cells/sample in three separate cultures ± SD. 2-HE fluorescence was recorded using 488-nm laser excitation and a 580/45 emission filter. (B) Median fluorescence/cell normalized to wild-type values in panel A for *ccp1*^{W191F} (solid diamonds) and *ccp1*Δ (open triangles). Data points are the averages of three separate cultures ± SD. The statistical significance in panel B between *ccp1*^{W191F} and *ccp1*Δ cells (**P* <0.05) was determined by Student's t-test and the lines between the data points in both panels were added for visualization only. Experimental data as in Fig. 2. 2 except that cells were stained with DHE for 1 h.

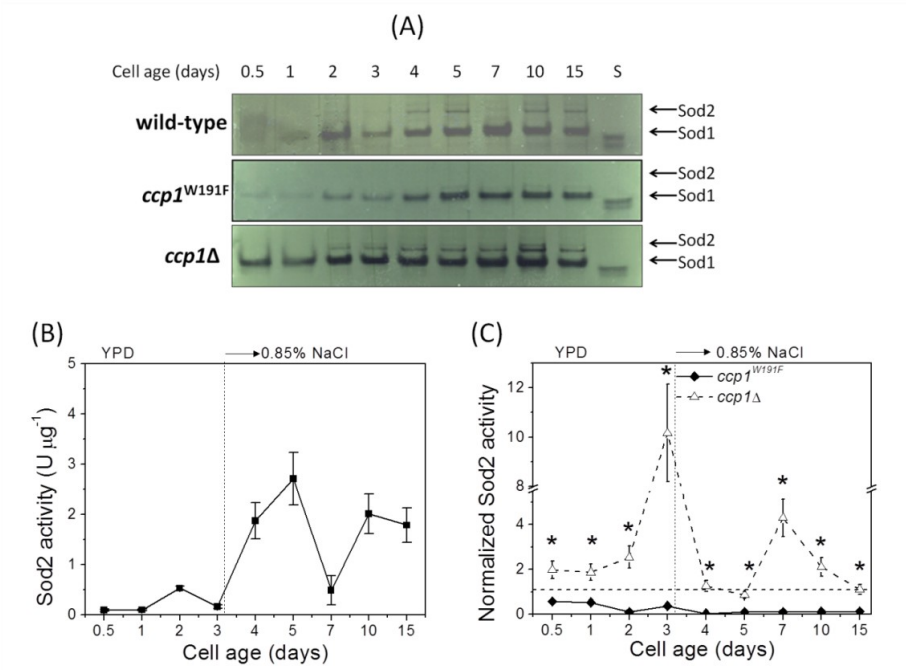

Fig. 2. 6 *Sod2 activity is upregulated in ccp1Δ but not in ccp1^{W191F} cells.* (A) In-gel analysis of superoxide dismutase (SOD) activity vs cell age in the soluble protein extracts (0.75 µg total protein/lane). The activity of 1 ng of purified recombinant human CuZnSOD is shown in lane S. (B) Sod2 activity in wild-type cells was determined from the calibration curve in Fig. S2. 2. (C) Sod2 activity normalized to wild-type values in panel B of *ccp1*^{W191F} (solid diamonds) and *ccp1*Δ (open triangles). Data points are the averages of three separate cultures ± SD. The statistical significance in panel C between *ccp1*^{W191F} and *ccp1*Δ cells (**P* <0.05) was determined by Student's t-test and the lines between the data points in panels B and C were added for visualization only. Enzyme activities were assayed following native PAGE as described under *Materials and methods*.

Sod2 activity is significantly lower in *ccp1*^{W191F} vs *ccp1*Δ cells (Fig. 2. 6C). Thus, low Sod2 activity combined with high Cta1 activity (Fig. 2. 3D) prevents H_2O_2 accumulation in *ccp1*^{W191F} cells (Fig. 2. 2) whereas the opposite situation permits H_2O_2 accumulation in *ccp1*Δ cells. Notably, staining with Rhod123 (a probe of mitochondrial membrane potential, Fig. S2. 3) reveals a post-diauxic drop at day 3 in mitochondrial function following the spike in $O_2^{\bullet-}$ accumulation in *ccp1*^{W191F} cells (Fig. 2. 5B). In contrast, elevated H_2O_2 in the null mutant (Fig. 2. 2B,E) has little effect on membrane potential (Fig. S2. 3). Also noteworthy is the surge in $O_2^{\bullet-}$

accumulation in wild-type and *ccp1*^{W191F} cells in stationary phase (Fig. S2. 5), which is partially offset by elevated Sod2 activity in *ccp1*Δ cells (Fig. S2. 6C). In sum, H_2O_2 sensing and signaling via Ccp1 strongly influence Sod2 activity and $O_2^{\bullet-}$ levels in respiring cells.

2.5.4) Ccp1 signaling protects exponentially growing cells against challenge with exogenous H_2O_2

Previously, we [83] and others [82, 84] reported that *ccp1*Δ cells in W303-1B, JM7490 and BY4741 genetic backgrounds exhibited poor viability when challenged with H_2O_2. We confirm here that exponentially growing BY4741 *ccp1*Δ cells are sensitive to 0.4 mM exogenous H_2O_2 whereas *ccp1*^{W191F} cells are resistant to this challenge (Fig. 2. 7A). Since Prx and catalase activities are depressed in *ccp1*^{W191F} and *ccp1*Δ cells, respectively (Fig. 2. 3B,C), we questioned how challenge with exogenous H_2O_2 might alter these activities. Surprisingly, Prx activity increased 10-fold in *ccp1*^{W191F} vs 2-fold in wild-type cells but remained uninduced in *ccp1*Δ (Fig. 2. 7B). Cytosolic Tsa1 (Tpx1) is the most abundant Prx in *S. cerevisiae* [116] and its mRNA was upregulated when exponentially growing wild-type and *ccp1*^{W191F} cells (in the CEN.PK2-1C genetic background) were challenged with exogenous H_2O_2 [86]. Furthermore, Tsa1 mRNA remained elevated longer in *ccp1*^{W191F} vs wild-type cells, consistent with Ccp1^{W191F} being a more persistent H_2O_2 signaling molecule than Ccp1 since the latter is readily deactivated by cyc1^{II} (Fig. 2. 1).

Exogenous H_2O_2 induces catalase activity by ~2.5-fold in wild-type cells to reach the high constitutive level found in *ccp1*^{W191F} (Fig. 2. 7C). The latter increases by ~20% on H_2O_2 challenge but remains at its constitutively low level in the *ccp1*Δ mutant (Fig. 2. 7C). A previous study of the yeast H_2O_2 stimulon [42] reported upregulation of cytosolic Ctt1 and Tsa1 protein expression. The catalase activity of Ctt1 will scavenge cytosolic H_2O_2 while Tsa1 functions both

as a ribosome-associated antioxidant [87] and chaperone [88]. Thus, the low viability of *ccp1*Δ cells under exogenous H_2O_2 challenge can be attributed in part to their failure to increase Ctt1 and Tsa1 production in the absence of Ccp1-mediated H_2O_2 signaling.

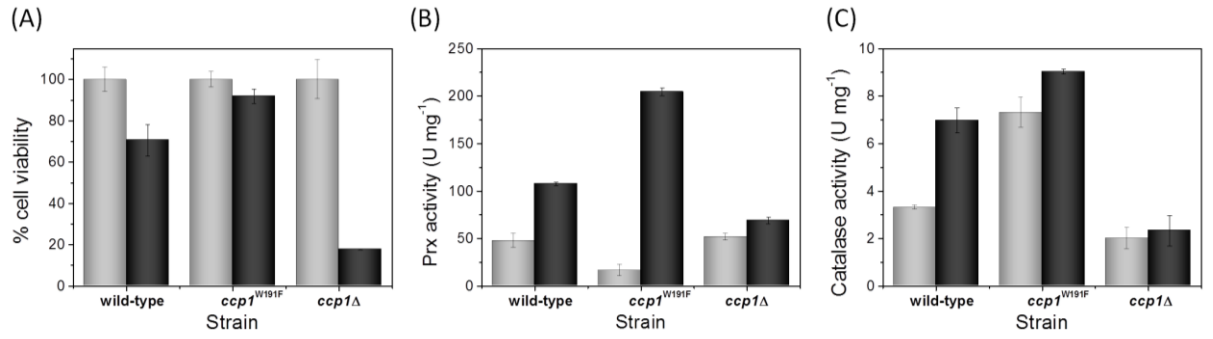

Fig. 2. 7 *ccp1Δ cells exhibit low viability and do not upregulate Prx or catalase activity following challenge with a bolus of exogenous H_2O_2.* (A) Viability of 0.5-day wild-type, *ccp1*^{W191F} and *ccp1*Δ cells after challenge with 0.4 mM H_2O_2. Total (B) Prx and (C) catalase activities with and without H_2O_2 challenge. Cultures at OD_{600} 0.5 were challenged with saline solution (control, grey bars) or 0.4 mM H_2O_2 (black bars) for 1.5 h at 30 ºC and 225 rpm. Cell viability and enzyme activities were assayed as described under *Materials and methods*. Data points are the averages for three separate cultures ± SD.

We previously reported that W303-1B *ccp1*Δ cells grown in SCD medium exhibited higher catalase activity on H_2O_2 challenge than wild-type cells [83]. Here we note that BY4741 *ccp1*Δ cells grown in SCD media possess *lower* catalase activity than wild-type cells both in the presence and absence of H_2O_2 challenge (Fig. S2. 7), although both cell viability and catalase induction are lower in SCD vs YPD (data not shown). Thus, the discrepancy in our previous [83] and present results may reflect differences in the parent strains. W303-1B cells have a nonsense mutation in the *YBP1* gene [117, 118] encoding Ybp1, a critical activator of the transcriptional regulatory protein, Yap1 [90, 117]. Since Yap1 is a master regulator of the H_2O_2 stimulon [42, 43], the dissimilar response to H_2O_2 challenge of cells in the W303-1B and BY4741 genetic backgrounds is not surprising. Additionally, in our previous study we expressed *CCP1* and

ccp1^{W191F} on a low copy number plasmid pYCplac33 [83] while for this present study all constructs were expressed chromosomally (Table 2. 1).

Interestingly, we observed that H_2O_2 challenge significantly decreases Sod2 activity in the three strains and Sod1 activity to a lesser extent (Fig. 2. 8). In contrast, Sod2 and Sod1 protein levels were induced ~6- and 4-fold, respectively, on H_2O_2 challenge of cells in the YPH98 genetic background [42, 43]. The divergence between Sod1 protein levels and activity may be explained in part by H_2O_2-induced inactivation of Sod1, which has been observed *in vitro* [119]. However, Sod2 is reportedly resistant to H_2O_2 *in vitro* [120] but a channel for H_2O_2-induced Sod2 inactivation may exist *in vivo* that is absent *in vitro*. Moreover, H_2O_2-induced expression of antioxidant defenses is transient and levels off after prolonged exposure to this compound [42], presumably due to H_2O_2 consumption by antioxidant enzymes. Thus, it is possible that expression of Sod1 and Sod2 are less persistent than Prx and catalases, since the SODs are not directly involved in metabolizing H_2O_2. While endogenous H_2O_2 induces SOD activity (Fig. 2. 6; Fig. S2. 6) and exogenous H_2O_2 [42, 43] induces Sod1 and Sod2 production, we speculate that the SODs may be inactivated at the post-translational level by the high H_2O_2 concentrations used to challenge cells (Fig. 2. 8).

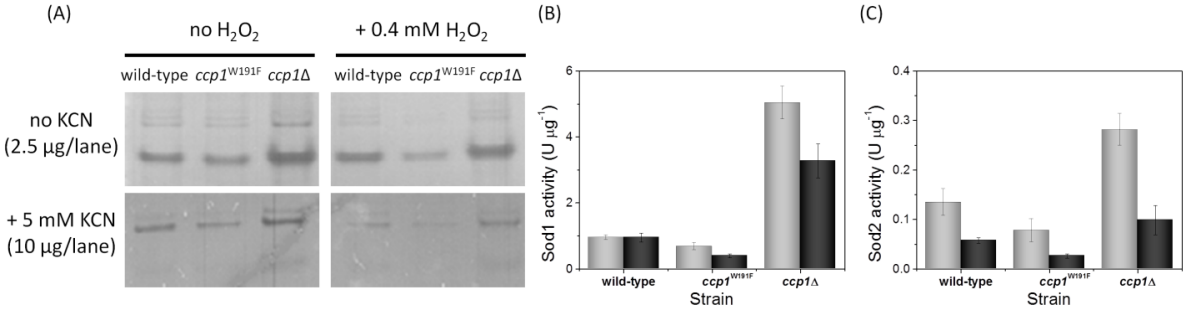

Fig. 2. 8 *Sod2 activity is more sensitive than Sod1 activity to challenge with a bolus (0.4 mM) of exogenous H_2O_2.* (A) Upper panel: in-gel superoxide dismutase (SOD) activity (2.5 µg total protein/lane). Lower panel: Sod2 activity (10 µg total protein/lane) following Sod1 inhibition with 5 mM KCN. (B) Sod1 and (C) Sod2 activities were determined from the calibration curve in Fig. S2. 2. Cultures at OD_{600}

0.5 were exposed to saline solution (control, grey bars) or 0.4 mM H_2O_2 (black bars) for 1.5 h at 30 ºC and 225 rpm. Sod1 and Sod2 activities were assayed following native PAGE as described under *Materials and methods*. Data points are the averages for three separate cultures ± SD.

2.6) Discussion

We provide data that identify Ccp1 as a mitochondrial H_2O_2 sensor and signaling molecule. Its role as a scavenger of H_2O_2 in respiring mitochondria appears secondary to its signaling role since H_2O_2 levels are higher in wild-type cells than in *ccp1*^{W191F} cells (Fig. 2. 2) with negligible CCP activity (Fig. 2. 1). Ccp1-mediated H_2O_2 signaling increases Cta1 activity (Fig. 2. 3D) and, although Ccp1^{W191F} and Ccp1 production are similar (Fig. 2. 4), Cta1 induction is higher in *ccp1*^{W191F} vs wild-type cells (Fig. 2. 3D) due to sluggish deactivation of activated Ccp1^{W191F} by cyc1^{II} (Steps b, c in Fig. 2. 1) [85]. Devoid of Ccp1, *ccp1*Δ cells accumulate the highest amount of H_2O_2 (Fig. 2. 2) and exhibit the lowest Cta1 activity (Fig. 2. 3). However, this is beneficial since H_2O_2 induces Sod2 [18, 19, 42] as reflected here in the elevated Sod2 activity in the null mutant vs *ccp1*^{W191F} (Fig. 2. 6C). Downregulation of this key mitochondrial antioxidant activity increases intracellular $O_2^{\bullet-}$ levels (Fig. 2. 5B) and impairs mitochondrial function in *ccp1*^{W191F} cells (Fig. S2. 3). Fig. 2. 9A summarizes how H_2O_2 sensing and signaling by Ccp1 influences endogenous ROS levels and antioxidant activities. Ccp1 is activated on oxidation by H_2O_2 and signaling by the active form, CmpdI (or a derivative), increases Cta1 activity, which scavenges H_2O_2. The drop in H_2O_2 levels inhibits stimulation of Sod2 activity, leading to increased $O_2^{\bullet-}$ levels (Fig. 2. 5B), and also depressed Prx activity (Fig. 2. 3B), especially in the presence of persistent signaling by Ccp1^{W191F}. Importantly, the opposing control of H_2O_2 and $O_2^{\bullet-}$ levels by Ccp1 signaling impacts yeast chronological lifespan since *ccp1*Δ and *ccp1*^{W191F} cells live longer and shorter, respectively, than wild-type cells [97]. Chronological lifespan extension has been previously reported for *ctt1*Δ and *cta1*Δ yeast strains which, like

*ccp1*Δ cells, accumulate more H_2O_2 and less $O_2^{\bullet-}$ that wild-type cells [19]. The effects of Ccp1 deletion on lifespan of yeast cells will be discussed in Chapter 4.

In contrast to its negative effect on mitochondrial fitness (measured as mitochondrial membrane potential, Fig. S2. 3), and lifespan [97], Ccp1 signaling clearly protects cells against exogenous H_2O_2 (Fig. 2. 7). Following challenge with a bolus (0.4 mM) of H_2O_2, *ccp1*Δ cells exhibit <20% viability and insignificant upregulation of catalase or Prx activities (Fig. 2. 7B,C). In contrast, *ccp1*^{W191F} cells are >95% viable and exhibit high catalase and Prx activities, whereas wild-type cells mount a slightly less effective defense (Fig. 2. 7). Increased catalase and Prx activities are consistent with the reported induction on challenge with exogenous H_2O_2 of Ctt1 and Tsa1 protein levels [42] as well as Tsa1 mRNA levels [86], as outlined in Fig. 2. 9B. Thus, Ccp1 signaling gives rise to different outcomes in response to endogenous and exogenous H_2O_2, the most striking example being the dramatic upregulation of Prx activity in *ccp1*^{W191F} cells in response to exogenous H_2O_2 (Fig. 2. 7B) vs the depression of this activity in unchallenged *ccp1*^{W191F} (Fig. 2. 3B). This serves as a clear example of how H_2O_2 signaling is site and concentration dependent [70], and more specifically how Ccp1-mediated H_2O_2 signaling reduces mitochondrial fitness but protects against H_2O_2 challenge. In essence, Ccp1 is nonessential in unstressed cells but strongly defends cells against exogenous H_2O_2 like other antioxidant enzymes studied in model organisms [50].

Heme-based H_2O_2-sensing has not been previously reported although heme proteins are known to sense gases including O_2, NO and CO [121]. Also, heme-activated O_2 sensors such as Hap1 and Hap2/3/4/5 modulate expression of antioxidant enzymes [122, 123] but do not respond to H_2O_2 [124]. Like thiol-based H_2O_2 sensors such as Gpx3 [70], Ccp1 is rapidly oxidized by H_2O_2 (Step a in Fig. 2. 1) [89] but it is unclear how H_2O_2 signals through Ccp1. We observe

accumulation of catalytically inactive and likely heme-free Ccp1 outside mitochondria following the diauxic shift [Kathiresan, Martins and English, manuscript in preparation] when catalase activity starts to increase in wild-type and *ccp1*^{W191F} strains (Fig. 2. 3C,D). This raises the intriguing possibility of heme transfer from "activated" Ccp1 to apoCta1, which we are currently investigating. This hypothesis gains credence from the fact that Ccp1 translation is independent of heme availability and apoCcp1 is rapidly converted to the holoprotein [125] once heme is synthesized [124] whereas translation of catalase T [126] but not A [127] requires heme.

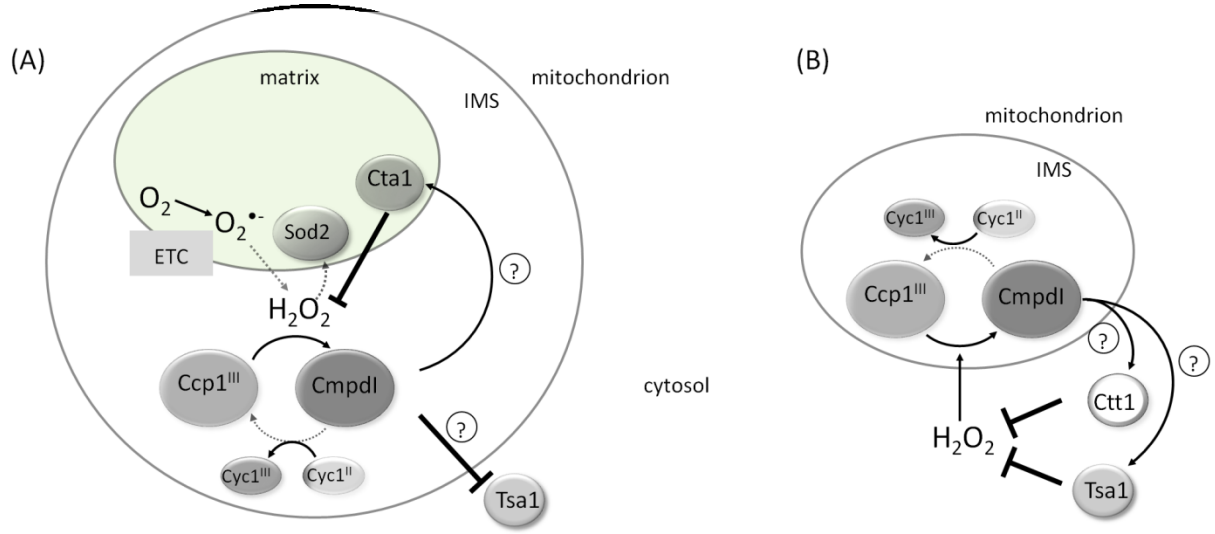

Fig. 2. 9 *Summary of Ccp1 sensing and signaling of mitochondrially generated H_2O_2 or of a bolus of exogenously added H_2O_2.* Solid and dashed arrows represent processes assumed to be stimulated and repressed, respectively by Ccp1 sensing/signaling. (A) Ccp1 in the mitochondrial intermembrane space (IMS) is oxidized to signaling competent CmpdI by H_2O_2 generated during mitochondrial respiration. CmpdI is deactivated by cyc1^{II} or signals to enhance Cta1 activity and suppress Prx activity by an unknown mechanism. Increased Cta1 activity blocks H_2O_2 accumulation, thereby downregulating Sod2, which increases $O_2^{\bullet-}$ levels. (B) Exogenously added H_2O_2 oxidizes Ccp1, which upregulates Ctt1 catalase and Tsa1 Prx activities to promote resistance to exogenous H_2O_2. We speculate that the Ccp1 signal is transmitted to the nucleus via the Skn7/Yap1 pathway, since Ccp1 was shown to activate Skn7 on H_2O_2 challenge also by an unknown mechanism [86].

Since Ccp1 is the first mitochondrial heme-based H_2O_2 sensor and signaling protein identified, unravelling its novel mechanism(s) should advance our understanding of mitochondrial retrograde signaling. Finally, we note that since Ccp1 shares its reducing substrate $cyc1^{II}$ with cytochrome c oxidase, reducing equivalents in the electron transport chain can be directed to H_2O_2 or O_2 to control respiration.

2.7) Supplementary information

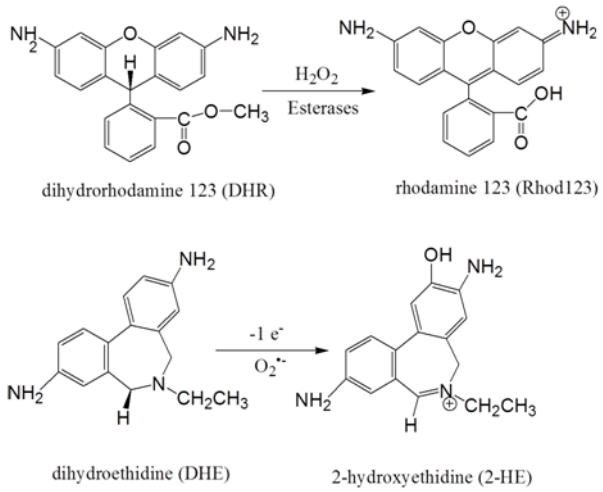

Fig. S2. 1 *Structures of the profluorescent dyes (DHR and DHE) and their fluorescent, oxidized forms (Rhod123 and 2-HE).* The probes are disposed to oxidation by H_2O_2 and $O_2^{\bullet-}$.

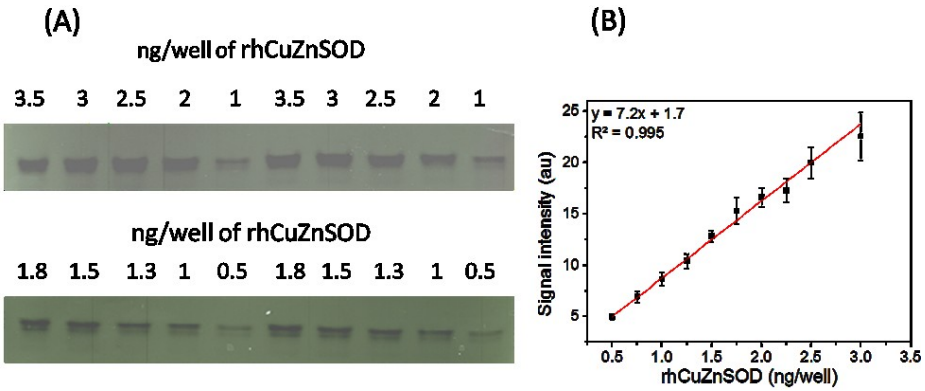

Fig. S2. 2 *Standard calibration plot for in-gel analysis of SOD activity*. (A) The activity of purified recombinant human Sod1 (rhCuZnSOD, 0.5 to 3.0 ng/well) in native polyacrylamide gels. (B) The signal intensity (arbitrary units, au) measured by densitometry is linear to ~2.5 ng/well with a detection limit of ~0.25 ng/well. Data points are the averages for three independent experiments ± SD. A unit of SOD activity in Fig. 2. 6, Fig. 2. 8 and Fig. S2. 6 corresponds to that of 1 ng of rhCuZnSOD. See *Materials and Methods* for additional information.

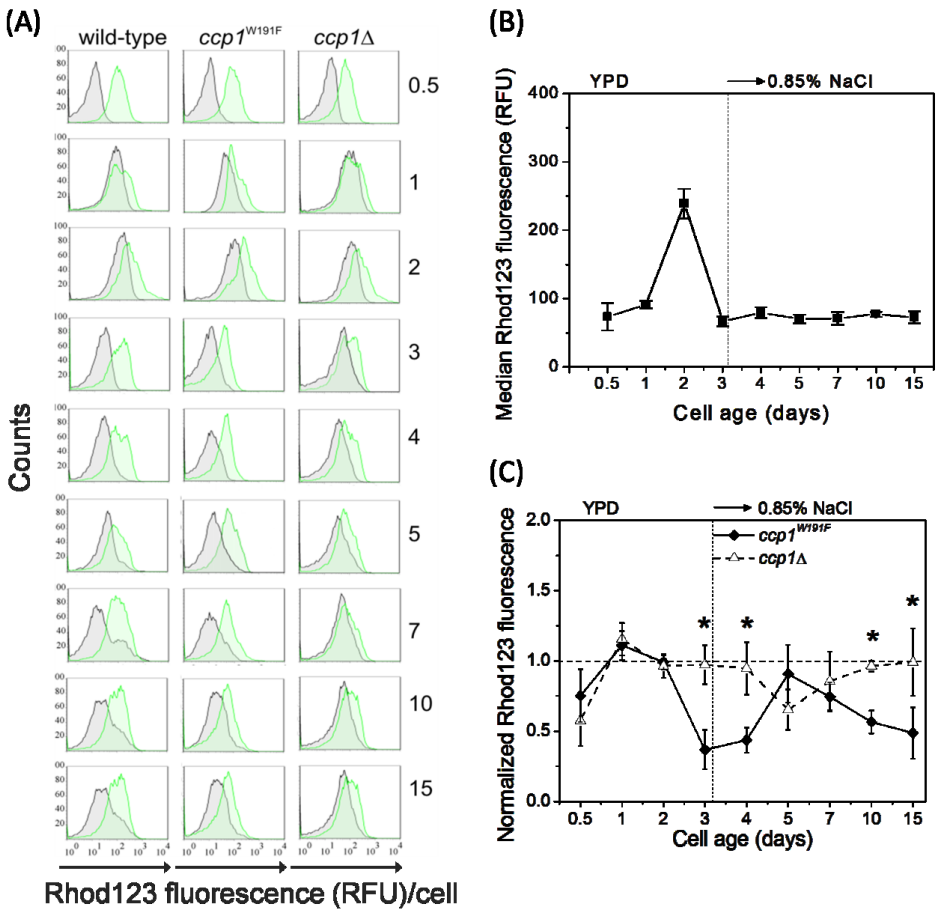

Fig. S2. 3. *Fluorescence from cells stained with DHR (a H_2O_2-senstive probe) or Rhod123 (a probe of membrane potential) reaches maximum intensity at the diauxic shift.* (A) Histograms of the FACS measurements over 15 days from wild-type (left panels), *ccp1*^{W191F} (middle panels) and *ccp1*Δ cells (right panels) stained with DHR (grey lines) and Rhod123 (green lines). (B) Variation vs cell age of Rhod123 fluorescence of wild-type cells. Data points indicate median ± SD fluorescence/cell in RFU (relative fluorescence units) measured in 10,000 cells/sample in three separate cultures. (C) Median fluorescence/cell after Rhod123 staining normalized to wild-type in panel B for *ccp1*^{W191F} (solid diamonds) and *ccp1*Δ (open triangles). Since the normalized Rhod123 fluorescence is <1.0 in post-diauxic *ccp1*^{W191F} cells we assume that these cells have low membrane potential and hence impaired membrane function. Yeast cells were grown as described under *Materials and Methods* and at each time point, 10^7 cells were stained with 1 mL of 5 µM DHR or Rhod123 for 2 h at 30 °C, harvested by centrifugation and diluted in PBS (pH 7.0) to 10^6 cells/mL. Cells were excited at 488 nm and emission was collected using a 530/30 bandpass filter. The statistical significance in panel C between *ccp1*^{W191F} and *ccp1*Δ cells (*P <0.05) was determined by Student's t-test and the lines between the data points in panels B and C were added for visualization only.

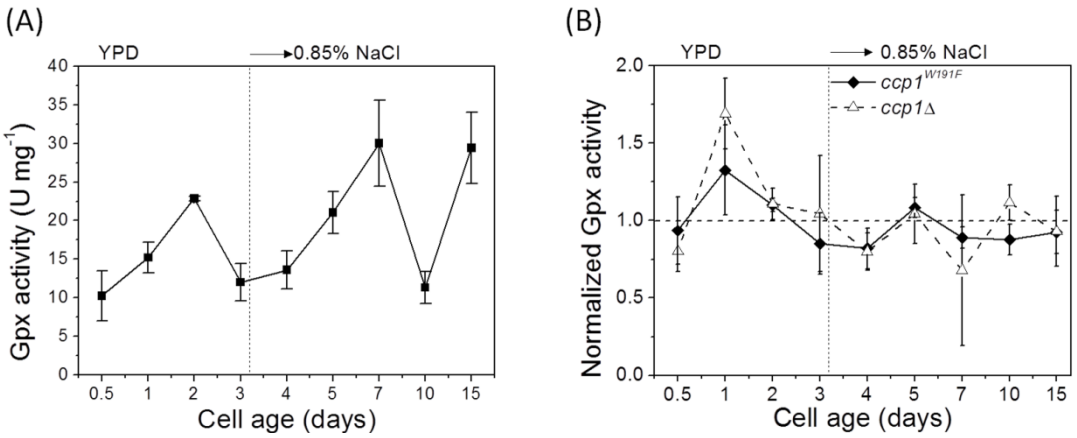

Fig. S2. 4 *Total glutathione peroxidase (Gpx) activity is comparable in wild-type, ccp1*^{W191F} *and ccp1*Δ *cells.* Gpx activity was assayed in the soluble protein extracts in a coupled reaction with glutathione-glutathione reductase, and 1 unit catalyzes the oxidation of 1 μmol of NADPH/min/mg total protein. (A) Specific Gpx activity in wild-type cells. (B) Gpx activity normalized to the wild-type values in panel A of *ccp1*^{W191F} (solid diamonds) and *ccp1*Δ (open triangles). Data points are the averages for three separate cultures ± SD. Statistical significance in panel B between *ccp1*^{W191F} and *ccp1*Δ cells (**P* <0.05) was determined by Student's t-test and the lines between the data points in both panels were added for visualization only. See *Materials and methods* for additional information.

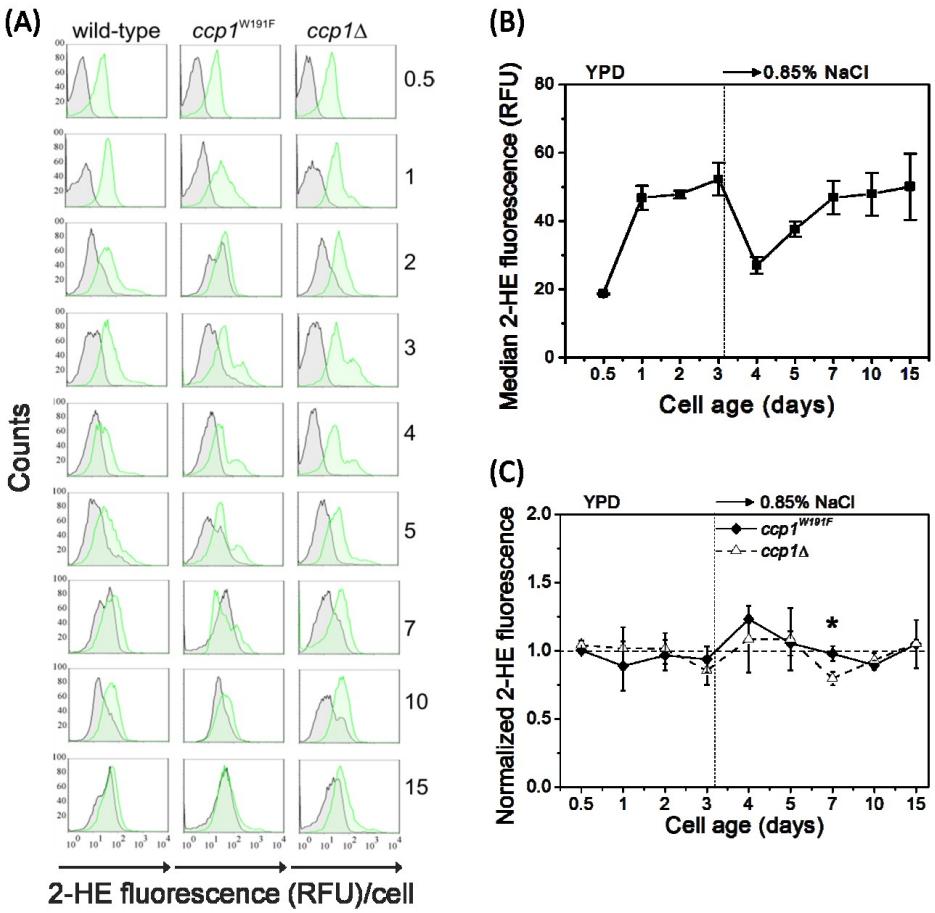

Fig. S2. 5 *Fluorescence from cells stained with DHE (a superoxide-sensitive probe) increases with cell age and uptake of 2-hydroxyethidine (2-HE) is comparable in wild-type, ccp1^{W191F} and ccp1Δ cells.* (A) Histograms of the FACS measurements over 15 days from wild-type (left panels), *ccp1*^{W191F} (middle panels) and *ccp1*Δ cells (right panels) stained with DHE (grey lines) and 2-HE (green lines). (B) Variation vs cell age of 2-HE uptake by wild-type cells. Data points indicate median ± SD fluorescence/cell in RFU (relative fluorescence units) measured in 10,000 cells/sample in three separate cultures. (C) Median fluorescence/cell after 2-HE staining normalized to the wild-type values in panel B for *ccp1*^{W191F} (solid diamonds) and *ccp1*Δ (open triangles). Since the normalized 2-HE fluorescence is close to 1.0 for the mutant strains we assume that 2-HE loading, and hence that of structurally similar DHE (Fig. S2. 1), is similar in the three strains. Experimental details are given in the legend to Fig. S2. 3 except that cells were stained with 5 μM DHE or 2-HE for 1 h. The statistical significance in panel C between *ccp1*^{W191F} and *ccp1*Δ cells (**P* <0.05) was determined by Student's t-test and the lines between the data points in panels B and C were added for visualization only.

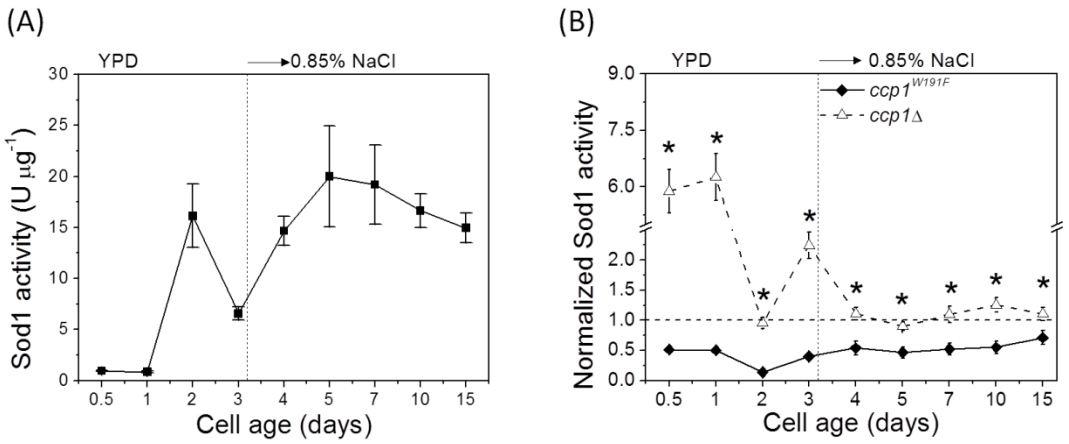

Fig. S2. 6 *Sod1 activity is upregulated in ccp1Δ but not in ccp1^{W191F} cells.* In-gel assay of Sod1 activity in the soluble protein extracts. (A) Sod1 activity in wild-type cells was determined from the calibration curve in Fig. S2. 2. (B) Sod1 activity normalized to the wild-type values in panel A of *ccp1*^{W191F} (solid diamonds) and *ccp1*Δ (open triangles). Data points are the averages for three separate cultures ± SD. The statistical significance in panel B between *ccp1*^{W191F} and *ccp1*Δ cells (**P* <0.05) was determined by Student's t-test and the lines between the data points in both panels were added for visualization only. See *Materials and methods* for additional information.

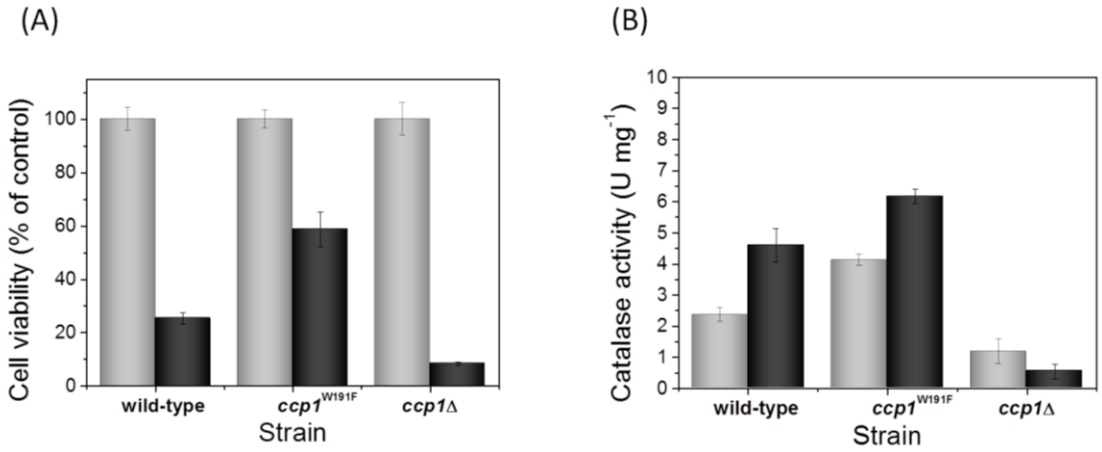

Fig. S2. 7 *Catalase activities increase in wild-type and ccp1^{W191F} cells but not in ccp1*Δ *on challenge with a bolus of exogenous H_2O_2 in SCD media.* (A) Viability of 0.5-day wild-type, *ccp1*^{W191F} and *ccp1*Δ cells after challenge with 0.4 mM H_2O_2 in SCD media. (B) Total catalase activities before and after H_2O_2 challenge. Cultures at OD_{600} 0.5 were exposed to saline solution (grey bars) or 0.4 mM H_2O_2 (black bars) for 1.5 h at 30 ºC and 225 rpm. Cell viability and enzyme activities were assayed as described under *Materials and Methods*. Data points are the averages for three separate cultures ± SD.

Chapter 3: Ccp1 as a peroxynitrite sensor

3.1) Preface

The work presented in Chapter 3 corresponds to the following manuscript in preparation: Martins D, Bakas I, McIntosh K, English AM. **Cytchrome c peroxidase (CCP) - a highly efficient peroxynitrite reductase**. Target Journal: Free Radical Biology and Medicine. The spectrophotometric and kinetic characterizations of the reaction of Ccp1 with peroxynitrite were performed by Iolie Bakas and Kelly McIntosh, respectively. I performed and analyzed all of the *in vivo* data, wrote and revised the manuscript. Dr. English analyzed the kinetic data and edited the paper.

3.2) Abstract of the manuscript

Peroxynitrite [ONOO(H)] is a reactive nitrogen species (RNS) that increases in pathologies such as amyotrophic lateral sclerosis, diabetes, and Alzheimer's, Parkinson's and cardiovascular diseases. Since ONOO(H) promotes cell damage by nitrating proteins, enzymes that efficiently scavenge this RNS are of interest. Herein, we report that cytochrome c peroxidase (Ccp1), a heme-based H_2O_2 sensor in yeast mitochondria, rapidly reacts with ONOO(H) *in vitro* ($k=1.4\pm0.5\times10^7$ $M^{-1}s^{-1}$). The Ccp1 product formed exhibits the same absorption spectrum as the well-characterized compound I (CmpdI) formed on Ccp1 oxidation by H_2O_2, and, like CmpdI, it oxidizes two equivalents of ferrocytochrome c. Nitrite, a product of the two-electron reduction of ONOO(H) does not reduce CmpdI, indicating that ONOO(H) is not converted by Ccp1 to the powerful nitrating agent, $^{\bullet}NO_2$. Ccp1 may therefore protect cells against RNS. As anticipated from these *in vitro* results, deletion of Ccp1 increases the sensitivity of yeast cells to challenge with SIN-1, a ONOO(H) generator. Challenge of wild-type Ccp1-producing yeast cells with

SIN-1 increases both catalase and peroxiredoxin activities, which are known to scavenge ONOO(H). Since we reported previously that Ccp1 similarly protects cells against H_2O_2 challenge, we conclude that exogenous ONOO(H) and H_2O_2 stimulate a common response pathway involving oxidation of Ccp1 to CmpdI, to signal a peroxide stress response. Our results implicate Ccp1 as a key player in protecting yeast cells against ROS and RNS.

3.3) Introduction

Nitric oxide (NO) serves as a critical mediator of cell signaling [128] and modulator of important physiological mechanisms such as vasodilation [129, 130], the immune response [130] and inhibition of platelet aggregation [131, 132]. However, excess of NO promotes deleterious effects such as mitochondrial respiratory-chain blockage [133], DNA damage and cell cycle arrest [134] and induction of apoptosis [135]. Some of these toxic effects can be attributed to the diffusion controlled reaction ($k=4\text{-}16\times10^9$ $M^{-1}s^{-1}$) between NO and $O_2^{\bullet-}$ [136] that produces ONOO(H) [137]:

$$NO + O_2^{\bullet-} \rightleftharpoons ONOO^- \quad (1)$$

$$ONOO^- + CO_2 \overset{a}{\rightleftharpoons} [ONO_2CO_2^-] \overset{b}{\rightleftharpoons} {}^{\bullet}NO_2 + {}^{\bullet}CO_3^- \quad (2)$$

Peroxynitrite has a pK_a of 6.8 and both the peroxynitrous acid (ONOOH) and its conjugate base ($ONOO^-$) undergo a series of reactions *in vivo*. ONOO(H) oxidizes cysteine residues to sulfinic and sulfonic acids in critical metabolic enzymes such as glyceraldehyde-3-phosphate dehydrogenase [138] and aconitase [139]. ONOO(H) also reacts with CO_2 present at millimolar levels in tissues to form nitrosoperoxicarbonate, $ONO_2CO_2^-$ (Reaction 2a; $k=3\times10^4$ $M^{-1}s^{-1}$). The latter rapidly decomposes to the carbonate (${}^{\bullet}CO_3^-$) and nitrogen dioxide radicals (${}^{\bullet}NO_2$, Reaction 2b) and both these radicals oxidize lipids, DNA and proteins [136]. Moreover, ${}^{\bullet}NO_2$ is a potent nitrating agent that attacks tyrosine residues and promotes 3-nitrotyrosine

formation and dityrosine crosslinks, which also inactivate aconitase [140] and the key antioxidant enzyme, manganese superoxide dismutase (Sod2) [141]. Not surprisingly, excessive ONOO(H) production has been associated with pathological conditions such as ALS [142], diabetes [143], Alzheimer's [144] and cardiovascular diseases [145]. Thus, mechanisms of ONOO(H) scavenging and metabolism have been extensively investigated.

Mammalian enzymes with ONOO(H)-metabolizing activity described so far can be divided into those that play a role in host immune defense and those that protect the host from RNS. Enzymes involved in defense include myeloperoxidase (MPO) and lactoperoxidase (LPO). These heme peroxidases react rapidly with ONOO(H) ($k=6.2x10^6$ and $3.3x10^5$ M^{-1} s^{-1}, respectively, for MPO and LPO at pH 7.4) [146] in a pH-dependent manner. Only ONOOH, which is an inorganic hydroperoxide, is a substrate of heme peroxidases [146] and it oxidizes the heme to a two-electron oxidized enzyme intermediate termed compound I (CmpdI) (Fig. 3. 1, step a). The NO_2^- produced on heterolytic cleavage of the ONO-OH peroxy bond does not diffuse from the active site of MPO or LPO but quickly reduces CmpdI by one electron to compound II (CmpdII, Fig. 3. 1, step b). The $^{\bullet}NO_2$ released in step b (Fig. 3. 1) can assist MPO and LPO in cellular defense [146] by nitrating tyrosines of proteins from invaders [147].

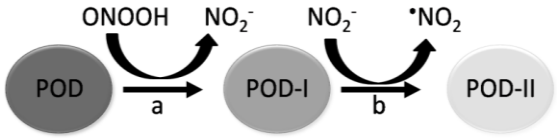

Fig. 3. 1 *A mechanism of the reaction between heme peroxidases and ONOO(H).* (a) the protonated form of ONOO(H) (peroxynitrous acid, ONOOH) oxidizes the heme center of a ferric heme peroxidase (POD) to the 2-electron oxidized form compound I (POD-I) and generates nitrite (NO_2^-). (b) the POD-I oxidizes the product NO_2^- and is converted to the 1-electron oxidized intermediate compound II (POD-II). Nitrogen dioxide ($^{\bullet}NO_2$), a powerful nitrating species, diffuses from POD.

Enzymes that protect the host against RNS rapidly scavenge intracellular ONOO(H) but do not oxidize NO_2^- to the harmful $^{\bullet}NO_2$ radical. Such enzymes and their bimolecular rates ($M^{-1}s^{-1}$) of ONOO(H) scavenging include peroxiredoxin 5 ($k=7x10^7$, pH 7.4) [148], selenium glutathione peroxidase ($k=8x10^6$, pH 7.4) [147], and catalase ($k=2x10^6$, pH 7.1) [149]. Also, a low-molecular-weight selenium glutathione peroxidase mimetic, ebselen, has been identified and this compound reacts rapidly with ONOOH ($k=2x10^6$ $M^{-1}s^{-1}$, pH 7.5) [150]. These scavengers differ in their mechanism of ONOO(H) degradation but none oxidize NO_2^-, which would lead to $^{\bullet}NO_2$, a more toxic species than ONOO(H).

To date, there are no reports of a heme peroxidase that protects cells against ONOO(H). Cytochrome c peroxidase (Ccp1) is a heme enzyme found in the intermembrane space of yeast mitochondria [81]. It exhibits highly efficient H_2O_2-metabolizing activity *in vitro* by coupling the two-electron reduction of H_2O_2 to the one-electron oxidation of ferrocytochrome c from yeast and other sources including horse heart (Cyc^{II}, Fig. 3. 2) [80]. Ccp1 scavenges H_2O_2 (Fig. 3. 2, step a) with a bimolecular rate constant of $k=4.5x10^7$ M^{-1} s^{-1} [151], and the two-electron oxidized CmpdI formed is rapidly reduced by two molecules of Cyc^{II} (Fig. 3. 2, steps b,c) [152]. Because of its efficient peroxidase activity, Ccp1 has long been viewed as a H_2O_2 scavenger *in vivo*. In fact, deletion of Ccp1 increases sensitivity to exogenous H_2O_2 [20, 82-84], and expression of Ccp1 [42] and of the *lacZ* reporter under the control of the Ccp1 promoter [82] increases on H_2O_2 challenge. However, cells expressing the $Ccp1^{W191F}$ variant with negligible Cyc^{II} oxidizing ability [85] are less sensitive to H_2O_2 challenge than wild-type cells [20, 82]. This demonstrates CCP activity is not required directly for protection against H_2O_2, which led us [20, 83] and others [86] to identify a role for Ccp1 in H_2O_2 sensing and signaling. Challenge of wild-type yeast with H_2O_2 increases Tsa1 (a homolog of human peroxiredoxin 2) mRNA expression [86] as well the

total peroxiredoxin and catalase activities [20]. The response of cells expressing Ccp1^{W191F} to H_2O_2 challenge surpasses that of the wild-type strain and the negligible response of the Ccp1-null mutant renders these cells highly sensitive to H_2O_2 [20]. Thus, we concluded that Ccp1 serves to communicate a H_2O_2 stress response, which likely involves formation of CmpdI since Ccp1^{W191F} is a more persistent H_2O_2 sensor *in vivo* [20] due to slow deactivation of its CmpdI by Cyc^{II} (Fig. 3. 2, steps b,c).

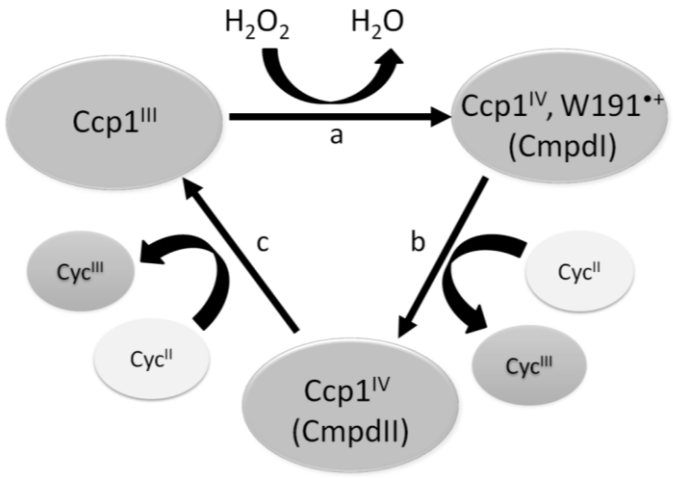

Fig. 3. 2 *Catalytic cycle of Ccp1 using H_2O_2 and cyc^{II} as substrates.* Resting ferric Ccp1 (Ccp1^{III}) undergoes a 2-electron oxidation upon reaction with H_2O_2 (step a, k=4.5x10^7 M^{-1} s^{-1}) and generates compound I (CmpdI), which contains an oxyferryl heme (Fe^{IV}=O) and a tryptophan cation radical at position 191 (W191$^{•+}$). CmpdI reacts with a molar equivalent of Cyc^{II} (step b, k=1.3x10^8 M^{-1} s^{-1}) and is reduced to compound II (CmpdII), which contains only the Fe^{IV}=O moiety. CmpdII oxidizes a second molar equivalent of Cyc^{II} to return to the resting state (step c, k=2.0x10^6 M^{-1} s^{-1}) [153]

Since ONOOH behaves as a peroxide in reaction with heme peroxidases, we hypothesized that Ccp1 would also react with this RNS *in vitro* and *in vivo*. In fact, it has been demonstrated that cells respond to ONOO(H) challenge by increasing the expression of *lac*Z under the control of the Ccp1 promoter [82]. We further investigated the role of Ccp1 as a protective enzyme in the presence of ONOO(H). Herein, we report that Ccp1 is rapidly oxidized

to CmpdI by ONOOH *in vitro* but unlike MPO, CmpdI of Ccp1 does not oxidize NO_2^- to $^{\bullet}NO_2$. These *in vitro* results suggest that Ccp1 protects cells from ONOO(H), which we confirm here. *In vivo*, Ccp1 acts as a ONOO(H) sensor that increases the cell's response to ONOO(H) challenge by boosting catalase and peroxiredoxin activity to effectively scavenge this RNS [149, 154]. Thus, Ccp1 emerges as the first heme peroxidase that neutralizes rather than potentiates ONOO(H) toxicity. As a heme-based general peroxide sensor, Ccp1 protects yeast cells against both ROS and RNS.

3.4) Materials and methods

3.4.1) Materials

Sephadex G25 resin, horse heart cytochrome c (type III), blue dextran and all buffer salts were purchased from Sigma. Potassium ferricyanide [$K_3Fe(CN)_6$], sodium dithionite ($Na_2S_2O_4$), glucose and 30% (w/w) hydrogen peroxide solution were obtained from Fisher Scientific. Diethylenentriamine pentaacetic acid (DTPA) and ethylenediaminetetraacetic acid (EDTA) were from ICN Biomedicals, sodium nitrite from Anachemia Chemicals and sodium nitrate from Allied Chemical. Peroxynitrite was purchased from Calbiochem in powder form as the tetramethylammonim salt [$ONOON(CH_3)_4$] in 0.3 M NaOH solution. Peroxynitrite was also prepared in NaOH by the ozone-azide method, aliquoted and stored at -16 °C [155]. Yeast cytochrome c peroxidase (Ccp1) was a generous gift from Professor James Erman (Northern Illinois University). All solutions were prepared using Nanopure water (specific resistance 18.2 MΩ cm) from a Barnstead Nanopure system (Thermo Scientific). Yeast extract, peptone and microbiology grade agar were purchased from Bioshop, and 3-morpholinosydnonimine (SIN-1) was obtained from Cayman Chemicals.

3.4.2) Protein sample preparation

Ccp1 stock solutions were prepared by dissolving the lyophilized enzyme in 100 mM potassium phosphate buffer, pH 7.0 (KPi) and the concentration was determined spectrophotometrically (ε_{408}=98.0 mM^{-1} cm^{-1}) [156]. All Ccp1 samples had a purity index (A408/A280) of 1.25–1.30 in KPi [157], and the A408/A380 (1.54±0.06) and A620/A647 (0.78±0.04) ratios were within the range of the reported values, which are characteristic for a 5-coordinate, high-spin heme protein [158].

A stock horse heart ferricytochrome c (Cyc^{III}) solution was prepared by dissolving the lyophilized protein in KPi and its concentration was determined both by weight (MW=12,384 Da) and spectrophotometrically with ε_{550}=9.1 mM^{-1} cm^{-1} [159]. Cyc^{III} was reduced with excess dithionite and passed through a 1x19-cm Sephadex G-25 column equilibrated with degassed KPi in a glove box (MBraun, Model MB 120-G) under N_2 to remove excess reducing agent. The reduced protein was stored in liquid N_2 for up to one month. Before and after each experiment, the CycII concentration was checked spectrophotometrically (ε_{550}=27.7 mM^{-1} cm^{-1}) [159], and in all cases Cyc was ≥ 90% reduced.

3.4.3) Titration of Ccp1 with ONOO(H) under N_2

A peroxynitrite stock solution (12.7 mM) in 0.3 M NaOH was diluted with ice cold deionized water, adjusted to pH 11.0 with NaOH, and the concentration determined spectrophotometrically (ε_{302}=1.670 mM^{-1} cm^{-1}) [154]. A solution of 0.1 mM DTPA in KPi (KPi/DTPA) was purged with N_2 gas for 30–40 min and added to a quartz cuvettete fitted with a septum. Ccp1 stock solution was added to the cuvettete using a gas-tight 25 µL Hamilton syringe to a concentration of 4–10 µM in 1.0 mL. Then, ONOO(H) was added in 10 µL aliquots using the gas-tight syringe and after each addition the spectrum was recorded over 250–700 nm on a

Agilent 8451A diode-array spectrophotometer at room temperature and corrected for dilution. Note that to minimize ONOO(H) decay, the syringe was rinsed with N_2-purged 10 mM EDTA followed by N_2-purged Nanopure water at pH 11.0. At the end of the titration the pH of the solution in the cuvettete remained at 7.0. To establish if commercial ONOO(H) contained any contaminants that reacted with Ccp1, a 12.7 mM stock ONOO(H) in KPi/EDTA was let stand at room temperature for 20 min to decompose. Ccp1 was titrated with this solution under aerobic conditions so that CO_2 in the buffer would eliminate any remaining ONOO(H).

3.4.4) Stopped-flow kinetics of the reaction of Ccp1 with ONOO(H) under N_2

In a glove bag, a NaOH pellet was added to 100 mL of N_2-purged Nanopure water. An aliquot of the concentrated (46 mM) ONOO(H) reaction solution (prepared by the ozone-azide method) was diluted into this NaOH solution to give a 20-30 μM ONOO(H) working solution. A 1-2 μM Ccp1 working solution was prepared by dissolving the lyophilized enzyme in 10 mL of N_2-purged 0.1 M sodium phosphate (NaPi) at pH 5.5-8.5, purging again with N_2 gas. Also, N_2-filled balloons were attached to the septa sealing each working solution to minimize introduction of air. The solutions were drawn into separate syringes attached to an Applied Photophysics SX-19MV stopped-flow analyzer with a deadtime of 1.3 ms at 25.2 °C. Equal volumes were injected into the mixing cell, and data collection was triggered. To establish the initial pH of the Ccp1 solution required to obtain the desired pH in the mixing cell, equal volumes of NaOH (1 NaOH pellet per 100 mL Nanopure water) and 0.1 M NaPi at different pHs were mixed and the pH recorded. The kinetics of Ccp1 oxidation to CmpdI by ONOO(H) were monitored at 424 nm on the 200 ms timescale, and the decay of excess ONOO(H) over 20 s was monitored at 302 nm ±Ccp1.

3.4.5) Titration of ONOO(H)-oxidized Ccp1 with Cyc^{II} under N_2

ONOO(H) (8 nmol) was added by gas-tight syringe to a 1-mL N_2-purged solution of 4 μM Ccp1 (4 nmol) in KPi/DTPA in a cuvette sealed with a septum. Aliquots (5 μL) of 210 μM Cyc^{II} were added with the gas-tight syringe and the Cyc absorbance at 550 nm was recorded following each addition on a Beckman DU 650 spectrophotometer at room temperature. After the equivalence point the absorbance at 550 nm increases sharply due to the higher absorbance of Cyc^{II} vs.Cyc^{III} (ε_{550}=18.5 mM^{-1} cm^{-1}) [159]

3.4.6) Probing nitrite oxidation by CmpdI

Ccp1 (11.5 μM) was oxidized with stoichiometric amount of H_2O_2 in KPi and the conversion to CmpdI was confirmed spectrophotometrically. A 10-fold molar excess of $NaNO_2$ in KPi was added to one aliquot and buffer only to a second aliquot and spectra (250-700 nm) were monitored in 30-min intervals over 120 min on a Beckman DU 650 spectrophotometer at room temperature. The ΔA424 nm at each time point was compared to ΔA424 nm at t=0 min to monitor the decay of CmpdI ± nitrite.

3.4.7) Yeast strains and growth conditions

The yeast strains in the BY4741 background used in this study are listed in Table 3. 1. The wild-type and Ccp1-null strain (*ccp1*Δ) were purchased from the European *Saccharomyces cerevisiae* Archive for Functional Analysis (EUROSCARF, Frankfurt, Germany). The mutant chromosomally expressing $Ccp1^{W191F}$, which exhibits negligible turnover with Cyc^{II} [85], was constructed by homologous recombination as previously reported [20]. All strains were grown to the exponential phase (OD600=0.5, ~12 h growth) in YPD liquid medium (1% yeast extract, 2% peptone and 2% glucose) at 30 °C with shaking at 225 rpm and a flask-to-medium volume ratio of 1:5.

Table 3. 1. *S. cerevisiae strains used in this study*

Strain	Description	Reference
wild-type BY4741	*MATa his3Δ1 leu2Δ0 met15Δ0 ura3Δ0*	EUROSCARF
*ccp1*Δ	BY4741 cells with *CCP1::KAN4MX*, a gene disruption cassette bearing a kanamycin resistance selection marker	EUROSCARF
ccp1^{W191F}	BY4741 cells with *CCP1::CCP1*^{W191F}	[20]

3.4.8) Challenge of yeast with SIN-1, a ONOO(H) generator

Cultures at OD_{600}=0.5 were challenged with 2 mM SIN-1 for 1.5 h at 30 °C with shaking at 225 rpm and a flask-to-medium volume ratio of 1:5. Following challenge, the cultures were serially diluted, plated on YPD agar medium and incubated for 2 days at 30 °C [20]. Cell viability was determined by counting the total colony forming units (cfu) in SIN-1 treated and untreated cultures. Data are represented as the averages for three separate cultures ±SD.

3.4.9) Preparation of soluble protein extracts and enzyme activity assays

Protein extracts from SIN-1 treated and control cultures were prepared as reported [20, 83]. Cells were washed twice with KPi, centrifuged at 2000xg, the pellets suspended in KPi with 0.1 mM PMSF and mixed with an equal volume of acid-washed glass beads. Cells were disrupted by vortexing for 4x15 s, the suspensions were centrifuged at 13000xg for 10 min at 4 ºC, and the total protein in the supernatant was determined by the Bradford assay with BSA as a standard [160].

Specific enzyme activities (U mg^{-1} protein) of 40–100 µL aliquots of the supernatant are represented as the averages for three independent cultures ±SD. Total catalase activity was determined by monitoring spectrophotometrically (ε_{240}=43.6 M^{-1} cm^{-1}) the decomposition of 20 mM H_2O_2 in 50 mM KPi (pH 7.0) at 22 °C after supernatant addition [105]. One unit of catalase

activity consumes 1 μmol of H_2O_2/min/mg protein. Total peroxiredoxin (Prx) activity was determined by monitoring NADPH peroxidation spectrophotometrically (ε_{340}=6.2 mM^{-1} cm^{-1}) in a coupled thioredoxin/thioredoxin reductase reaction [107] following supernatant addition to the assay solution (90 μM H_2O_2, 6 μg/mL thioredoxin, 1 μg/mL thioredoxin reductase and 250 μM NADPH in 50 mM HEPES-NaOH, pH 7.0). One unit of Prx activity catalyzes the peroxidation of 1 μmol NADPH/min/mg protein.

3.5) Results

3.5.1) ONOO(H) converts Ccp1 to CmpdI which oxidizes two equivalents of Cyc^{II}

We anticipated that ONOOH, an inorganic peroxide, would oxidize Ccp1 to CmpdI as reported for other heme peroxidases (Fig. 3. 1). This was confirmed since addition of excess ONOO(H) to Ccp1 in N_2-purged KPi gives a species with an absorption spectrum identical to that of CmpdI generated with H_2O_2 (Fig. 3. 3A,B) [161]. The CmpdI-Ccp1 difference spectrum shows a maximum at 424 nm (Appendix 3. 1) [161] and a plot of ΔA424 vs. [ONOO(H)] exhibits an inflection point at ~10 μM ONOO(H) when 6.0 μM Ccp1 was titrated with this peroxide (Fig. 3. 4A). However, in three titrations, 1.65±0.10 molar equivalents of ONOO(H) were required to fully convert Ccp1 to CmpdI vs. 1.0 molar equivalents of H_2O_2 (data not shown). The titrations were performed in N_2-purged buffer to eliminate CO_2 and prevent reaction 2 but ONOOH will isomerize to NO_3^- during manual mixing (~1–2 s) at pH 7.0 in the cuvette. We measured by stopped-flow a first-order rate constant of ~0.5 s^{-1} for ONOO(H) decomposition in the absence of Ccp1 at pH 7.0 (data not shown), which corresponds to a half-life of ~1.4 s. Thus, competition between ONOO(H) isomerization to NO_3^- [136] and its reduction by Ccp1 during the mixing time in the cuvette will increase the apparent stoichiometry of this reaction with Ccp1.

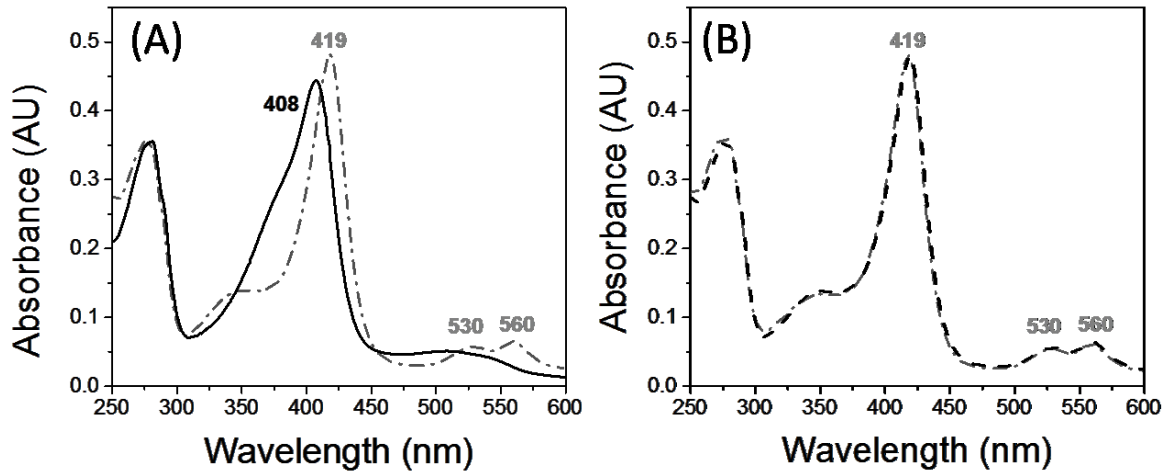

Fig. 3. 3 *Ccp1 is oxidized by ONOO(H) to CmpdI.* (A) UV-vis spectrum in N_2-purged KPi in 1-cm cuvette recorded at room temperature of 4 μM Ccp1 (solid black line) and of 4 μM Ccp1 plus 8 μM ONOO(H) (dashed-dotted grey line). (B) Overlay of the UV-vis spectra of 4 μM Ccp1 plus 8 μM ONOO(H) (dashed-dotted grey line); and of 4 μM Ccp1 plus 8 μM H_2O_2 (dashed black line) recorded under the same conditions as the spectra in panel A. The spectrum of Ccp1 plus ONOO(H) is identical to that plus H_2O_2, exhibiting the Soret (419 nm) and charge transfer bands (530 and 560 nm) expected for CmpdI.

CmpdI and CmpdII, the two- and one-electron oxidized Ccp1 intermediates, respectively, possess essentially identical spectral properties. This is because the second oxidizing equivalent in CmpdI is localized on residue Trp191, which forms a cation radical that does not significantly perturb the electronic environment of the heme as probed by electronic absorption and MCD spectroscopy [162]. Thus, we titrated the oxidizing equivalents in ONOO(H)-generated CmpdI with horse heart Cyc^{II}, which is highly similar to Ccp1's physiological reducing substrate (Fig. 3. 2). As shown in Fig. 3. 4B, an inflection point at 7.5 μM in the titration of 4 μM CmpdI revealed that 1.9 oxidizing-equivalents are stored between the heme and polypeptide in good agreement with the theoretical value of 2.0.

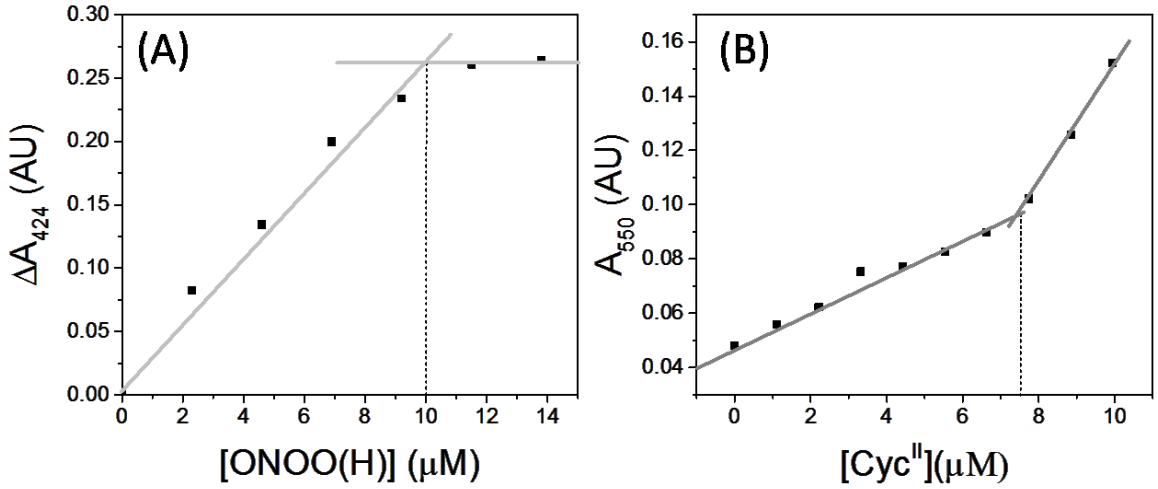

Fig. 3. 4 *Ccp1 is oxidized to CmpdI by ONOO(H).* (A) Aliquots (10 μL) of 200 μM ONOO(H) were added with a gas-tight syringe to 6.0 μM Ccp1 in 1.0 mL of N_2-purged KPi/DTPA in a sealed cuvette and the spectrum recorded at room temperature. Following correction for dilution, subtraction of the Ccp1 spectrum revealed a maximum at 424 nm in the difference spectrum and ΔA424 is plotted vs. [ONOO(H)] added. (B) Ccp1 (4 μM) was reacted with 8 μM ONOO(H) in 1 mL of N_2-purged KPi/ DTPA in a cuvette. The sample was titrated with 210 μM Cyc^{II} in the same buffer by adding 5 μL aliquots to the cuvette with a gas-tight syringe and recording the absorbance at 550 nm and correcting for dilution. The inflection point at 7.5 μM Cyc^{II} corresponds to the titration endpoint and reveals that 1.9 molar equivalents of Cyc^{II} are oxidized by ONOO(H)-oxidized Ccp1, consistent with its identification as CmpdI (Fig. 3. 2).

3.5.2) Nitrite oxidizing activity of CmpdI

As shown in Fig. 3. 3, ONOO(H) reacts with Ccp1 to yield CmpdI, and the NO_2^- formed in this reaction may be converted $^{\bullet}NO_2$ as seen for MPO and LPO (Fig. 3. 1). Thus, we examined the effect of NO_2^- on the decay of CmpdI over 2 h. When present at 0.1 mM, NO_2^- doubles the rate of CmpdI decay (Fig. 3. 5) but this reaction ($k=3x10^2$ M^{-1} s^{-1}) is 10^4-fold slower than the rate of CmpdI reduction by Cyc^{II} ($k=2x10^6$ M^{-1} s^{-1}), suggesting that oxidation of NO_2^- to $^{\bullet}NO_2$ by CmpdI *in vivo* would be negligible. Importantly, oxidation of NO_2^- by MPO-I, which yields significant amounts of $^{\bullet}NO_2$, is also 10^4-fold faster ($k=2x10^6$ M^{-1} s^{-1}, pH 7.0, [163]) than that

estimated here for CmpdI (Fig. 3. 5). Thus, the insignificant reactivity of NO_2^- with CmpdI supports a protective role for Ccp1 against ONOO(H).

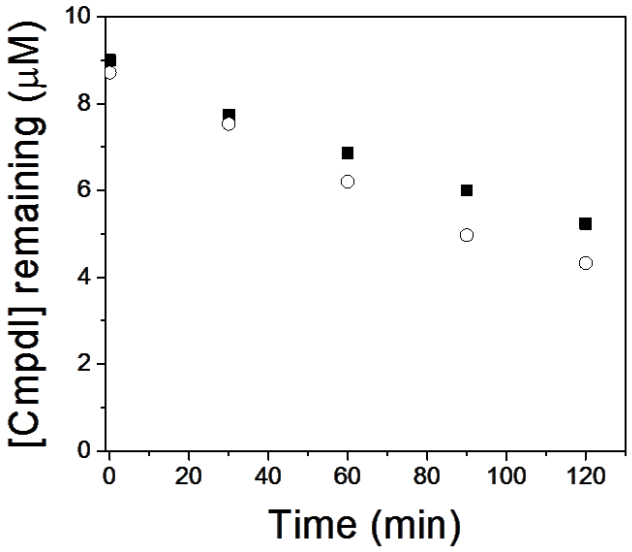

Fig. 3. 5 *NO_2^- at 0.1 mM slightly accelerates the decay of CmpdI.* Ccp1 (11.5 μM) was oxidized to CmpdI with stoichiometric H_2O_2. The decay of CmpdI was monitored at 424 nm in KPi at room temperature in the absence (black squares) and presence (white circles) of 0.1 mM $NaNO_2$ as described under *Materials and methods*. Note that 11.5 μM $NaNO_2$ had no effect on CmpdI decay (data not shown).

3.5.3) Apparent biomolecular rate constants k_2' for the reaction of Ccp1 with ONOO(H) at pH 7.0

Ccp1 does not scavenge bulk ONOO(H) since addition of Ccp1 does not alter the rate of 167 mM ONOO(H) decay on the 20 s timescale (Fig. 3. 6A). This reinforces that the reaction between Ccp1 and ONOO(H) is stoichiometric and not a disproportionation-type reaction as observed for catalase [149]. There are three possible routes for ONOO(H) decay at pH 7.0 in the presence of Ccp1 and CO_2 (Reaction 2). However, the CO_2 dissolved in the phosphate buffer was removed by purging the solution with N_2 for 30–40 min, and the titration was performed in a cuvette fitted with a septum to ensure that the system remained essentially CO_2-free. Therefore, Reaction 2 is assumed to have been eliminated. Thus, only the oxidation of Ccp1 by ONOO(H)

is occurring on the 200 ms timescale. The observed bimolecular rate constants (k_2, M^{-1} s^{-1}) are plotted in Fig. 3. 6B and revealed that k_2 increases and becomes pH independent at pH 6.5. Since the pK_a of ONOO(H) is 6.8 [96], Ccp1 is oxidized by peroxynitrous acid, ONOOH, as observed for MPO, LPO and HRP [146]. The pH-independent k_2 ($M^{-1}s^{-1}$) for Ccp1 reaction with ONOOH is $1.4\pm0.5x10^7$, which is higher than the pH-independent k_2 ($M^{-1}s^{-1}$) values for MPO ($6.2x10^6$), HRP ($6.4x10^5$), LPO ($3.3x10^5$) [146] and selenium glutathione peroxidase ($k=8x10^6$, pH 7.4) [164] but lower than that observed for peroxiredoxin 5 ($k=7x10^7$ $M^{-1}s^{-1}$, pH 7.4) [148]. Moreover, Ccp1 is 10-fold more efficient in metabolizing ONOO(H) than the selenium glutathione peroxidase mimetic ebselen ($k=2x10^6$, pH 7.5) [150]. The highest k_2 for Ccp1 oxidation by ONOO(H) was found at pH 6.5 (Fig. 3. 3A). This pH is below the pK_a of ONOOH [154] and a significant drop in k_2 was observed at pH >7.5 above the pK_a of ONOOH.

Notably, at pH 6.0 Ccp1's ONOO(H)-metabolizing activity drops dramatically (Fig. 3. 6). It is reported that the k_2 for Ccp1 oxidation by H_2O_2 is maximal at pH 7-9 and drops at pH <5.5 [151], which reflects the protonation state of the distal His52 with an apparent pK_a of 5.2 [165]. This might explain in part the drop in Ccp1's reactivity with ONOO(H), but it does not rule out inhibition by binding of NO_2^- to the heme moiety of Ccp1, as reported for other heme proteins such as methemoglobin [166].

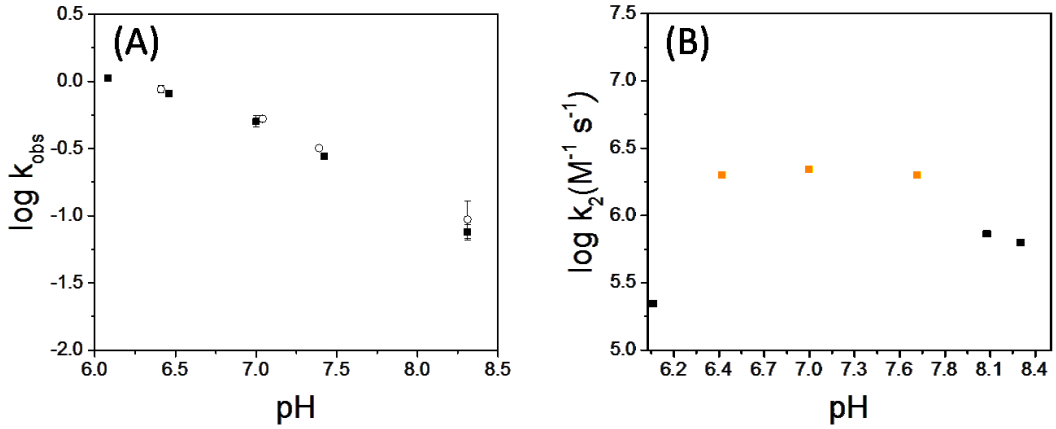

Fig. 3. 6 *Ccp1 and ONOO(H) undergo a rapid stoichiometric reaction that is pH dependent.* (A) Log of the observed rate constants for bulk ONOO(H) decay (k_{obs}, s^{-1}) vs. pH as monitored by stopped-flow absorbance at 302 nm in the presence (empty circles) and absence (solid squares) of 2.5 µM Ccp1. The rate of bulk ONOO(H) decay decreases at high pH but is not catalyzed by Ccp1, confirming that Ccp1 reacts stoichiometrically with ONOO(H). (B) Log of the apparent second-order rate constants (k_2, $M^{-1}s^{-1}$) vs. pH for the reaction between Ccp1 and ONOO(H). The reaction was monitored by stopped-flow absorbance at 408 nm (Ccp1 decay) and 424 nm (CmpdI growth). Log k_2 increases at low pH indicating that Ccp1 reacts with peroxynitrous acid (ONOOH, pK_a=6.8) [96]. Note that the data point at pH 6.03 is considered an outlier as discussed in the text.All reactions were monitored in 0.1 M NaPi at 25 °C as described under *Materials and methods*. Data points are the averages ±SD of triplicate determinations.

3.5.4) Wild-type Ccp1 and Ccp1^{W191F} variants protect yeast cells against SIN-1 challenge

Since Ccp1 is able to efficiently scavenge ONOO(H) *in vitro,* we next addressed whether the production of this enzyme protects yeast cells against ONOO(H) insult. We used SIN-1, a well-established ONOO(H) generator that releases NO and $O_2^{\bullet-}$ with 1-4% efficiency at rates of 1.4 to 3.6 µM/min [167]. As seen in Fig. 3. 7A, the viability of the wild-type strain decreases by only 15% after 2 mM SIN-1 challenge, whereas its isogenic knockout strain *ccp1*Δ displays a 40% reduction in survival following the insult. This suggests a protective role of Ccp1 when cells are challenged with ONOO(H). However, the strain expressing the variant Ccp1^{W191F}

(*ccp1*^{W191F}), which has impaired turnover with Cyc^{II} (Fig. 3. 2; [85]) and hence negligible CCP activity, is fully resistant to challenge with SIN-1, suggesting that the catalytic activity of Ccp1 is not critical in protecting cells against ONOO(H). We previously observed a similar effect after challenging the strains with 0.4 mM exogenous H_2O_2 (Fig. 3. 7B, adapted Fig. 2. 7).

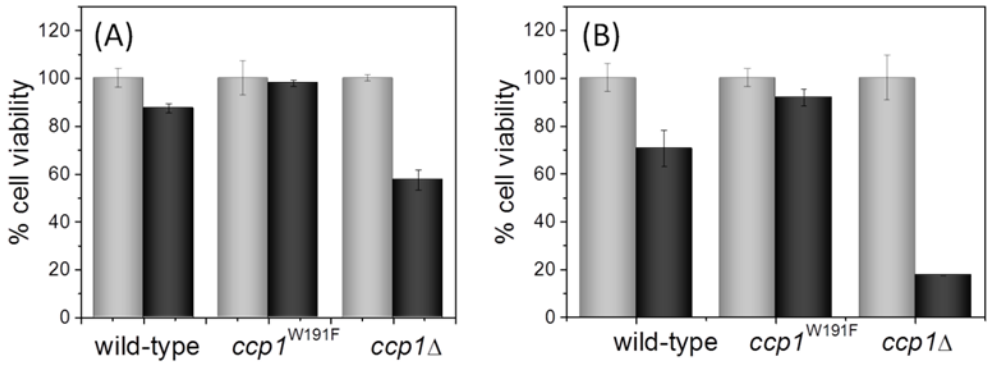

Fig. 3. 7 *Ccp1 and its catalytically impaired variant Ccp1*^{W191F} *protect yeast cells against challenge with the ONOO(H) generator SIN-1 or a bolus of* H_2O_2. Exponentially growing yeast cells expressing wild-type Ccp1, the Ccp1^{W191F} variant (*ccp1*^{W191F}) with negligible CCP activity, and the Ccp1-null mutant (*ccp1*Δ) were adjusted to an OD_{600} of 0.5 and challenged with saline (grey bars), (A) 2 mM SIN-1 (black bars) or (B) a bolus of 0.4 mM H_2O_2 (black bars) for 1.5 h at 30ºC and 225 rpm. Cell viability was measured by counting the total colony forming units (cfu) in treated and untreated (control) cultures. Data are represented as the averages ±SD for three separate cultures.

The *ccp1*^{W191F} strain increased its catalase and peroxiredoxin activities more than the wild-type strain after H_2O_2 challenge (Fig. 2. 7), which indicates a H_2O_2 sensing and signaling function for Ccp1 [20]. Thus, we measured total catalase (Fig. 3. 8A) and peroxiredoxin (Fig. 3. 8B) activities after SIN-1 challenge. These activities were upregulated in the wild-type and *ccp1*^{W191F} strains but not in c*cp1*Δ cells. Catalase activity doubles in wild-type cells after SIN-1 challenge and approaches the levels found in *ccp1*^{W191F} cells (Fig. 3. 8A), which display almost 3-fold higher catalase activity than wild-type cells before challenge (Fig. 3. 8A). An impressive 10-fold induction of peroxiredoxin activity was observed in *ccp1*^{W191F} cells after SIN-1 exposure

(Fig. 3. 8B), which mirrors that seen after challenge with 0.4 mM H_2O_2 (Fig. 3. 8C,D, adapted from Fig. 2. 7). Notably, the constitutively high catalase activity combined with the 10-fold induction of peroxiredoxin activity after SIN-1 challenge can be associated with the high survival of *ccp1*^{W191F} cells on exposure to the ONOO(H)-generator. We conclude that Ccp1 and Ccp1^{W191F} rapidly sense ONOO(H) *in vivo* to amplify the cell's response to this RNS by increasing catalase and peroxiredoxin activities.

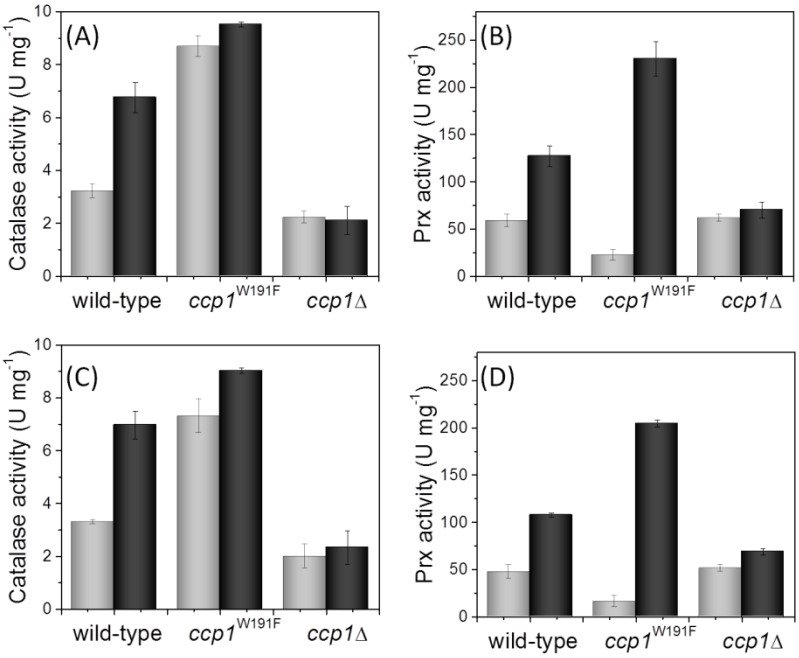

Fig. 3. 8 *Challenge with the ONOO(H) generator SIN-1 or H_2O_2 triggers the same Ccp1-mediated stress response.* Exponentially growing yeast cells expressing wild-type Ccp1, the catalytically impaired Ccp1^{W191F} variant (*ccp1*^{W191F}) and the Ccp1-null mutant (*ccp1*Δ) were treated as described in the legend of Fig. 3. 7. (A) Total catalase and (B) total peroxiredoxin (Prx) activities of cells challenged with saline (grey bars) or 2 mM SIN-1 (black bars). (C) Total catalase and (D) total peroxiredoxin (Prx) activities of cells challenged with saline (grey bars) or a bolus of 0.4 mM H_2O_2 (black bars). Activities were assayed as described under *Materials and methods*. Data points are the averages ±SD for three separate cultures.

3.6) Discussion

Peroxynitrite production from NO and $O_2^{\bullet-}$ during the inflammatory response is of grave concern due to its potential toxicity. It has been shown *in vitro* that ONOO(H) reacts with a variety of biological structures such as lipid membranes and DNA [136], causing lipid peroxidation, and DNA lesions and mutations. Reaction of ONOO(H) with tyrosine residues in proteins to form 3-nitrotyrosine is also of concern since extensive protein nitration was observed around macrophages and neutrophils in lung specimens from humans with respiratory distress syndrome or pneumonia [168]. During normal metabolism, small amounts of ONOO(H) are generated but it has been questioned whether this could promote significant damage since ONOO(H) has a short half-life due to its relatively rapid isomerization to NO_3^- ($k=0.26\ s^{-1}$, 25 °C and pH 7.4) [136]. However, it has been demonstrated that chronic exposure to low ONOO(H) levels can promote significant cellular damage over time [168, 169]. Thus, ONOO(H) toxicity is of interest not only under pathologic conditions or after acute exposure, but also during aging and in aging-related diseases [142, 143, 145]. Given the growing appreciation for ONOO(H) toxicity, the search for biological ONOO(H) scavengers has begun [146, 148, 149, 154, 164]. Heme peroxidases, including MPO and LPO possess efficient ONOO(H)-reductase activity, but these enzymes generate the potentially toxic product $^{\bullet}NO_2$ [146]. Cellular scavengers of ONOO(H) such as peroxiredoxin, glutathione peroxidase and catalase have been reported to protect cells against nitrosative stress by scavenging ONOOH without $^{\bullet}NO_2$ generation. However, to the best of our knowledge, no heme peroxidase that protects cells against ONOO(H) has been reported.

In this work, we provide compelling evidence that Ccp1 is an efficient ONOO(H) scavenger *in vitro* and a sensor of this RNS *in vivo.* The titration of Ccp1 with ONOO(H) yields

a species with a spectrum identical to that of CmpdI formed on reaction with H_2O_2 (Fig. 3. 3). Furthermore, two equivalents of Cyc^{II} convert the ONOO(H)-Ccp1 reaction product to resting Ccp1 so we conclude that ONOO(H) indeed oxidizes Ccp1 to CmpdI. Supporting evidence that CmpdI is indeed formed comes from an inspection of its charge-transfer bands. The ratio of the α (560 nm) to β band (530 nm) for CmpdI is 1.13 whereas for CmpdII it drops to 1.04 [161]. We found a ratio of 1.14 for the Ccp1-ONOO(H) reaction product, identifying it as CmpdI. A plot of ΔA_{424} vs [ONOO(H)] (Fig. 3. 4A), revealed that 1.6 mol of ONOO(H) are necessary to convert 1.0 mol of Ccp1 to CmpdI instead of the expected 1:1 ratio. We speculate that extra ONOO(H) is required to fully oxidize Ccp1 due to its quick isomerization to NO_3^- [136] under the conditions employed here (pH 7.0, room temperature). Thus, not all of the ONOO(H) added to Ccp1 will be available to form CmpdI and the 1.6 molar ratio is acceptable.

The stopped-flow rate data in Fig. 3. 6 show that k_2 ($M^{-1}s^{-1}$) for the reaction of Ccp1 with ONOO(H) at pH 7.0 is $1.4\pm0.5x10^7$. Surprisingly, this is only 2-fold smaller than k_2 for the reaction with H_2O_2 ($4.5x10^7$) [151], but double the k_2 for the reaction of ONOO(H) with MPO ($6.2x10^6$), and ~20 and ~40-fold higher than those for HRP ($6.4x10^5$, pH 7.4) and LPO ($3.3x10^5$, pH 7.2) with ONOO(H), respectively [146]. Thus, Ccp1 appears to be a highly efficient ONOO(H) scavenger, having a k_2 that is second only to that reported for peroxiredoxin 5 ($7x10^7$, pH 7.4) [148]. Furthermore, unlike MPO and LPO, Ccp1 exhibits negligible NO_2^- oxidizing activity (Fig. 3. 1), so we can assume that it scavenges ONOO(H) to protect cells. The *CCP1* promoter has been shown to be responsive to ONOO(H) [82], which provides indirect evidence that Ccp1 plays a role in protecting cells against ONOO(H) insult.

We find that, although Ccp1 rapidly reacts with ONOO(H) *in vitro*, it may not scavenge significant amounts of this RNS *in vivo.* Production of $Ccp1^{W191F}$, which is catalytically

impaired, provides more protection than wild-type Ccp1 when cells are challenged with the ONOO(H) generator SIN-1 (Fig. 3. 7A). We have previously shown that Ccp1 or Ccp1^{W191F} production provide protection against exogenous H_2O_2 by increasing catalase and peroxiredoxin activities (Fig. 3. 8B). Also, Ccp1^{W191F} appears to be a more persistent sensor than Ccp1 (Fig. 3. 8C,D), presumably due to the slow deactivation of its CmpdI by Cyc^{II} (Fig. 3. 2, step b). A similar effect to that induced by H_2O_2 was observed when the Ccp1- and Ccp1^{W191F}-expressing strains were challenged with SIN-1 (Fig. 3. 8A,B), which reinforces the role of CmpdI as the peroxide signaling species that increases catalase and peroxiredoxin activity.

CmpdI-mediated peroxide signaling in the mitochondria may be linked to the Yap1/Skn7-dependent peroxide signaling in the cytosol that increases production of cytosolic catalase T (Ctt1) and Tsa1 [43]. Furthermore, Yap1 deletion results in hypersensitivity to nitrosative stress generated by GSNO and sodium nitroprusside [170], suggesting that yeast responds to RNS and H_2O_2 by a common pathway. The high Ccp1 reactivity towards ONOO(H) (Fig. 3. 6) and Ccp1's signaling function when cells are challenged with SIN-1 (Fig. 3. 7) suggest that cells may detoxify RNS via ONOO(H) formation. In fact, conversion of NO and $O_2^{\bullet-}$ to ONOO(H) would benefit cells by allowing them to simultaneously detoxify both radicals via peroxide stress response. Notably, the ~10^{10} M^{-1} s^{-1} rate of the $O_2^{\bullet-}$ and NO reaction [96] is comparable to the rate of $O_2^{\bullet-}$ dismutation catalyzed by Sod1 and Sod2 (10^9-10^{10} M^{-1} s^{-1}, [24, 25]), thus allowing $O_2^{\bullet-}$ to detoxify NO via ONOO(H) formation using cell's peroxide scavenging system.

Interestingly, 2 mM SIN-1 is less toxic than 0.4 mM H_2O_2 (Fig. 3. 7A,B) but both compounds induce similar increases in catalase and Prx activity (Fig. 3. 8). Considering the steady-state rate of SIN-1 decay to ONOO(H) (1.4 to 3.6 μM/min, [167]), the maximum

concentration of ONOO(H) generated by 2 mM SIN-1 at 4% efficiency after 1.5 h would be ~0.3 mM. We observed a higher induction of catalase activity in wild-type BY4741 cells following challenge with a bolus of 0.2 mM vs 0.4 mM H_2O_2, and reduction of catalase activity as the H_2O_2 concentration is increased (See Chapter 5, Fig. 5. 2) [171]. Thus, we conclude that the relatively low toxicity of SIN-1 to *ccp1*Δ cells compared to bolus H_2O_2 is associated with the low steady-state level of ONOO(H) within the cell, which nonetheless effectively induces catalase activity.

In summary, we have identified Ccp1 as the first heme peroxidase that protects cells against ONOO(H) since its fast reaction with this peroxide is not followed by the generation of toxic $^{\bullet}NO_2$ as in other heme peroxidases (Fig. 3. 1). However, Ccp1 was designed to act as a ONOO(H) sensor *in vivo*, and like the thiol-based H_2O_2 sensors such as glutathione peroxidase 3 [70], Ccp1 reacts rapidly with H_2O_2 and ONOO(H). Furthermore, it reacts with a small electron-transfer protein, Cyc^{II}, its reducing substrate (Fig. 3. 2) to deactivate the signaling, analogous to the deactivation of oxidized glutathione peroxidase by its thiol disulfide reducing substrate thioredoxin [49]. Although NO signaling and sensing have been extensively described [166], little is known about the signaling of very reactive molecules such as $O_2^{\bullet-}$ and ONOO(H). In fact, it is claimed that unlike H_2O_2 [79] and NO [166], $O_2^{\bullet-}$ and ONOO(H) lack sufficient specificity in their reactions to act as second messengers [79]. However, we provide compelling evidence here that ONOO(H) triggers the same stress response as H_2O_2 and both are mediated via the heme peroxidase sensor, Ccp1. Additionally, Ccp1 scavenging of ONOO(H) to generate NO_2^- would protect the bioactivity of NO and stores it in a less toxic reactive form [172].

Chapter 4: Ccp1 and yeast lifespan

4.1) Preface

The work presented in Chapter 4 corresponds to the following manuscript: Martins D, Titorenko VI, English AM (2014). **Cells with impaired mitochondrial H_2O_2 sensing generate less $^{\bullet}OH$ radicals and live longer**. Antioxidants and Redox Signaling, *in press,* doi:10.1089/ars.2013.5575. I performed all of the experiments and interpreted the results. I also wrote the first draft of the manuscript and prepared the revisions. Dr. English contributed helpful discussions, data analysis and revisions of the manuscript. Dr. Titorenko contributed with helpful discussions, revisions of the manuscript and also provided the yeast anti-Aco1 antibody. The permission for using the manuscript's content in this thesis was granted by Mrs. Karen Ballen, manager of copyright permissions for Antioxidants and Redox Signaling (Liebertpub).

4.2) Abstract of the manuscript

AIM: Mitochondria are major sites of reactive oxygen species (ROS) generation and adaptive mitochondrial ROS signaling extends longevity. We aim to link the genetic manipulation of mitochondrial H_2O_2 sensing in live cells to mechanisms driving aging in the model organism, *Saccharomyces cerevisiae*. To this end, we compare *in vivo* ROS ($O_2^{\bullet-}$, H_2O_2 and $^{\bullet}OH$) accumulation, antioxidant enzyme activities, labile iron levels, GSH depletion and protein oxidative damage during the chronological aging of three yeast strains: *ccp1*Δ that does not produce the mitochondrial H_2O_2 sensor protein, cytochrome c peroxidase (Ccp1); *ccp1*^{W191F} that produces a hyperactive variant of this sensor protein (Ccp1^{W191F}), and the isogenic wild-type strain. **RESULTS:** Young *ccp1*Δ cells accumulate mitochondrial high H_2O_2 but low superoxide ($O_2^{\bullet-}$) levels because they possess elevated manganese superoxide dismutase (Sod2) activity. These cells exhibit stable aconitase activity and contain low amounts of labile iron or hydroxyl

radicals ($^{\bullet}$OH). Furthermore, they undergo late glutathione (GSH) depletion, less mitochondrial protein oxidative damage and live longer than wild-type cells. In contrast, young *ccp1*^{W191F}cells accumulate little H_2O_2, possess depressed Sod2 activity allowing their $O_2^{\bullet-}$ level to spike and deactivate aconitase, which ultimately leads to greater mitochondrial oxidative damage, early GSH depletion, and a shorter lifespan than wild-type cells. **INNOVATION:** Modulation of mitochondrial H_2O_2 sensing offers a novel interventional approach to alter mitochondrial H_2O_2 levels in live cells and probe the pro- vs anti-aging effects of ROS. **CONCLUSION:** The strength of mitochondrial H_2O_2 sensing modulates adaptive mitochondrial ROS signaling and hence lifespan.

4.3) Introduction

High levels of mitochondrially generated ROS are assumed to promote cell damage and accelerate aging [6, 7]. In contrast, mildly elevated ROS induce a mitohormesis effect [16] that increases the expression of stress-related proteins and extends lifespan via adaptive mitochondrial ROS signaling [17-19, 173]. Although the dual effects of ROS on longevity have been reported and their cross-talk with aging-regulating routes such as the target of rapamycin-serine threonine kinase Sch9 (Tor/Sch9) pathway has been suggested [174], little is understood about how ROS production is synchronized to modulate aging. Presumably, the effects of a ROS on aging depend on its chemical nature as well as its concentration. For example, H_2O_2 is a diffusible mediator that signals a stress response [70] but activated thiols or redox-active metals are required to implement this beneficial biological action [79]. Although less diffusible and not very reactive, $O_2^{\bullet-}$ efficiently removes iron from the iron-sulfur (4Fe4S) catalytic sites of dehydratases such as aconitase to catalyze $^{\bullet}$OH formation from H_2O_2 [175, 176]. However, $O_2^{\bullet-}$ has a short half-life in cells since it spontaneously dismutates to H_2O_2 [25] and cells possess

many superoxide dismutases to catalyze this reaction [177]. The $^{\bullet}OH$ radical is highly reactive and indiscriminately attacks cellular components and organelles at diffusion-controlled rates [9].

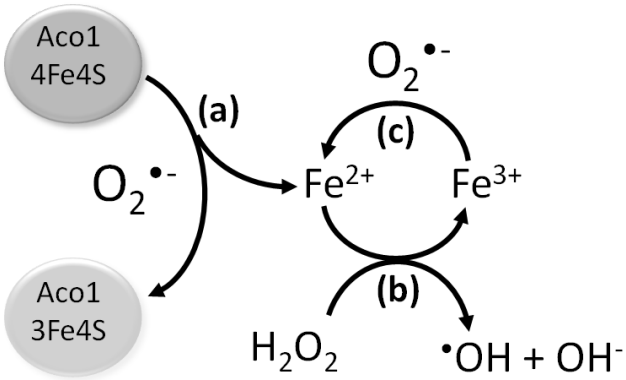

Fig. 4. 1 *The proposed mechanism of $^{\bullet}OH$ generation in mitochondria.* In reaction *a*, $O_2^{\bullet-}$ donates an electron to the 4Fe4S catalytic site of aconitase (Aco1) and the labilized Fe^{2+} is released to give the catalytically inactive 3Fe4S enzyme. This provides Fe^{2+} to catalyze reaction *b* and the Fe^{2+} catalyst is regenerated by $O_2^{\bullet-}$ in reaction *c*. The generation of $^{\bullet}OH$ from H_2O_2 and $O_2^{\bullet-}$ (the Haber-Weiss reaction) is very slow in the absence of the Fe^{2+} catalyst. Thus, formation of the catalyst (reaction *a* and reaction *c*) will limit $^{\bullet}OH$ formation when H_2O_2 is abundant. When H_2O_2 levels are depressed and $O_2^{\bullet-}$ is abundant, $^{\bullet}OH$ formation will be limited by reaction *b*.

Synchronization between $O_2^{\bullet-}$-mediated removal of iron from aconitase and the Fenton reaction involving H_2O_2 reduction is required for $^{\bullet}OH$ generation (Fig. 4. 1). Thus, limiting H_2O_2 and/or $O_2^{\bullet-}$ accumulation should control $^{\bullet}OH$ production and be protective to cells. Given its chemical properties, H_2O_2 is considered to be the most suitable ROS for signaling longevity extension and oxidative stress [79]. Moreover, enhanced H_2O_2 accumulation and signaling in yeast strains deleted for catalase A (*CTA1*) and/or T (*CTT1*) are linked to extended their chronological lifespans relative to the wild-type strain [19]. H_2O_2 signaling activates manganese superoxide dismutase (Sod2) and consequently the catalase-null mutants exhibit low $O_2^{\bullet-}$ levels [19]. Very recently, we described a mutant yeast strain (*ccp1*Δ) that also accumulates high H_2O_2

levels [20]. Deletion of the *CCP1* gene encoding cytochrome c peroxidase (Ccp1) reduces catalase A (Cta1) activity and increases manganese superoxide dismutase (Sod2) activity to significantly lower the $O_2^{\bullet-}/H_2O_2$ balance relative to that in wild-type cells [20]. Since the rapid reaction of H_2O_2 with its heme triggers these cellular responses, Ccp1 functions as a heme-based mitochondrial H_2O_2 sensor and signaling molecule in yeast [20]. Importantly, elevated H_2O_2 in *CCP1*-null cells (*ccp1*Δ) is not simply related to the absence of CCP activity since the isogenic mutant strain (*ccp1*^{W191F}) expressing the catalytically inactive Ccp1^{W191F} protein variant accumulates *less* H_2O_2 but more $O_2^{\bullet-}$ than wild-type cells. Although essentially devoid of CCP activity [85], Ccp1^{W191F} is a hyperactive H_2O_2 sensor and *ccp1*^{W191F} cells exhibit higher Cta1 activity than wild-type cells [20].

The *ccp1*Δ and *ccp1*^{W191F} mutant strains together with their isogenic wild-type strain provide a unique opportunity to investigate how changes in mitochondrial H_2O_2 signaling influence aging of differentiated eukaryotic cells. Since baker's yeast is a popular and robust model system for studying aging in postmitotic eukaryotic cells [18, 19, 64, 67, 68, 174, 178, 179], we determined how the chronological lifespan of *ccp1*Δ, *ccp1*^{W191F} and wild-type yeast is influenced by the strength of their mitochondrial H_2O_2 signaling. We also compared the three strains regarding key factors that are correlated with cell fitness: aconitase activity, $^{\bullet}OH$ levels, mitochondrial protein carbonylation, labile, and GSH levels. Our results reveal that hyperactive mitochondrial H_2O_2 signaling by Ccp1^{W191F} depresses *in vivo* H_2O_2 accumulation and the ROS adaptive response in exponentially growing and early stationary phase cells, increases aconitase inactivation, $^{\bullet}OH$ production *in vivo*, mitochondrial labile iron, and protein oxidative damage. These deleterious events lower GSH levels and shorten lifespan. In contrast, impairing mitochondrial H_2O_2 sensing by deleting *CCP1* allows H_2O_2 to rise [20], which depresses *in vivo*

$O_2^{\bullet-}$ accumulation in late exponential and early stationary phase cells and extends lifespan, consistent with the results obtained for the catalase knockout strains [19] and for yeast subjected to calorie restriction [18, 19]. Importantly, we provide the first systematic analysis identifying the intracellular $O_2^{\bullet-}/H_2O_2$ balance in early life as a critical parameter in shaping the anti- vs pro-aging effects of ROS. The potential implications of controlling the $O_2^{\bullet-}/H_2O_2$ balance in the lifespan of higher eukaryotes lifespan is also discussed.

4.4) Materials and methods

4.4.1) Yeast strains, media and growth conditions

The *Saccharomyces cerevisiae* strains used are listed in Table 4. 1. The wild-type Ccp1-expressing strain and the Ccp1 null mutant (*ccp1*Δ) were purchased from EUROSCARF. The mutant strain (*ccp1*^{W191F}) chromosomally expressing the gene encoding the catalytically impaired Ccp1^{W191F} protein variant was constructed as described previously [20]. Yeast cells were grown in YPD liquid medium (1% yeast extract, 2% peptone, and 2% glucose) with a medium-to-air ratio of 1:5. Incubations were carried out at 30 °C and 225 rpm at an initial OD_{600} of 0.01. The spent medium was replaced with 0.85% (wt/v) NaCl solution after 72 h (3 days) to maximize lifespan and prevent re-growth in stationary phase [69].

Table 4. 1 *S. cerevisiae* strains used in this study

Strain, plasmid or primer	Description	Reference
wild-type BY4741 strain	*MATa his3Δ1 leu2Δ0 met15Δ0 ura3Δ0*	EUROSCARF
*ccp1*Δ strain	*ccp1::KAN4MX*	EUROSCARF
ccp1^{W191F} strain	BY4741 cells with *ccp1::*m*ccp1*^{W191F}	[20]

4.4.2) Aconitase activity assay

Cells were lysed and total soluble protein extracts were prepared as previously described [20, 83]. Protein concentrations were determined by the Bradford method [104] using bovine serum albumin (BSA) as a standard. Aconitase activity was monitored by following NAD^+ reduction at 340 nm in a coupled reaction with citrate and isocitrate dehydrogenase [180]. The assay solution contained 5 mM sodium citrate, 0.2 mM NAD^+, 0.6 mM $MnCl_2$, 2 units of isocitrate dehydrogenase in 50 mM Tris-Cl buffer (pH 7.4). To determine the extent of reversible aconitase inactivation, the protein extracts were also assayed after pre-incubation with 1 mM DTT and 0.2 mM $FeSO_4$ for 20 min at 4 ºC. Aconitase activity was initiated by adding 100 µL of assay solution to 5-20 µL of extract in a 96-well plate reader (TecanSpectraFluor Plus). One unit of aconitase activity produces 1 nmol of NADH/min/mg protein [180].

4.4.3) Aconitase 1 (Aco1) protein levels

Rabbit anti-Aco1 serum was a kind gift from Prof. Ronald A. Butow (University of Texas, Southern Medical Center at Dallas). All procedures were performed at room temperature unless otherwise indicated. Soluble protein extracts were fractionated by SDS-PAGE under reducing conditions in 6% stacking and 12% resolving gels for 1 h at 150 V. The electrophoresed proteins were transferred to a polyvinylidene fluoride (PVDF, BioRad) membrane for 3 h using a constant current of 100 mA, the membranes were blocked with 5% (w/v) skim milk in TBST (50 mM Tris, 150 mM NaCl and 0.05% v/v Tween 20, pH 7.6) for 1 h, incubated with rabbit anti-Aco1 serum (1:10,000 dilution) for 12 h, washed 3 times with TBST, and incubated with goat anti-rabbit HRP-conjugated secondary antibody (1:20,000, Biorad) for 1.5 h. Anti-Aco1 reactive bands were visualized using the Super Signal West Pico Enhanced Chemiluminscence (ECL) kit from Thermo Fisher in an AlphaImager (Alpha Innotech). After immunodetection membranes

were stained with Commassie (ICN Biomedicals), and the integrated intensity of the Aco1 bands was normalized by the sum of the integrated intensity of all Commassie bands in the same lane as loading controls [109]. Each lane contained 5-12.5 μg of total protein since the Aco1 signal (2 min exposure) was linear over 3-7.5 μg of total protein in 3-day cells, which exhibited the highest Aco1 levels (Fig. 4. 2D).

4.4.4) FACS analysis of intracellular ROS and autofluorescence

Intracellular H_2O_2 and $O_2^{\bullet-}$ levels were measured *in vivo* using dihydrorhodamine 123 (DHR) and dihydroethidine (DHE), respectively, as previously described [20], and measurements were extended to 89 days. Intracellular $^{\bullet}OH$ levels were detected in living cells stained with 3'-(p-hydroxyphenyl) fluorescein (HPF), which specifically detects very reactive ROS such as $^{\bullet}OH$ (Appendix 4. 1) and does not cross-react with H_2O_2 or $O_2^{\bullet-}$ [181].

HPF staining was performed following the literature procedure [181] with slight modifications. Briefly, 10^7 cells were harvested at 2,000xg for 10 min, incubated for 60 min with 5 μM HPF in PBS (10 mM sodium phosphate and 150 mM NaCl, pH 7.0) at 30 ºC, re-harvested, and diluted in PBS to 10^6 cells/mL. HPF-loaded and unstained cells were excited with a 488-nm argon laser in a Becton Dickinson (BD) FACScan flow cytometer, and the fluorescence was monitored using a 530/30 nm bandpass filter. The fluorescence intensity distributions of cells stained with HPF are shown in Fig. S4. 1 and Fig. S4. 2. Experiments were performed on three independent cultures and 10,000 cells were analyzed per sample. To probe for HPF loading, HPF-stained cells were washed twice with PBS, lysed using glass beads as previously described [20, 83], and centrifuged at 10,000xg. The HPF in the supernatants was oxidized to fluorescein and detected by fluorescence in a Cary Eclipse fluorometer (Agilent) as described in the legend

of Fig. S4. 3. As an indicator of nonspecific oxidative damage, the autofluorescence of unstained cells [182] was measured by flow cytometry with a 620 nm longpass filter.

4.4.5) Subcellular fractionation

Subcellular compartments were separated as described previously [20, 103]. Cells were grown in 50 mL of YPD medium at 30 °C, harvested and washed twice with aqueous 0.85% NaCl. The cell pellets were resuspended in 10 mL of pre-warmed 100 mM Tris-H_2SO_4 (pH 9.4) with 10 mM DTT, incubated for 10 min at 30 °C and 80 rpm, harvested, washed twice with 10 mL of 10 mM potassium phosphate buffer (pH 7.4) containing 1.2 M sorbitol, and treated for 40 min with 3 mg of zymolyase 20T/g of wet cells at 30 ºC. The resulting spheroplasts were washed twice with 10 mL of the same buffer and resuspended in 5 mL of 10 mM Tris-HCl (pH 7.4) containing 0.6 M sorbitol, 1 mM EDTA, 1 mM PMSF and Complete™ Protease Inhibitor Cocktail. Spheroplasts at 4 ºC were disrupted by 15 strokes of a glass-Teflon homogenizer, the homogenates were centrifuged at 2,000xg and the supernatants, which correspond to the denucleated lysates (S2 fractions), were collected. The S2 fractions were further centrifuged at 10,000xg for 15 min at 4 °C, and the mitochondria-depleted supernatants (S10 fractions) were separated from the mitochondria-enriched pellets (P10 fractions). For determining labile iron in P10 fractions, two modifications were done in the original procedure. First, the cells were not incubated with 100 mM Tris-H_2SO_4 (pH 9.4) with 10 mM DTT. Second, the homogenization of spheroplasts was carried out in 10 mM KPi (pH 7.4) containing 0.6 M sorbitol.

4.4.6) Mitochondrial labile and total iron analyses

The pool of labile iron in the mitochondria-enriched fractions (P10) was measured using the chelator ferrozine, which coordinates selectively with Fe^{2+} to form a complex with a strong absorbance between 500 and 600 nm, with maximum a at 562 nm (ε_{562}=27.9 mM^{-1} cm^{-1}) [183,

184]. Briefly, P10 fractions were suspended in 100 mM KPi buffer (pH 7.0) and diluted 10-fold in a solution containing 1 mM ferrozine in MilliQ water. The variation in absorbance at 550 nm (ΔA550 nm) over time was determined using a 96-well plate reader (TecanSpectraFluor Plus) and the total amount of $[Fe(ferrozine)_3]^{4-}$ complex formed after 50 min per mg of P10 protein used in the assay (nmol/min mg protein) was normalized against the average of rates for wild-type cells at each data-point. For total iron measurements, S2 and P10 fractions were first digested in 40% metal trace HNO_3 (v/v) for 16 h at 20 °C, diluted 4-fold and injected into an Agilent 7500ce inductively coupled plasma mass spectrometer (ICP/MS). The parameters used in the run were radio frequency (RF) power = 1550 W; RF matching= 1.7 V; octapole RF= 160 V; ion lenses extract 2= -110 V; helium gas flow= 4 mL/min. The total iron content was normalized by mg of protein in each sample (nmol/mg protein).

4.4.7) Protein oxidative damage

Protein carbonylation, a measure of protein oxidative damage, was determined by reaction with 2,4-dinitrophenylhydrazine (DNPH) as described elsewhere [185] with minor modifications. Briefly, the S2, S10 and P10 fractions at 1-2 mg protein/mL were incubated in diluted aqueous HCl (pH 2) containing 30 mM *n*-octylglucoside and 10 mM DNPH at 22 ºC for 1 h. Then 500 µL aliquots were mixed with 500 µL of 1:1 (v/v) ethyl acetate:ethanol to precipitate the proteins, the samples were centrifuged at 10,000xg for 10 min, and the pellets were washed twice with 1:1 ethylacetate:ethanol to remove unreacted DNPH. After suspending the pellets in PBS (pH 7.0), absorbances were measured at 355 nm and 390 nm, and the carbonyl content (nmol/mg protein) was calculated from $(A_{355}-A_{390})DF/45.45[Prot]$, where DF is the

dilution factor and [Prot] the total protein concentration in mg/mL. Samples treated in the same manner without DNPH were used as negative controls.

4.4.8) GSH/GSSG measurements

Total GSH and GSSG were measured following previously described procedures [186] with slight modification. Briefly, protein soluble extracts, prepared as described previously [20, 83], were incubated for 10 min at 4 °C with 10% TCA (v/v). The proteins were precipitated by centrifuging the solutions at 10,000xg for 10 min at 4 °C. The supernatants were collected and 20 µL aliquots were measured for total GSH in an assay solution containing 0.25 mM NADPH, 0.7 mM DTNB, 1 µg/mL glutathione reductase diluted in 0.1 M Tris-HCl and 5 mM EDTA (pH 8). The increase in absorbance at 412 nm over time due to formation of TNB^{2-} via S-S exchange with GSH [187] was measured using a 96-well plate reader (TecanSpectraFluor Plus). For GSSG measurement, free GSH was initially quenched using 10 mM 4-VP in 0.1 M Tris-HCl and 5 mM EDTA (pH 8) for 1 h at 20 °C in the dark and the samples were mixed with the assay solution as described above. The concentrations of total GSH and GSSG were determined using a calibration curve using purified GSH as standard.

4.4.9) Chronological lifespan

Survival in stationary-phase defines the chronological lifespan reported here [18]. Cells were grown in liquid YPD medium as described in Section 4.4.1 and exchanged into 0.85% NaCl on day 3. Since cells enter a quiescent state in 0.85% NaCl [69], stationary-phase begins on day 4 under our experimental conditions. At selected time-points, 100 µL aliquots of stationary-phase cells were serially diluted into aqueous 0.85% NaCl, plated onto YPD-agar, incubated at 30 ºC for 2 days, and the total colony forming units (cfu) were counted to monitor cell survival.

The chronological lifespan corresponds to the number of days in stationary phase required to reach a 2-log drop in cfu.

4.4.10) Statistical analyses

Protein carbonyl content and median fluorescence or autofluorescence were measured over time for three separate cultures. Average values for the mutant strains are normalized to the average wild-type values such that plots reveal fold-increase or fold-decrease relative to wild-type. Duplicate or triplicate measurements of aconitase activity and chronological lifespan were carried out on three separate cultures. Statistical analyses were performed using Student's *t*-test in Origin 9.0 software and probabilities lower than 5% (P <0.05) are considered significant.

4.5) Results

4.5.1) Aconitase activity is higher in post-diauxic and early stationary phase *ccp1Δ* cells with impaired mitochondrial H_2O_2 sensing

Although *ccp1*^{W191F} cells initially display the highest aconitase activity during exponential growth (0.5 days, Fig. 4. 2), this drops to wild-type levels by day 1, and only weakly increases after the diauxic shift (day 3) when cells are respiring [18]. Aconitase activity rises sharply in the null mutant and is significantly higher in this strain than in wild-type and *ccp1*^{W191F} cells by day 3 (Fig. 4. 2A-C). It is well-documented that $O_2^{\bullet-}$ efficiently removes labile iron from aconitase's catalytic 4Fe4S cluster [175, 176], and activity can be restored on reconstitution of the enzyme with ferrous iron (Fe^{2+}) and dithiothreitol (DTT). Notably, *ccp1*^{W191F} cells undergo a large spike in $O_2^{\bullet-}$ accumulation around day 2 (Fig. S4. 4) [20] leading to a high level (~65-90%) of reversibly inactivated aconitase (Fig. 4. 2B). In sharp contrast, the aconitase activity of *ccp1*Δ cells, which accumulate little $O_2^{\bullet-}$ (Fig. S4. 4) [20], increases by only ~10-20% on reconstitution while ~40-60% activity is restored in wild-type cells (Fig. 4. 2A-C).

Hence, $O_2^{\bullet-}$-mediated inactivation of aconitase by iron is significantly inhibited by deleting *CCP1* and impairing mitochondrial H_2O_2 sensing. However, aconitase protein levels are comparable in the three strains and exhibit a similar decline with age (Fig. 4. 2D), which explains in large part the overall decline in aconitase activity in early stationary phase (days 3 to 15) even following reconstitution (Fig. 4. 2C).

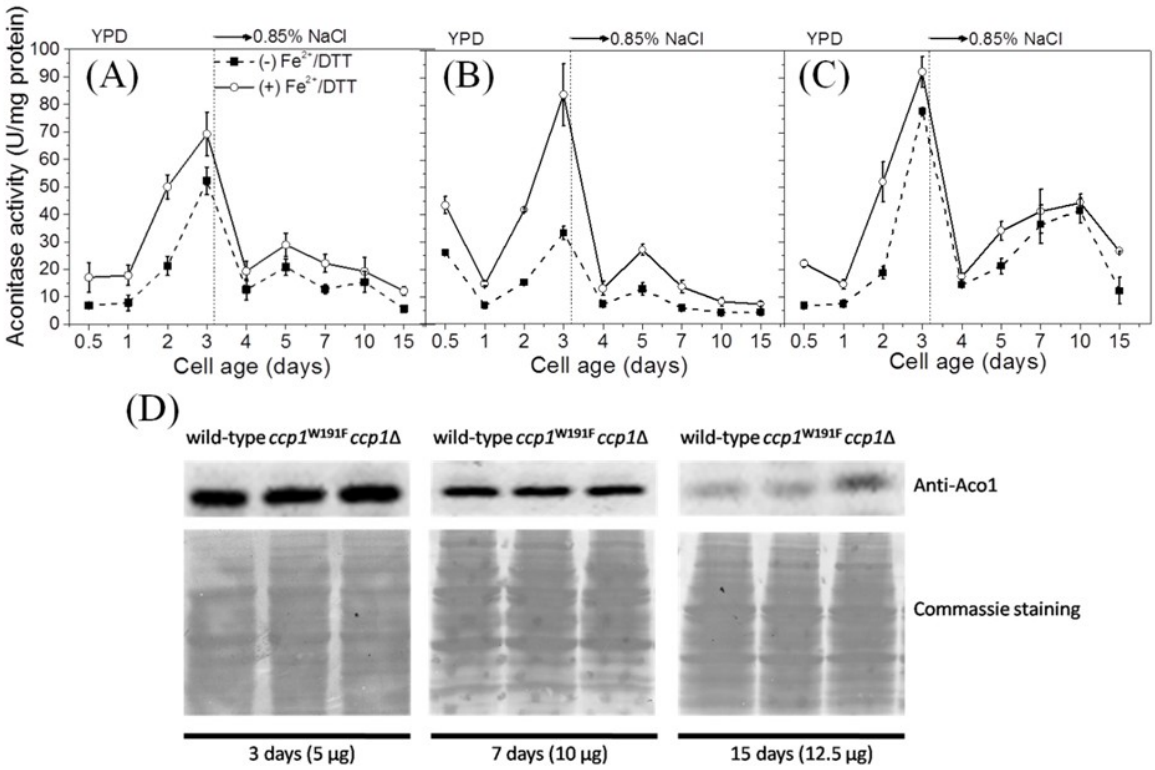

Fig. 4. 2 *Aconitase activity peaks in respiring ccp1Δ cells but Aco1 protein levels are comparable in the wild-type, ccp1^{W191F} and ccp1Δ strains.* Soluble protein extracts from (A) wild-type, (B) *ccp1*^{W191F} and (C) *ccp1*Δ cells were assayed for aconitase activity before (solid squares) and after reconstitution (open circles) with Fe^{2+} and DTT as described under *Materials and methods*. Yeast cells were grown at 30 °C with 225 rpm stirring and changed to 0.85% NaCl at the vertical dotted line. One unit of aconitase activity produces 1 nmol of NADH/min/mg total protein in a coupled reaction with citrate and isocitrate dehydrogenase. Data points are the average activities of three independent cultures±SD and the lines were added as a visualization aid. (D) Western blot analysis using anti-Aco1 antibody of Aco1 protein levels in soluble protein extracts from wild-type, *ccp1*^{W191F}, and *ccp1*Δ cells at 3, 7, and 15 days. Membranes were stained with Commassie after probing for Aco1 and the sum of Commassie band intensities in each lane serves as a loading control [109]. See *Materials and methods* for further details.

4.5.2) Lower •OH levels are detected in live *ccp1*Δ cells with impaired mitochondrial H_2O_2 sensing

Since iron released from aconitase is available to catalyze •OH formation from H_2O_2, we measured intracellular •OH levels by 3'-(*p*-hydroxyphenyl)fluorescein (HPF) staining [181] *in vivo* (Fig. 4. 3). HPF loading of the three strains was comparable (Fig. S4. 3), hence the variation in HPF fluorescence reflects the relative amounts of •OH generated in the cells. Interestingly, the FACS histograms reveal a bimodal distribution of •OH levels in *ccp1*Δ cells after the diauxic shift at day 2 (Fig. 4. 3A; Fig. S4. 1; Fig. S4. 2). Why the distribution is bimodal is not obvious at present, but this indicates that a large population of *ccp1*Δ cells limit •OH formation more effectively than wild-type or *ccp1*^{W191F} cells between 2 and 25 days (Fig. 4. 3A). In fact, the median •OH levels in *ccp1*Δ cells after the diauxic shift are about half those of wild-type cells (Fig. 4. 3C) and do not oscillate around wild-type levels until late stationary phase after day 30 (Fig. 4. 3D). In contrast, young *ccp1*^{W191F} cells possess wild-type •OH levels (Fig. 4. 3A,C) but these spike above wild-type values after 30 days (Fig. 4. 3D) as the viability of the mutant is waning.

4.5.3) *ccp1*Δ cells possess a low mitochondrial pool of labile iron consistent with their high aconitase activity

Significantly less •OH is generated in live *ccp1*Δ cells compared to *ccp1*^{W191F} or wild-type cells (Fig. 4. 3). Bearing in mind the mechanism of intracellular •OH generation (Fig. 4. 1), we asked if less labile iron (i.e., iron complexed to low-molecular-weight ligands or loosely bound to proteins) was available to catalyze the Fenton reaction (step b in Fig. 4. 1) in the mitochondria of the null mutant. On addition of the Fe^{2+}-selective chelator, ferrozine [183, 184], to the P10 fractions, the absorbance at 550 nm increased within the mixing time, indicating the

presence of highly labile Fe^{2+} (Fig. 4. 4B). An additional small increased in 550-nm absorbance occurred over ~60 min before the signal reached a plateau, and we attribute this to Fe^{2+} that can be slowly stripped by ferrozine. Notably, the chelator does not cross-react with other abundant transition metals such as zinc, manganese and copper present in yeast mitochondria (Fig. 4. 4A).

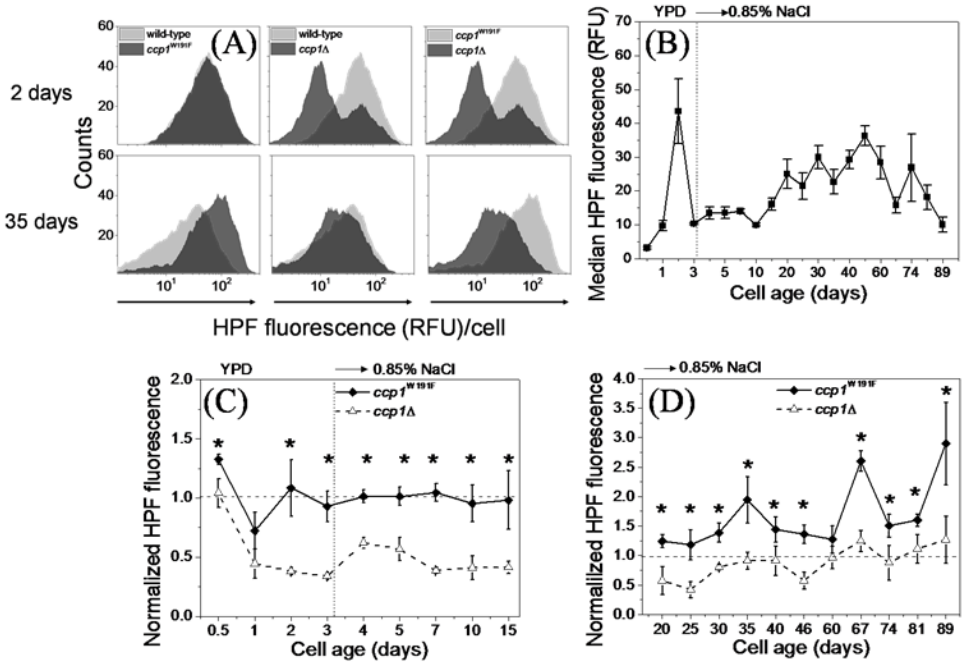

Fig. 4. 3 *Less* $^{\bullet}OH$ *is detected in ccp1*Δ *vs ccp1*^{W191F} *cells.* (A) FACS histograms of HPF-derived fluorescence in relative fluorescence units (RFU)/cell from 10,000 cells/sample of 2- and 35-day wild-type (grey traces in left and middle panels), *ccp1*^{W191F} (black traces in left panel; grey traces in right panel) and *ccp1*Δ (black traces in middle and right panels) cells (Counts = number of cells with a given RFU). (B) Median RFU/cell for 10,000 wild-type cells/sample for three independent cultures±SD over 89 days. (C),(D) Median RFU/cell normalized to wild-type values in panel B for *ccp1*^{W191F} (solid diamonds) and *ccp1*Δ cells (open triangles) from (C) young and (D) old cultures. Yeast cells were grown at 30 °C with 225 rpm stirring and changed to 0.85% NaCl at the vertical dotted line. Fluorescence was recorded at a density of 10^6 cells/mL in a FACScan flow cytometer with excitation at 488 nm and a 530/30 nm bandpass filter. The statistical significance in panels C and D between *ccp1*Δ and *ccp1*^{W191F} cells(*P<0.05) was determined by Student's *t*-test. The lines between the data points in panels B, C and D were added as a visualization aid.

The difference in absorbance (ΔA) between the plateau (>60 min) and the background was used to estimate labile Fe^{2+} accumulation in the cells. Strikingly, we detected very little ferrozine-reactive Fe^{2+} in mitochondria (P10 fractions) of 3-day *ccp1*Δ cells, which contain less labile Fe^{2+} than wild-type cells until about day 30 (Fig. 4. 4C,D). On the other hand, 30-day *ccp1*^{W191F}cells contain twice as much labile Fe^{2+}as wild-type cells, which is associated with the spike in their $^{\bullet}OH$ levels (Fig. 4. 3D). Importantly, the variation in ferrozine-reactive iron in young cells (≤ 15 days) cannot be attributed to differences in iron uptake or storage since the total iron content in both the denucleated lysates (Fig. S4. 5A) and in the mitochondria-enriched fractions is largely strain independent (Fig. S4. 5B). However, the strains do exhibit differences in total iron levels at 30 days for reasons which are not clear at present.

$O_2^{\bullet-}$ inactivates aconitase by removing the labile iron from its catalytic 4Fe4S cluster [175, 176, 180]. Consequently, yeast strains deleted for *sod1*and *sod2* that accumulate above wild-type $O_2^{\bullet-}$ [35, 36] also exhibit high levels of aconitase inactivation and non-protein-bound iron [188]. In contrast, we find that our yeast strain deleted for *CCP1* with low $O_2^{\bullet-}$ levels (Fig. S4. 4) displays significantly less aconitase inactivation (Fig. 4. 2C) and also significantly less ferrozine-reactive mitochondrial Fe^{2+} (Fig. 4. 4D) relative to wild-type and *ccp1*^{W191F} cells, confirming that aconitase contributes Fe^{2+} to the mitochondrial labile iron pool. By serving as a catalyst for Fenton chemistry (step b in Fig. 4. 1), aconitase-derived, ferrozine-reactive Fe^{2+} enhances $^{\bullet}OH$ generation. Hence, young *ccp1*Δ cells with low labile iron also exhibit low $^{\bullet}OH$ levels (Fig. 4. 3C) as predicted by Fig. 4. 1. Notably, the amount of ferrozine-reactive Fe^{2+} (Fig. 4. 4C,D) represents about ~1−10% of the total iron detected in the P10 fractions (Fig. S4. 5B), which brackets the levels of EPR-detectable labile intracellular iron reported for stationary-phase yeast [188].

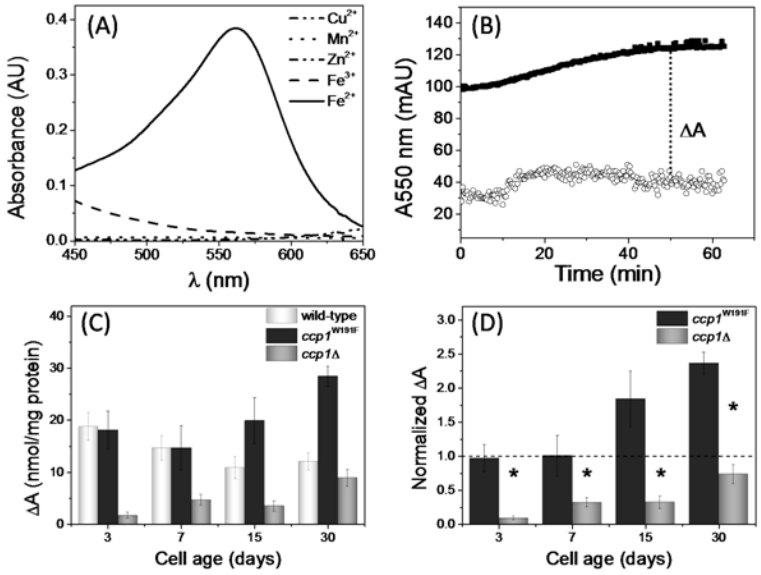

Fig. 4. 4 *Mitochondria of ccp1Δ cells generate less ferrozine-reactive Fe^{2+} than wild-type or ccp1^{W191F} cells.* (A) Spectra recorded in a 1 cm cuvette of solutions containing 67 μM ferrozine and 23 μM Cu^{2+}, Mn^{2+}, Zn^{2+} or Fe^{3+}; or 2.3 μM Fe^{2+}. (B) $[Fe(ferrozine)_3]^{4-}$ complex formation monitored at 550 nm following mixing of 1 mM ferrozine in 10 mM KPi buffer (pH 7.0) with an equal volume of 10 mM KPi buffer (open circles) or P10 lysate (50 μg protein/mL in 10 mM KPi buffer; solid squares) from 3-day wild-type cells. (C) Ferrozine-reactive iron (nmol/mg protein) in the P10 fractions from wild-type, *ccp1*^{W191F} and *ccp1*Δ cells calculated from the background-corrected absorbance at 550 nm (ΔA) at 50 min. The background corrected absorbance was obtained by subtracting from the sample absorbance the sum of the absorbance of the assay solution containing ferrozine plus the average absorbance of the P10 fractions without ferrozine. (D) Ferrozine-reactive iron normalized to the wild-type values in panel C for *ccp1*^{W191F} (black bars) and *ccp1*Δ cells (grey bars). The statistical significance between *ccp1*^{W191F} and *ccp1*Δ cells (**P*<0.05) in panel (D) was determined by Student's *t*-test and the ΔA values are the averages from three independent cultures ±SD.

4.5.4) Oxidative damage to mitochondrial proteins increases with •OH levels

Because of its high reactivity, •OH indiscriminately oxidizes proteins, nucleic acids, sugars and lipids at close proximity to its site of formation [8, 9]. Autofluorescence is a non-specific marker of oxidative modification in live cells [182] and over 2 to 46 days the *ccp1*Δ strain exhibits approximately half the median autofluorescence of wild-type or *ccp1*^{W191F} cells

(Fig. 4. 5B,C), reflecting the low •OH levels in the null strain (Fig. 4. 3C,D). In contrast, the autofluorescence of *ccp1*^{W191F} cells oscillates above wild-type after ~20 days (Fig. 4. 5C), roughly tracking the spikes in their *in vivo* •OH levels (Fig. 4. 3D).

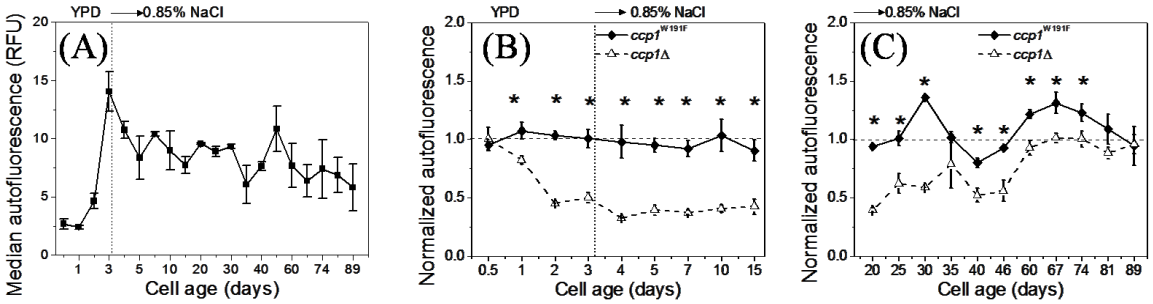

Fig. 4. 5 *Less oxidative damage accumulates in ccp1Δ vs ccp1*^{W191F} *cells.* The autofluorescence of yeast cells was measured (in relative fluorescence units, RFU) as an indicator of global oxidative damage. (A) Median RFU/cell of 10,000 wild-type cells/sample over 89 days measured for three independent cultures±SD. (B),(C) Median RFU/cell normalized to the wild-type values in panel A for *ccp1*^{W191F} (solid diamonds) and *ccp1*Δ (open triangles) from (B) young and (C) old cultures. Yeast cells were grown at 30 °C with 225 rpm stirring and changed to 0.85% NaCl at the vertical dotted line. The autofluorescence of unstained cells at a density of 10^6 cells/mL was recorded in a FACScan flow cytometer with excitation at 488 nm and a 620 nm longpass filter. The statistical significance in panels B and C between *ccp1*^{W191F} and *ccp1*Δ cells (*P<0.05) was determined by Student's *t*-test. The lines between the data points in all panels were added as a visualization aid.

Mitochondrial proteins are reported to be the main targets of oxidative damage by respiration-derived ROS [179, 189]. Thus, we compared protein carbonylation, a marker of protein oxidation [185], in the mitochondria-enriched (P10) and mitochondria-depleted fractions (S10). As expected, the mitochondria-enriched P10 fractions isolated from the wild-type strain possess dramatically higher carbonylation than the corresponding S10 fractions as cells begin to respire around day 1 (Fig. 4. 6A). Significantly, the wild-type and *ccp1*^{W191F} P10 fractions display significantly higher carbonylation than the corresponding fractions (Fig. 4. 6B) from *ccp1*Δ cells with low •OH levels (Fig. 4. 3C), implicating this radical in protein oxidation. In fact, protein carbonylation in the P10 fractions from 1-day *ccp1*^{W191F}cells is double that of wild-type

cells (Fig. 4. 6B) presumably because the mutant's high $O_2^{\bullet-}/H_2O_2$ balance during growth (Fig. S4. 4) leads to an early $^{\bullet}OH$ spike (Fig. 4. 3) via the reactions in Fig. 4. 1.

Following the rise in Cta1 activity [20], H_2O_2 levels in young *ccp1*^{W191F} cells drop below wild-type values (Fig. S4. 4). Since H_2O_2 is its chemical precursor (steb b in Fig. 4. 1), $^{\bullet}OH$ levels also drop in the mutant (Fig. 4. 3C), which surprisingly contains wild-type levels of ferrozine-reactive Fe^{2+} (Fig. 4. 4C,D) despite a high fraction of reversibly inactivated aconitase (Fig. 4. 2B) and oxidatively damaged mitochondrial proteins (Fig. 4. 6B). Hence, we speculate that some of the Fe^{2+} released from aconitase in *ccp1*^{W191F} cells may be immobilized (i.e., non-ferrozine-reactive) in insoluble Fe-phosphate nanoparticles, which can contribute to mitochondrial damage [190]. Also, repair or assembly of the aconitase 4Fe4S cluster may be defective in *ccp1*^{W191F} cells since Aco1 protein levels are comparable in the three strains (Fig. 4. 2D). Consistent with their depressed aconitase activity (Fig. 4. 2B) and extensive mitochondrial protein oxidation (Fig. 4. 6B), young *ccp1*^{W191F} cells possess a lower mitochondrial membrane potential than either wild-type or *ccp1*Δ cells [20]. Furthermore, in old *ccp1*^{W191F} cells, $^{\bullet}OH$ (Fig. 4. 3D) and ferrozine-reactive-Fe^{2+} levels (Fig. 4. 4D) again spike above wild-type levels, which undoubtedly shortens their lifespan.

It is noteworthy that protein carbonylation is also lower in the mitochondria-depleted S10 fractions of *ccp1*Δ cells as compared to those of *ccp1*^{W191F} or wild-type cells (Fig. 4. 6D).This reveals that extramitochondrial proteins also undergo less oxidative damage as *ccp1*Δ cells age, consistent with their relatively weak autofluorescence (Fig. 4. 5B,C). Since their mitochondria release 3-fold more H_2O_2 than wild-type mitochondria [20], *ccp1*Δ cells may experience increased activation of Yap1, a H_2O_2-sensitive cytosolic transcription factor that controls expression of cytosolic antioxidant enzymes [43]. Thus, enhanced activation of the H_2O_2 stress

response by relatively high levels of mitochondrial H_2O_2, as seen on *CCP1* deletion, serves to protect cells against cytosolic as well as mitochondrial oxidative damage.

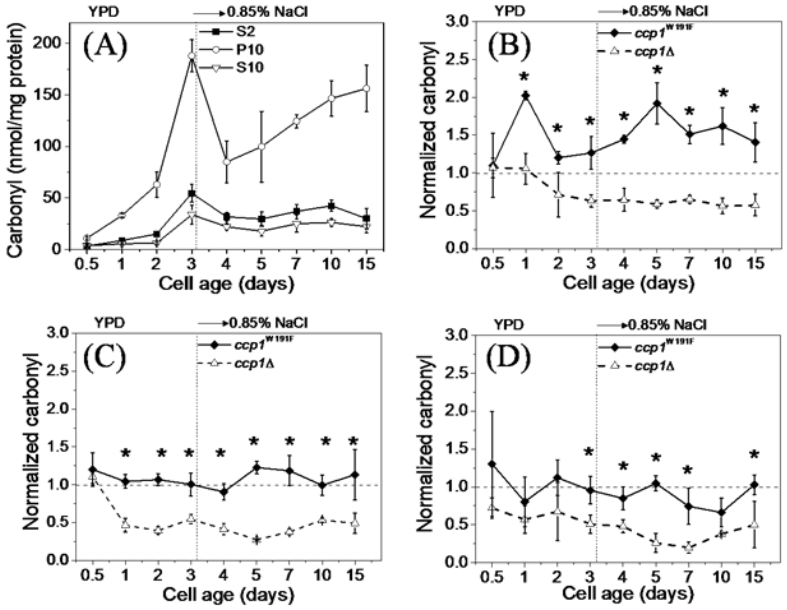

Fig. 4. 6 *Mitochondrial protein carbonylation is lower in ccp1Δ vs ccp1^{W191F} cells.* (A) Protein carbonyl levels in denucleated lysates (S2 fractions, solid squares), mitochondria-enriched pellets (P10 fractions, open circles) and mitochondria-depleted supernatants (S10 fractions, open triangles) of wild-type cells from 3 independent cultures ±SD. Protein carbonyl content per mg protein in (B) P10, (C) S2, and (D) S10 fractions from *ccp1*^{W191F} (solid diamonds) and *ccp1*Δ cells (open triangles) normalized to the wild-type values in panel A. Protein carbonylation was assayed using DNPH and the subcellular fractions were prepared as described under *Materials and methods*. The statistical significance in panels B, C and D between *ccp1*^{W191F} and *ccp1*Δ cells (*P<0.05) was determined by Student's *t*-test. The lines between the data points in all panels were added as a visualization aid.

The wild-type and *ccp1*^{W191F} strains exhibit similar autofluorescence (Fig. 4. 5B) and total protein carbonylation (Fig. 4. 6C) over 15 days. This suggests that these cells experience comparable global oxidative damage over this time period despite the increased damage to mitochondrial proteins in the mutant (Fig. 4. 6B). Hence, differences in mitochondrial oxidative damage may be masked when probing global oxidative damage or protein carbonylation in

samples such as our S2 fractions since mitochondria contribute <10% of the total cellular protein.

4.5.5) Total intracellular GSX and the GSH/GSSG ratio are elevated in ccp1Δ cells with impaired mitochondrial H_2O_2 sensing

Chronological aging in yeast is marked by a progressively more oxidizing intracellular environment due to increased GSH oxidation [64]. Consistent with this, we observe that both the total GSX (i.e., GSH+GSSG) content and the GSH/GSSG ratio decline dramatically with age in wild-type cells (Fig. 4. 7A) and in the mutant strains (Fig. 4. 7B,C). Although the three strains have similar levels on day 3 (Fig. 4. 7B), rates of GSX depletion with age follow the order: *ccp1*Δ < wild-type < *ccp1*^{W191F}. Also, the GSH/GSSG ratio is significantly higher in *ccp1*Δ compared to the two other strains (Fig. 4. 7C), and the effects of enhanced intracellular redox buffering on lifespan are discussed in the next section.

4.5.6) *ccp1*Δ cells with impaired mitochondrial H_2O_2 sensing live longer

The average chronological lifespan measured in stationary phase of *ccp1*Δ cells is 72 days vs 47 and 32 days for wild-type and *ccp1*^{W191F} cells, respectively (Fig. 4. 8). Significantly, the absence of CCP enzyme activity in mitochondria does not negatively impact longevity since *ccp1*Δ cells live longer than wild-type cells. Notably, *ccp1*Δ cells live twice as long as *ccp1*^{W191F} cells producing the Ccp1^{W191F} protein variant (Fig. 4. 8) with no CCP activity but with hyperactive H_2O_2 sensing and signaling properties. Thus, *CCP1* deletion extends chronological lifespan by impairing mitochondrial H_2O_2 sensing, thereby allowing increased mitochondrial H_2O_2 accumulation, which triggers mitohormesis in exponentially growing and early stationary phase cells (Fig. S4. 4) [20]. This in turn lowers the $O_2^{\bullet-}/H_2O_2$ balance, protects aconitase activity (Fig. 4. 2), shrinks the labile iron pool (Fig. 4. 4), depresses $^{\bullet}OH$ levels (Fig. 4. 3) and

diminishes global and mitochondrial oxidative damage (Fig. 4. 5; Fig. 4. 6). Since lifespan correlates inversely with the extent of mitochondrial protein carbonylation in young cells (Fig. 4. 8C), we conclude that mitochondrial oxidative damage in early life is a critical determinant of lifespan. We noted above that measurements of global oxidative damage may not reveal differences in mitochondrial damage since we observe that young *ccp1*^{W191F} and wild-type cells exhibit comparable global oxidative damage (Fig. 4. 5; Fig. 4. 6C) but young wild-type cells accumulate less mitochondrial protein carbonylation and live 1.4-fold longer (Fig. 4. 8).

Critically, lifespan is also associated with a decline in the effective intracellular redox buffering capacity of GSH/GSSG [64]. Since GSH is a highly efficient $^{\bullet}$OH scavenger [22, 23], the relatively high GSX levels and GSH/GSSG ratios found in the long-lived *ccp1*Δ cells (Fig. 4. 7) will lower $^{\bullet}$OH levels (Fig. 4. 3B) and extend lifespan by protecting mitochondrial proteins from this highly reactive ROS (Fig. 4. 8A,B).

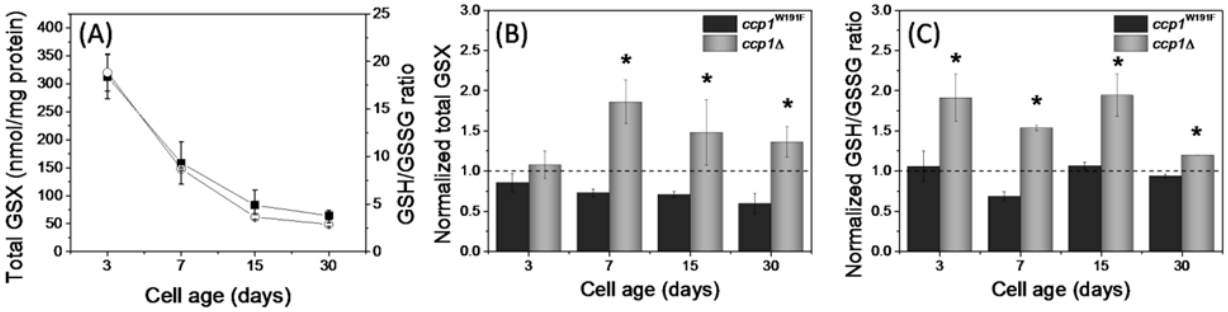

Fig. 4. 7 *GSX levels and the GSH/GSSG ratios are higher in ccp1*Δ *vs ccp1*^{W191F} *cells.* (A) Variation with age in total GSX (GSH+GSSG, solid squares) and the GSH/GSSG ratio (open circles) in wild-type cells. (B) Total GSX and (C) GSH/GSSG ratios in *ccp1*Δ (grey bars) and *ccp1*^{W191F} cells (black bars) normalized to the wild-type values in panel A. GSX was assayed using DTNB in protein-free extracts following GSSG reduction by glutathione reductase and NADPH. GSSG was determined by blocking free GSH with 10 mM 4-vinyl pyridine prior to GSSG reduction. Data are averages ±SD for cells from three independent cultures. The statistical significance in panels B, and C between *ccp1*^{W191F} and *ccp1*Δ cells (*P<0.05) was determined by Student's *t*-test. The lines between the data points in panel A were added as a visualization aid.

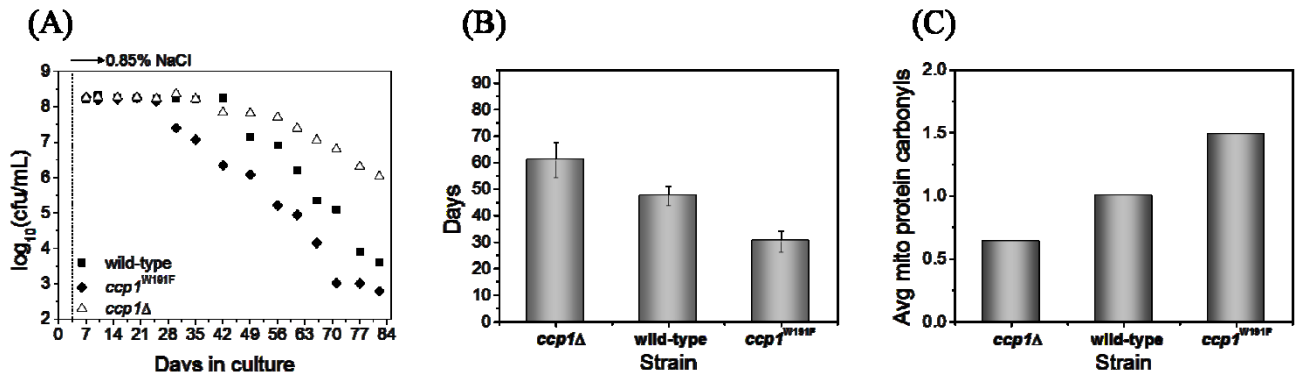

Fig. 4. 8 *ccp1*Δ *cells accumulate less mitochondrial protein damage in early life and live 2-fold longer than ccp1*^{W191F} *cells.*(A) Cell viability in colony forming units (cfu) vs days in culture of *ccp1*^{W191F} (solid diamonds), wild-type (solid squares) and *ccp1*Δ cells (open triangles). Aliquots (100 µL) of culture were withdrawn at the times indicated, serially diluted, plated on YPD agar medium, and the number of cfu was counted following 2 days incubation at 30 °C. (B) Average viability ±SD of cells from three independent cultures for each strain. Cell viability is defined here as the time in days required for a 2-log drop in cfu of stationary-phase cells. Note that stationary phase begins at day 4 under our experimental conditions (see *Materials and methods*). (C) Mitochondrial protein carbonyls averaged over the first 15 days for each strain (P10 fractions, Fig. 4. 6B) and normalized to the wild-type value.

4.6) Discussion

4.6.1) Impaired H_2O_2 sensing lowers the intracellular $O_2^{\bullet-}/H_2O_2$ balance in young cells and extends lifespan

We demonstrate here that deletion of Ccp1, a mitochondrial H_2O_2 sensing and signaling protein [20], extends yeast lifespan (Fig. 4. 9). Notably, the intracellular ROS levels we report in our respiring yeast strains [20] largely reflect those present in mitochondria since these organelles are the main sites of endogenous ROS accumulation in eukaryotes, including yeast [179]. Young cells (≤ 15 days) of the long-lived *ccp1*Δ strain accumulate more H_2O_2 but less $O_2^{\bullet-}$ than young wild-type cells, giving rise to a low $O_2^{\bullet-}/H_2O_2$ balance (Fig. S4. 4) [20]. The extended lifespan of these cells demonstrates that the beneficial effects of maintaining a low intracellular $O_2^{\bullet-}/H_2O_2$ balance in early life include the protection of aconitase activity (Fig. 4. 2), diminution

of the mitochondrial labile iron pool (Fig. 4. 4C,D) and greater persistence of a reducing intracellular environment (Fig. 4. 7).

Mitochondrial Aco1 is a target of $O_2^{\bullet-}$ generated in the respiratory chain [175]. $O_2^{\bullet-}$ inactivates the enzyme by removing a labile Fe^{2+} ion from its 4Fe4S catalytic site (step a in Fig. 4. 1). This provides protein-free Fe^{2+} to reduce H_2O_2 and generate highly reactive $^{\bullet}OH$ radicals (step b in Fig. 4. 1). Free Fe^{3+} can be cycled back to Fe^{2+} by a second $O_2^{\bullet-}$molecule (step c in Fig. 4. 1) in competition with further Fe^{2+} removal from aconitase [191]. However, little iron is released from aconitase in *ccp1*Δ cells (Fig. 4. 4) since they exhibit only a 10-20% increase in aconitase activity vs 65-90% increase for *ccp1*^{W191F} cells after reconstitution with Fe^{2+} and DTT (Fig. 4. 2A-C). Redox cycling of free iron (steps b and c in Fig. 4. 1) will also be attenuated in *ccp1*Δ cells because of this strain's low $O_2^{\bullet-}$ levels in early life (Fig. S4. 4) [20]. Hence, increased accumulation of mitochondrial H_2O_2 is not damaging to cells when $O_2^{\bullet-}$ levels are low. On the contrary, stable high-level mitochondrial H_2O_2 production in early life promotes mitohormesis [16], an adaptive mitochondrial stress response that increases Sod2 expression [18, 42] and activity [19, 20]. The latter lowers $O_2^{\bullet-}$ accumulation and attenuates $^{\bullet}OH$ generation, thereby slowing down GSH oxidation and GSX depletion (Fig. 4. 7), which marks the loss of redox buffering and cell death [64, 192]. In essence, a low mitochondrial $O_2^{\bullet-}/H_2O_2$ balance in early life protects mitochondrial proteins and allows cells to live longer (Fig. 4. 9). Our results concur with other studies involving genetic intervention of yeast ROS-metabolizing enzymes. For example, *CTA1* and/or *CTT1* deletion [19] or *SOD*2 overexpression lowers the $O_2^{\bullet-}/H_2O_2$ balance and extends chronological lifespan [59], whereas deletion of *SOD2* and/or *SOD1* increases the $O_2^{\bullet-}/H_2O_2$ balance and shortens yeast lifespan [35]. Because it is a mitochondrial H_2O_2 sensor, Ccp1 functions as an upstream regulator of both Cta1 and Sod2 activities [20] and hence of the

mitochondrial $O_2^{\bullet-}/H_2O_2$ balance, and ultimately lifespan. Mesquita *et al.* [19] report contradictory results on the extent of oxidative damage in yeast with elevated H_2O_2 levels. Their *cta1*Δ and *ctt*1Δ mutant strains exhibit higher oxidative damage (measured as autofluorescence and global protein carbonylation) than wild-type cells, whereas enhanced H_2O_2 accumulation in wild-type cells due to calorie restriction (0.5 vs 2% glucose) resulted in decreased oxidative damage analogous to our *ccp1*Δ strain (Fig. 4. 5; Fig. 4. 6). *CCP1* deletion down-regulates peroxisomal/mitochondrial Cta1 activity but not cytosolic Ctt1 activity [20] so in contrast to the *ctt1*Δ strain, *ccp1*Δ cells possess wild-type Ctt1 activity to protect the cytosol and control global oxidative damage (Fig. 4. 5; Fig. 4. 6). Furthermore, lifespan correlates with mitochondrial protein carbonylation levels (Fig. 4. 8) so these should be measured in the *cta1*Δ and *ctt*1Δ strains in addition to the reported global analyses [19].

4.6.2) *In vivo* ROS levels fluctuate in older cells

As Fig. 4. 3B reveals for wild-type cells, $^{\bullet}OH$ levels fluctuate considerably with age due to corresponding fluctuations in $O_2^{\bullet-}$ and H_2O_2 levels (Fig. S4. 4). The viability of *ccp1*^{W191F} cells clearly declines after 30 days (Fig. 4. 8A) when their $^{\bullet}OH$ levels spike relative to wild-type (Fig. 4. 3D). A second $^{\bullet}OH$ spike above wild-type around day 60 further impacts this strain's viability (Fig. 4. 8A). Notably, the *ccp1*Δ strain also exhibits an $O_2^{\bullet-}$ spike around day 60 (Fig. S4. 4) but without a corresponding spike in $^{\bullet}OH$ (Fig. 4. 3D) or H_2O_2 (Fig. S4. 4). Thus, $^{\bullet}OH$ generation in old cells appears to also vary with their mitochondrial $O_2^{\bullet-}/H_2O_2$ balance and diminished control over this balance can be associated with loss of viability. In other words, aging can be linked to increased $^{\bullet}OH$ generation within mitochondria, and spikes in $^{\bullet}OH$ levels indicate that old cells lose their capacity to counteract this stress, in part due to loss of redox buffering on GSX depletion [64]. Hence, our results are in agreement with the free radical theory of aging proposed

four decades ago [6, 7], which predicts that cells age due to the accumulation of free radical damage over time.

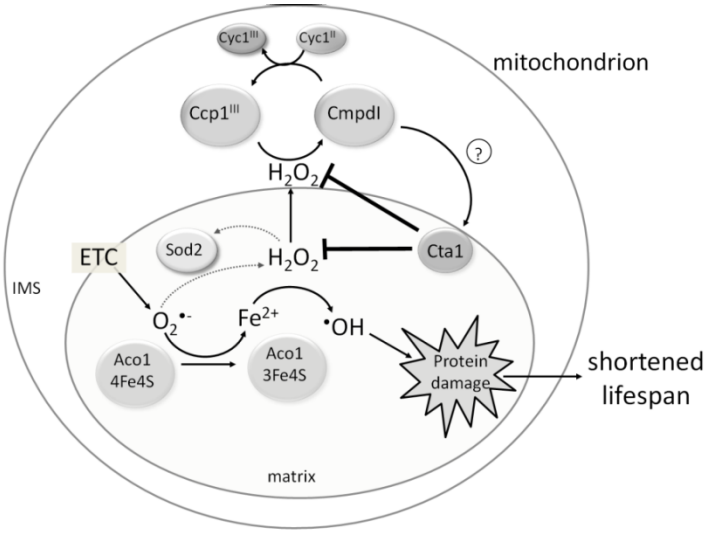

Fig. 4. 9 *Sensing of mitochondrial H_2O_2 by Ccp1 shortens lifespan.* Localized in the intermembrane space (IMS), Ccp1 senses H_2O_2, a product of the $O_2^{\bullet-}$ derived from the electron transport chain (ETC). Ccp1 is rapidly 2-electron oxidized by H_2O_2 to Compound I (CmpdI), which is either reduced (*i.e.*, deactivated) by $Cyc1^{II}$or in its oxidized form upregulates Cta1 activity by an unknown mechanism that likely involves heme transfer. Cta1 scavenges H_2O_2 and weakens the H_2O_2 stress response whereas *CCP1* deletion allows enhanced mitochondrial H_2O_2 accumulation and strengthens the H_2O_2stress response. This response includes a signaling event that is transmitted to the nucleus to upregulate the expression of Sod2, which is directed to the mitochondrial matrix to dismutate ETC-derived $O_2^{\bullet-}$ [35, 36]. Suppression of the H_2O_2 stress response raises $O_2^{\bullet-}$ levels and increases Aco1-derived free Fe^{2+} to catalyze $^{\bullet}OH$ formation from H_2O_2 (Fig. 4. 1). The $^{\bullet}OH$ radicals damage mitochondrial proteins and curtail longevity (Fig. 4. 8). Note that the two dotted arrows represent the key components of the H_2O_2 stress response that are repressed by Ccp1 signaling: H_2O_2-induced upregulation of Sod2 (which involves H_2O_2-dependent mitochondrial retrograde signaling that is omitted for clarity) and Sod2-catalyzed dismutation of $O_2^{\bullet-}$.

4.6.3) Interpretation of genetic intervention in higher eukaryotes is complex

Genetic intervention by knockout or overexpression of antioxidant enzymes has not provided consistent results in flies, mice and worms [50]. Deletion of the *Sod2* [193] or *Sod1* [194] gene shortens lifespan of fruit flies, while overexpression of *Cat* with *Sod1* [51] or *Sod2*

with *Sod1* [195] extends lifespan but overexpression of just one of these genes has questionable effects on longevity [50].

Sod2-knockout (*Sod2*$^{-/-}$) mice are not viable [54], whereas heterozygous (*Sod2*$^{+/-}$) animals live a normal lifespan but experience increased tumor incidence [196]. *Sod1*-knockout mice (*Sod1*$^{-/-}$) experience a shortened lifespan [197] but *Sod1* or *Sod2* overexpression has no effect on murine lifespan [198]. Likewise, mice overexpressing non-mitochondrially targeted *Cat* do not live longer [198] but those overexpressing mitochondrially targeted *Cat* do live longer [52]. *Caenorhabditis elegans* deleted for *sod*-2 or treated with the $O_2^{\bullet-}$ generator paraquat early in life exhibits lifespan extension [199]. Also, the simultaneous knockout of all five *sod* genes in *C. elegans* has no effect on lifespan but increases the worm's susceptibility to multiple stressors [53].

Unlike the clonal populations of yeast examined here, differentiated cells in higher eukaryotes maytolerate a broader spectrum of mitochondrial ROS. Furthermore, oxidative damage will differentially impact different tissues in multicellular organisms, which adds extra complexity to the analysis of ROS and aging in these models. For example, a lifelong gradual increase in oxidative damage-related apoptosis has been reported in the muscles but not in the brain of fruit flies [200]. Nonetheless, we speculate that maintaining an appropriate level of mitochondrial H_2O_2 sensing to optimize the mitochondrial $O_2^{\bullet-}/H_2O_2$ balance is critical in modulating $^{\bullet}OH$ generation and ROS-induced aging in eukaryotic cells. However, detailed biochemical analyses of antioxidant enzyme activities and ROS levels in different tissues of these genetically altered organisms need to be compared to their wild-type values as carried out in our studies on yeast.

4.7) Conclusions

We observed the somewhat counter-intuitive phenomenon that deleting a mitochondrial H_2O_2 sensor and signaling protein, Ccp1, significantly increases the fitness of a eukaryotic cell. Impaired H_2O_2 sensing *in vivo* allows greater H_2O_2 accumulation and promotes the mitohormetic effects of this biochemical messenger [16]. Combined with our previous results [20] we conclude that Ccp1 senses H_2O_2 and upregulates Cta1 activity. This lowers the H_2O_2 concentration and weakens the H_2O_2 stress response whereas *CCP1* deletion allows more H_2O_2 accumulation and strengthens the H_2O_2 stress response. This response likely includes a signaling event that is transmitted to the nucleus to stimulate the expression of the mitochondria-directed antioxidant enzyme, Sod2. Such H_2O_2-dependent mitochondrial retrograde signaling, or communication between the mitochondria and nucleus, regulates the mitochondrial $O_2^{\bullet-}/H_2O_2$ balance and controls chronological aging of yeast. As confirmed here, these effects include enhanced $O_2^{\bullet-}$ scavenging, higher aconitase activity and lower $^{\bullet}OH$ generation leading to decreased oxidative damage to mitochondrial proteins in early life and extended lifespan (Fig. 4. 9). On the other hand, hyperactive mitochondrial H_2O_2 sensing weakens the H_2O_2 stress response, which allows greater $O_2^{\bullet-}$ accumulation, thereby increasing the pool of mitochondrial free iron, $^{\bullet}OH$ generation and mitochondrial protein damage that depletes cellular reducing power and curtails lifespan (Fig. 4. 9). Importantly, supported by extensive biochemical analyses of aconitase activity, labile iron levels, protein and GSX oxidation, our results identify the intracellular $O_2^{\bullet-}/H_2O_2$ balance in early life as a critical parameter in modulating the anti- vs pro-aging effects of ROS. Since other pathways that modulate lifespan, including those controlled by Ras, Sch9 and Tor, are conserved between yeast and metazoans [67-69, 174], further elucidation of H_2O_2-dependent mitochondrial retrograde signaling (or adaptive mitochondrial ROS signaling [201]) in yeast will increase our

understanding of lifespan modulation by ROS in other postmitotic cells despite the fact that a Ccp1 homolog has not been identified in metazoans.

This is the first study to directly link H_2O_2 sensing with lifespan. By selecting yeast strains with impaired (*ccp1*Δ) and hyperactive (*ccp1*^{W191F}) mitochondrial H_2O_2 sensing, we demonstrate that the mitochondrial H_2O_2 stress response involves H_2O_2-dependent mitochondrial retrograde signaling that upregulates Sod2 activity to protect mitochondria against $^{\bullet}OH$-induced protein damage that curtains lifespan. Notably, the 2-fold lifespan extension on suppression (*ccp1*Δ) versus activation (*ccp1*^{W191F}) of mitochondrial H_2O_2 sensing is comparable to that reported on suppression of the Tor/Sch9 pathway [174]. However, the effects on lifespan of deleting the well-characterized yeast cytosolic H_2O_2 sensor Gpx3 [70] have not been reported.

4.8) Supplementary information

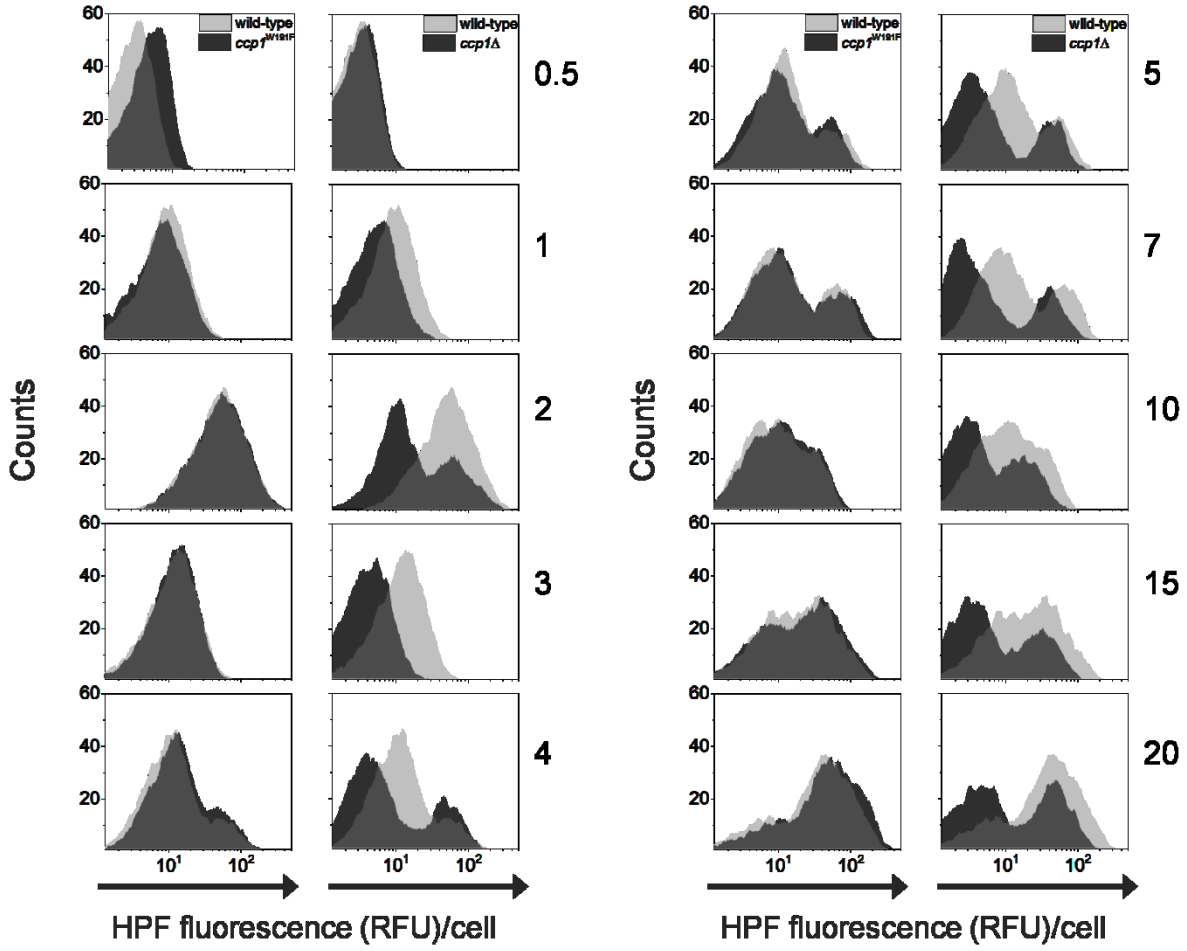

Fig. S4. 1 *Fluorescence from live young cells (0.5 to 20 days) stained with the* $^{\bullet}$*OH-sensitive probe HPF.* FACS histograms of HPF-derived fluorescence in RFU/cell from 10,000 cells/sample of wild-type (grey traces), *ccp1*^{W191F} (black traces, left panels) and *ccp1*Δ cells (black traces, right panels). Yeast were grown as described in *Materials and methods* and at each time point, 10^7 cells/mL were stained in 5 µM HPF for 1 h at 30 °C, harvested by centrifugation, diluted into PBS (pH 7.0) to 10^6 cells/mL, and fluorescence was recorded with excitation at 488 nm and a 530/30 nm bandpass filter. "Counts" on the y-axis gives the number of cells with a given RFU.

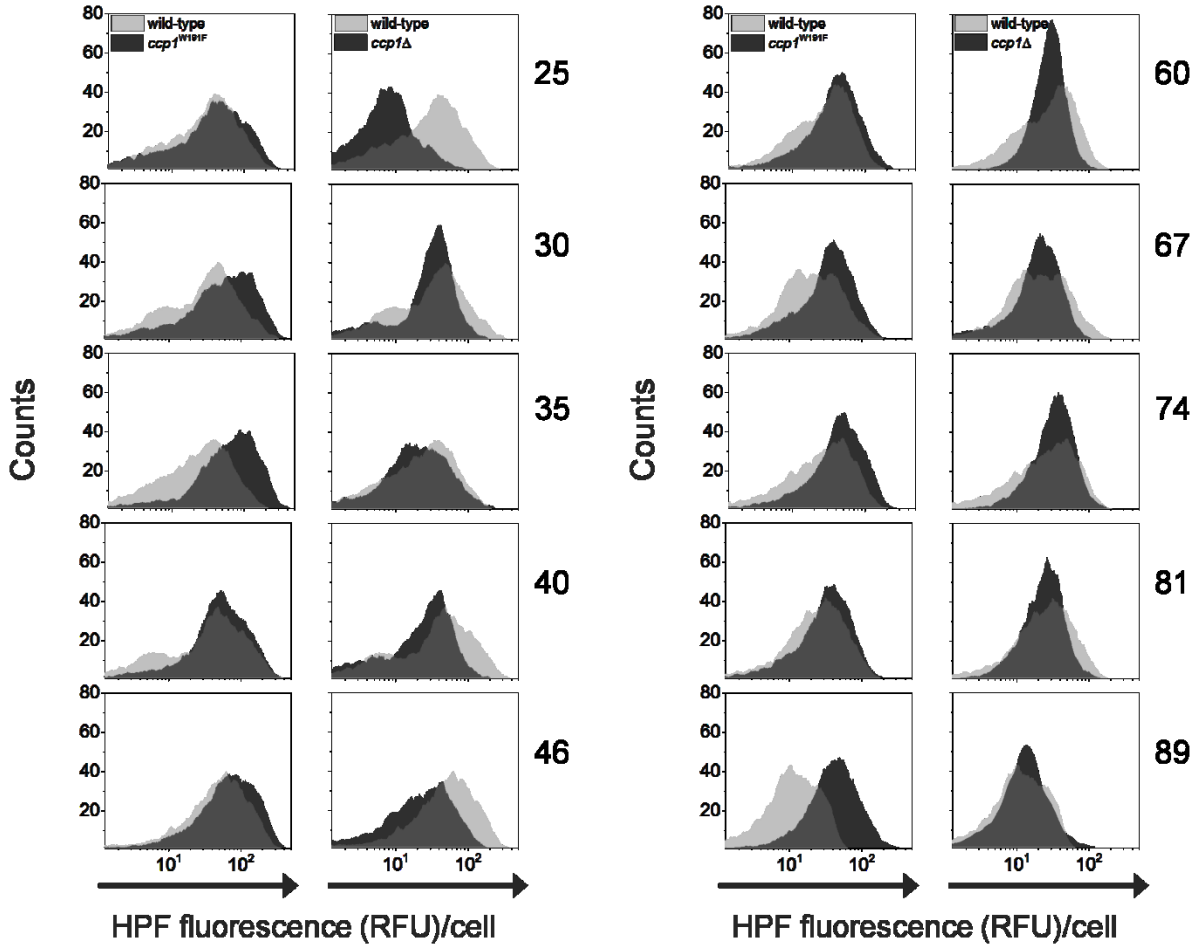

Fig. S4. 2 *Fluorescence from live old cells (25 to 89 days) stained with the* ˙*OH-sensitive probe HPF*. FACS histograms of HPF-derived fluorescence in RFU/cell from 10,000 cells/sample of wild-type (grey traces), *ccp1*^{W191F} (black traces, left panels) and *ccp1*Δ cells (black traces, right panels).

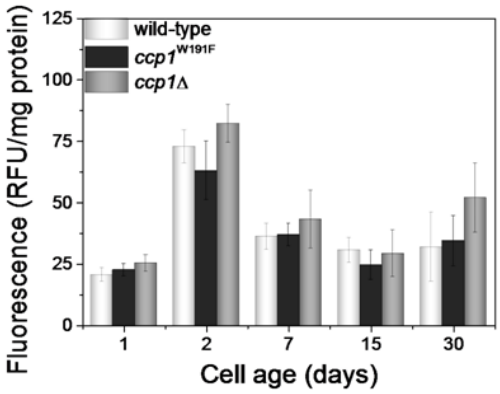

Fig. S4. 3 *Loading of the ˙OH-sensitive probe HPF is comparable in wild-type, ccp1*^{W191F} *and ccp1*Δ *cells*. Fluorescence in RFU (relative fluorescence units) vs cell age following oxidation of HPF in the soluble protein extracts from HPF-stained wild-type (white bars), *ccp1*^{W191F} (black bars) and *ccp1*Δ cells (grey bars) from three separate cultures ±SD. Yeast cells were grown at 30 °C with 225 rpm stirring in YPD medium and switched to 0.85% NaCl after 3 days. At each time point, 10^7 cells/mL were stained in 5 μM HPF for 1 h at 30 °C, harvested, washed twice in PBS (pH 7.0), lysed using glass beads, and the supernatants were treated with 10 mM H_2O_2 and 1 mM Fe_2SO_4 for 15 min at 20 ºC to oxidize HPF to fluorescein.The steady-state fluorescence of the supernatants at 520 nm, reported as RFU/mg protein, was measured in a fluorometer with excitation at 488 nm.

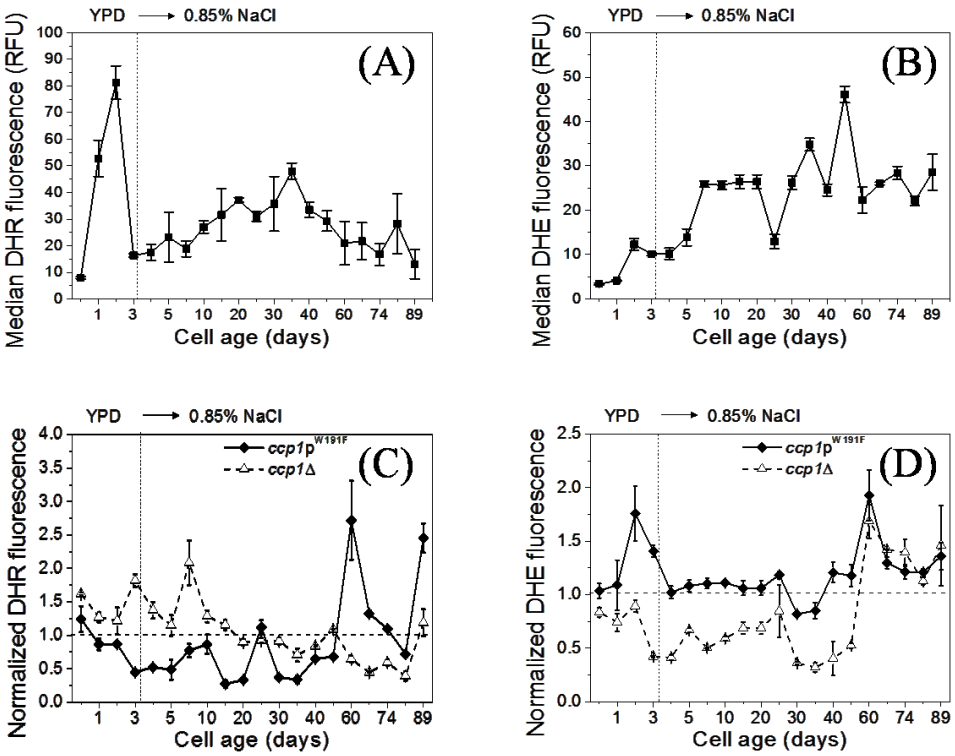

Fig. S4. 4 *H_2O_2 and $O_2^{\bullet-}$ levels in live wild-type, ccp1^{W191F} and ccp1Δ cells over 89 days.* Fluorescence in RFU (relative fluorescence units) of wild-type cells stained with (A) the H_2O_2-sensitive probe DHR and (B) the $O_2^{\bullet-}$-sensitive probe DHE. Data points are the median RFU/cell measured for 10,000 cells from three separate cultures ±SD. Median RFU/cell normalized to wild-type values for *ccp1*^{W191F} (solid diamonds) and *ccp1*Δ cells (open triangles) stained with (C) DHR and (D) DHE. Yeast cells were grown at 30 °C with stirring at 225 rpm in YPD medium and switched to 0.85% NaCl after 3 days. At the times indicated, 10^7 cells/mL were stained in 5 μM dye for 2 (DHR) and 1 h (DHE) at 30 °C. After dilution to 10^6 cells/mL with PBS (pH 7.0), FACS analysis was performed using 488 nm excitation with 530/30 nm (DHR) and 580/45 nm (DHE) emission filters. The statistical significance in panels C and D between *ccp1*^{W191F} and *ccp1*Δ cells (*P<0.05) was determined by Student's *t*-test. The lines between the data points in all panels were added as a visualization aid.

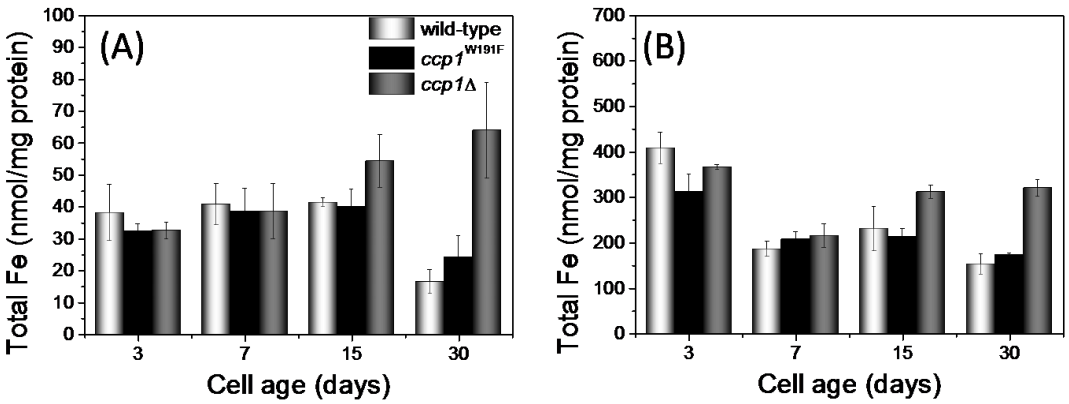

Fig. S4. 5 *Total iron content is comparable up to 15 days in the S2 and P10 fractions from the three strains.* Iron content vs cell age in (A) denucleated lysates (S2 fractions), and (B) mitochondria-enriched (P10 fractions) of wild-type (white bars), *ccp1*^{W191F} (black bars) and *ccp1*Δ cells (grey bars) from three independent cultures ±SD. Yeast cells were grown at 30 °C with 225 rpm stirring in YPD medium and switched to 0.85% NaCl after 72 h. At each time point, the cells were fractionated and the total iron content in the S2 and P10 fractions was determined by ICP/MS as described under *Materials and methods*.

Chapter 5: Catalases and resistance to exogenous H_2O_2

5.1) Preface

The work presented in Chapter 5 corresponds to the following manuscript: Martins D, English AM (2014). **Catalase activity is stimulated by H_2O_2 in rich culture medium and is required for H_2O_2 resistance and adaptation in yeast**. Redox Biology, 2, 308-313. I performed the experiments and interpreted the results, wrote the first draft of the manuscript and and provided revisions. Dr. English contributed with discussions, data analysis and revisions of the paper. The graphical abstract of the original paper was included in this chapter as Fig. 5. 6. Redox Biology is an open-access journal, and the manuscript's copyright is owned by the authors.

5.2) Abstract of the manuscript

Catalases are efficient scavengers of H_2O_2 and protect cells against H_2O_2 stress. Examination of the H_2O_2 stimulon in *Saccharomyces cerevisiae* revealed that the cytosolic catalase T (Ctt1) protein level increases 15-fold on H_2O_2 challenge in synthetic complete medium although previous work revealed that deletion of the *CCT1* or *CTA1* genes (encoding peroxisomal/mitochondrial catalase A) does not increase the H_2O_2 sensitivity of yeast challenged in phosphate buffer (pH 7.4). This we attributed to our observation that catalase activity is depressed when yeast are challenged with H_2O_2 in nutrient-poor media. Hence, we performed a systematic comparison of catalase activity and cell viability of wild-type yeast and of the single catalase knockouts, *ctt1*Δ and *cta1*Δ, following H_2O_2 challenge in nutrient-rich medium (YPD) and in phosphate buffer (pH 7.4). Ctt1 but not Cta1 activity is strongly induced by H_2O_2 when cells are challenged in YPD but suppressed when cells are challenged in buffer. Consistent with

the activity results, exponentially growing *ctt1*Δ cells in YPD are more sensitive to H_2O_2 than wild-type or *cta1*Δ cells, whereas in buffer all three strains exhibit comparable H_2O_2 hypersensitivity. Furthermore, catalase activity is increased during adaptation to sublethal H_2O_2 concentrations in YPD but not in buffer. We conclude that induction of cytosolic Ctt1 activity is vital in protecting yeast against exogenous H_2O_2 but this activity is inhibited by H_2O_2 when cells are challenged in nutrient-free medium.

5.3) Introduction

H_2O_2 is an inorganic messenger produced by cells during aerobic respiration [70]. At low levels, this hormone triggers adaptive responses that increase cell resistance to oxidants by augmenting the expression of antioxidant enzymes and stress related proteins [16, 18, 19]. In contrast, H_2O_2 is toxic at high concentration, triggering programmed cell death [99] and generating hydroxyl radicals catalyzed by redox-active transition metals [191]. Thus, intracellular H_2O_2 levels are tightly regulated by the activity of H_2O_2 metabolizing enzymes.

Catalases are tetrameric heme-containing enzymes that catalyze the disproportionation of H_2O_2 to H_2O and O_2 [27, 28] (*k*cat/Km 10^6-10^7 M^{-1} s^{-1}) without consuming additional electron-donor substrates [27]. Thus, these enzymes can metabolize high levels of H_2O_2 and the intracellular reducing environment is preserved [202, 203]. Nonetheless, conflicting results have been published on the importance of catalase activity in protecting yeast cells against H_2O_2. Analysis of the yeast H_2O_2 stimulon revealed that the protein levels of Cta1, the catalase isoform found in yeast peroxisomes and mitochondria, remained unchanged [42] but production of Ctt1, a cytosolic catalase, increased 15-fold after challenge with a bolus of H_2O_2 [42], indicating a role for this catalase in combating H_2O_2 stress. Our group reported that induction of catalase activity by Ccp1 is associated to resistance to exogenous H_2O_2 [20]. However, deletion of *CTT1* or both

CTT1 and *CTA1* did not render growth-phase yeast hypersensitive to bolus H_2O_2 but impaired the H_2O_2 adaptive response [38]. Also, a questionable linear correlation between catalase activity and yeast survival on H_2O_2 challenge has been reported [71].

Differences in yeast phenotype can frequently be attributed to variation in genetic background [71]. However, nutrient availability during H_2O_2 challenge was dramatically different in the studies that examined H_2O_2-induced protein expression [42] vs cell viability [38][71]. For instance, Godon *et al.* [42] looked at changes in protein expression after challenging exponentially growing wild-type YPH98 cells in synthetic complete dextrose (SCD). We looked at catalase activity after challenging exponentially growing BY4741 cells with H_2O_2 in YPD medium [20]. Izawa *et al.* [38] and Bayliak *et al.* [71] grew YPH250 cells in yeast extract peptone dextrose (YPD) but switched them to 100 mM potassium phosphate buffer, pH 7.4 (KPi) for the H_2O_2 challenge. Since nutrients are required for protein synthesis and repair [204], the comparable H_2O_2 hypersensitivity of wild-type, *ctt1*Δ, and acatalasemic yeast [38] may be a consequence of starvation when cells are challenged in KPi.

Thus, here we compare catalase activity and cell viability of wild-type, *ctt1*Δ and *cta1*Δ cells after H_2O_2 challenge in YPD and KPi. We find that the H_2O_2 sensitivity of wild-type cells depends on their genetic background and resistance requires stimulation of catalase activity. Ctt1 activity is upregulated by H_2O_2 challenge in nutrient-rich YPD and *ctt1*Δ cells exhibit lower survival than wild-type or *cta1*Δ cells. However, the three strains are equally hypersensitive to H_2O_2 when challenged in KPi since catalase activity falls below basal levels. Furthermore, wild-type and *cta1*Δ cells adapt to pre-challenge with a sublethal H_2O_2 dose in YPD [38] but not in KPi. Thus, we conclude that Ctt1 is stimulated by H_2O_2 and this activity is essential in protecting

yeast cells against H_2O_2 challenge. However, starvation impairs the H_2O_2-adaptive response by preventing induction of Ctt1 activity and masks its contribution to H_2O_2 resistance.

5.4) Materials and methods

5.4.1) Yeast strains, media, and growth conditions

The *Saccharomyces cerevisiae* strains used in this study are listed in Table 5. 1. Wild-type BY4741 was purchased from the European *Saccharomyces cerevisiae* Archive for Functional Analysis (EUROSCARF, Frankfurt, Germany). Catalase knockouts (*cta1*Δ and *ctt1*Δ) in the BY4741 genetic background were kindly provided by Prof. Christopher Brett (Department of Biology, Concordia University). Profs Philip Hieter (Department of Medical Genetics, University of British Columbia) and Shingo Izawa (Department of Applied Biology, Kyoto Institute of Technology) generously supplied wild-type YPH250 cells, and *cta1*Δ and *ctt1*Δ cells in the YPH250 background, respectively. All strains were inoculated at an initial OD_{600} of 0.01 in liquid YPD medium (1% yeast extract, 2% peptone, and 2% glucose) and incubated at 30 °C with shaking at 225 rpm using a flask-to-medium volume ratio of 1:5.

Table 5. 1 *S. cerevisiae strains used in this study*

Strain	Description	Reference
wild-type YPH250	*MATa ade2Δ101 his3Δ200 leu2Δ1 lys2Δ801 trpΔ1 ura3Δ52*	[38]
*cta1*Δ strain	YPH250 cells with *cta1::TRP1*	[38]
*ctt1*Δ strain	YPH250 cells with *ctt1::URA3*	[38]
wild-type BY4741	*MATahis3Δ1 leu2Δ0 met15Δ0 ura3Δ0*	EUROSCARF
*cta1*Δ strain	BY4741 cells with *cta1::KAN4MX*	EUROSCARF
*ctt1*Δ strain	BY4741 cells with *ctt1::KAN4MX*	EUROSCARF

5.4.2) Challenge of yeast cells with exogenous H_2O_2

Cultures were grown to mid-exponential phase (12 h; OD_{600}=0.5) under the conditions described above. Cells were washed twice with 100 mM potassium phosphate buffer, pH 7.4 (KPi), collected by centrifugation at 2000xg for 10 min at 25 °C and divided into two fractions. The fractions were resuspended in the YPD from the original culture (spent YPD) or in KPi, and challenged with H_2O_2 at 30 °C for 1.5 h with shaking at 225 rpm and a flask-to-medium volume ratio of 1:5. Following the challenge, the cultures were serially diluted, plated on YPD agar medium and incubated at 30 °C for 2 days [20]. Cell viability was determined by counting the total colony forming units (cfu) in H_2O_2-challenged and untreated cultures.

To examine adaptation, cells grown for 12 h in YPD as described above, were pre-challenged with 0.2 mM H_2O_2 at 30 °C for 1 h, switched to KPi and challenged with 2 mM H_2O_2 at 30 °C for 1.5 h (YPD/KPi column, Fig. 5. 1). Alternatively, cells grown for 12 h in YPD were switched to KPi and pre-challenged and challenged in this medium without buffer exchange (KPi column, Fig. 5. 1). Viability of pre-adapted cells (Fig. 5. 5B) is expressed as the ratio of the cfu following the lethal H_2O_2 challenge divided by the cfu following the 1 h pre-adaption.

5.4.3) Preparation of soluble protein extracts

These were prepared as previously described [20, 83] with slight modification. Cells were collected at 2000xg, washed twice with KPi containing 0.1 mM PMSF, the pellets were suspended in the same buffer, and mixed with an equal volume of acid-washed glass beads. Cell suspensions were vortexed (4x15s cycles), cell debris was removed by centrifugation at 13000xg for 10 min at 4 ºC, and the total protein concentration in the supernatants (*i.e.*, the soluble protein extracts) was determined by the Bradford assay with bovine serum albumin as a standard [104].

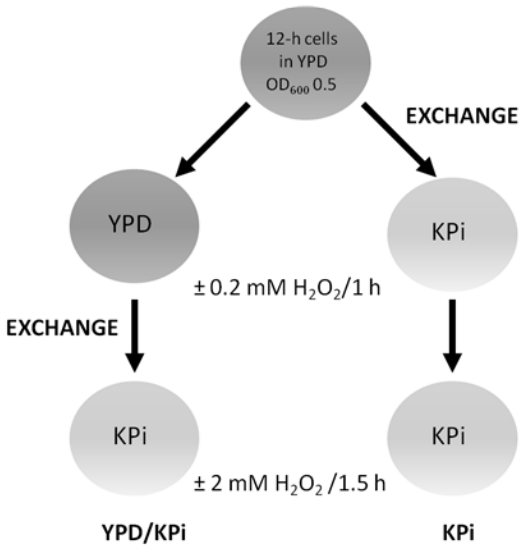

Fig. 5. 1 *Pre-adaptation of YPH250 yeast cells to H_2O_2.* Left row (YPD/KPi): Cells grown in YPD for 12 hat 30 °C were pre-challenged with 0.2 mM H_2O_2 at 30 °C for 1 h, switched to KPi and challenged with 2 mM at 30 °C for 1.5 h. Right row (KPi): cells grown in YPD for 12 h at 30 °C were switched to KPi, pre-challenged with 0.2 mM H_2O_2 at 30 °C for 1 h, and challenged with 2 mM at 30 °C for 1.5 h. Following challenge, both cultures were assayed for cell viability and catalase activity as described under *Materials and Methods*.

5.4.4) Catalase activity assay

The catalase activity of the soluble protein extracts was assayed as described previously [105]. Briefly, 40–100 μL of extract was added to 1.0 mL of 20 mM H_2O_2 in 50 mM KPi buffer (pH 7.0), and H_2O_2 decomposition was monitored at 240 nm (ε_{240}=43.6 M^{-1} cm^{-1}) [105]. One unit of catalase activity catalyzed the degradation of 1 μmol of H_2O_2 per min.

5.5) Results

5.5.1) Ctt1 activity is stimulated on H_2O_2 challenge in YPD and increases cell survival

We first compared catalase activity and cell viability after exposing wild-typeYPH250 and wild-type BY4741 cells to increasing doses of H_2O_2 in nutrient-rich YPD medium. Challenge of YPH250 cells with 0.2 and 0.4 mM H_2O_2 stimulates their catalase activity by 8- and

10-fold, respectively (Fig. 5. 2A), and the cells remain 100% viable (Fig. 5. 2B). Increasing the H_2O_2 dose to 1 mM and 2 mM results in weak catalase simulation and inhibition, respectively (Fig. 5. 2A) and a 50-80% drop in cell viability (Fig. 5. 2B). Notably, H_2O_2 induces loss of viability in YPH250 cells with ~7 U of catalase activity per mg protein (Fig. 5. 2A) which, significantly, is also observed for wild-type BY4741 cells (Fig. 5. 2C,D). In this strain the maximum stimulated catalase activity is close to 10 U per mg protein (Fig. 5. 2C) and cells become sensitive to H_2O_2 at 0.4 mM (Fig. 5. 2D). Interestingly, both strains require ~10 U of catalase activity per mg protein for protection against a bolus of H_2O_2 in the low millimolar range and in the absence of catalase stimulation, the observed viability drops below 25% (Fig. 5. 2; Fig. 5. 3). In sum, stimulation of catalase activity is required for protection of exponentially growing yeast against exogenous H_2O_2, and enhanced catalase stimulation renders YPH250 cells more resistant to H_2O_2 than BY4741 cells (Fig. 5. 2A,B vs Fig. 5. 2C,D).

S. cerevisiae possess two catalase isoforms, a peroxisomal/mitochondrial Cta1 [111] and an atypical cytosolic Ctt1 [110]. Hence, we next addressed the relative importance of each isoform in protecting cells against H_2O_2 challenge using the single catalase knockouts, *ctt1*Δ and *cta1*Δ. Comparable catalase activity is induced in wild-type and *cta1*Δ YPH250 cells after H_2O_2 (Fig. 5. 3A,B,D) but negligible catalase induction occurs in the *ctt1*Δ mutant strain (Fig. 5. 3C,D). Similar results were observed for the catalase knockouts in the BY4741 genetic background (data not shown). Combined, our data indicate that cytosolic Ctt1 activity is stimulated ~ 10-fold by exogenous H_2O_2 in YPD, consistent with the 15-fold increase in production of the Ctt1 protein on H_2O_2 challenge in SCD [42]. Furthermore, *cta1*Δ cells exhibit wild-type resistance to H_2O_2 (Fig. 5. 3E), whereas the *ctt1*Δ mutant exhibits H_2O_2 hypersensitivity with cell viability dropping by 30% on challenge with 0.2 mM H_2O_2 (Fig. 5.

3E). H_2O_2 challenge in YPD does not upregulate Cta1 activity (Fig. 5. 3C) and no increase in Cta1 protein levels were detected on H_2O_2 challenge in SCD [42]. Thus, we conclude that stimulation of cytosolic Ctt1 activity on H_2O_2 challenge in YPD is a critical factor in protecting cells against this ROS.

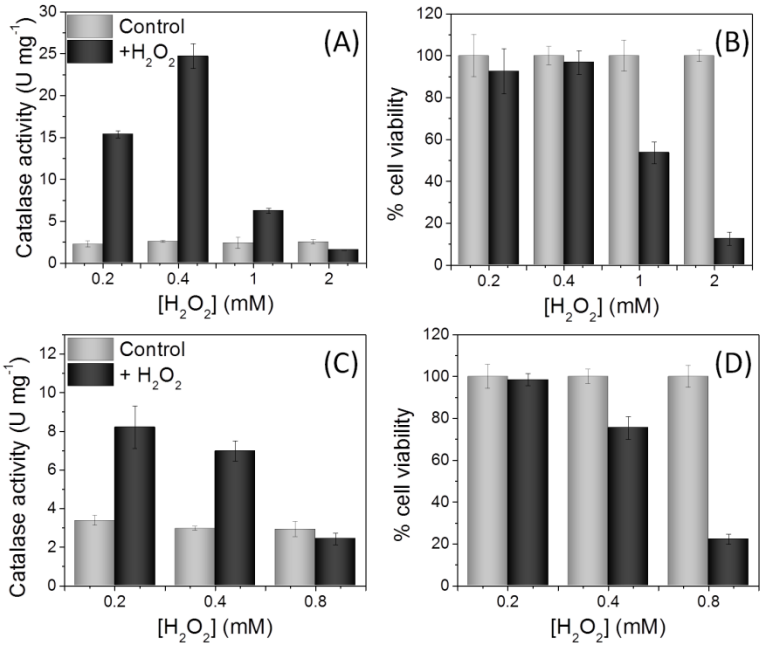

Fig. 5. 2 *Induction of catalase activity correlates with survival of exponentially growing yeast on H_2O_2 challenge in YPD medium.* Total catalase activity (left panels) and cell viability (right panels) of wild-type yeast cells in the YPH250 (A and B, respectively) and BY4741 (C and D, respectively) genetic backgrounds following H_2O_2 challenge. Exponentially growing cells (12 h, OD_{600}=0.5) in YPD medium were exposed to KPi (control, grey bars) or challenged with 0.2–2 mM H_2O_2 (black bars) for 1.5 h at 30 °C and 225 rpm. Catalase activity and cell viability were measured as described under *Materials and methods*.

5.5.2) Ctt1 upregulation is abolished on H_2O_2 challenge in KPi and cell viability is lower

Izawa *et al.* [38] reported that single or double deletion of the catalase isoforms does not alter sensitivity to H_2O_2 when YPH250 cells are challenged in KPi. We hypothesized that H_2O_2 challenge of starving wild-type cells in KPi might lead to negligible stimulation of Ctt1 activity

since this involves *de novo* Ctt1 protein synthesis [42] and in addition NADPH is required to prevent catalase inactivation during turnover [205]. Hence, we switched YPH250 cells from YPD to KPi and found that challenge in buffer with >0.2 mM H_2O_2 significantly inhibits catalase activity in wild-type and *cta1*Δ cells (Fig. 5. 4A,B,D) in contrast to the stimulation observed in YPD (Fig. 5. 3A,B,D). Thus, we propose that starvation prevents induction of Ctt1 activity by attenuating *de novo* Ctt1 synthesis and/or by promoting NADPH depletion. Furthermore, we speculate that variation in NAPDH depletion rates following the YPD-KPi switch may contribute to the relatively large variation in catalase activity of unchallenged cells in KPi (Fig. 5. 4A-C). Nevertheless, all three strains exhibit comparable H_2O_2 hypersensitivity in KPi (Fig. 5. 4) and the protective effect of Ctt1activity seen in YPD (Fig. 5. 3E) is obliterated on nutrient withdrawal.

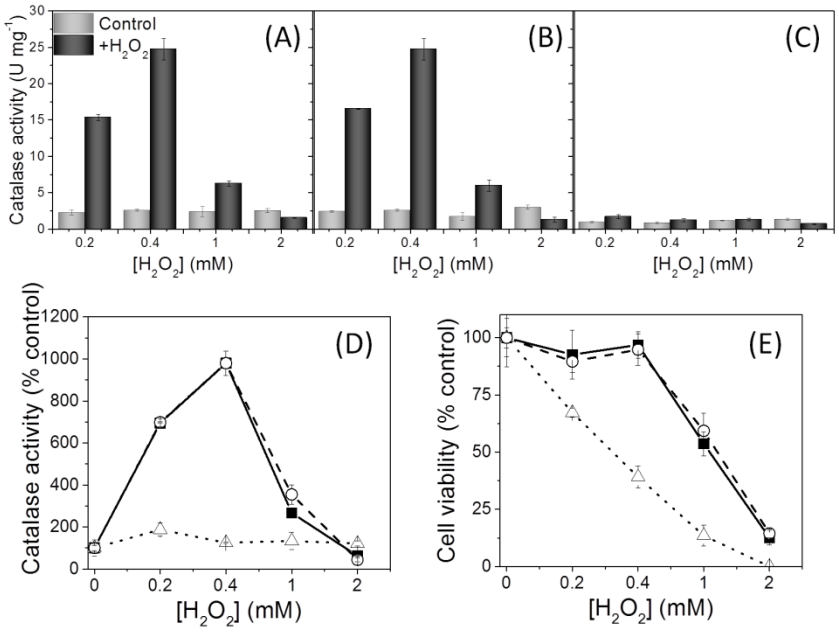

Fig. 5. 3 *Deletion of cytosolic catalase T (CTT1) results in hypersensitivity of exponentially growing YPH250 cells to H_2O_2 challenge in YPD medium.* Catalase activity before and after H_2O_2 challenge of: (A) wild-type cells producing both Ctt1 and Cta1; (B) *cta1*Δ cells producing cytosolic Ctt1 only; and (C) *ctt1*Δ cells producing peroxisomal/mitochondrial Cta1 only. (D) Catalase activity and (E) cell viability following H_2O_2 exposure relative to the control (no H_2O_2) for wild-type (solid squares), *cta1*Δ (open

circles) and *ctt1*Δ cells (open triangles). Exponentially growing cells in YPD medium were challenged after 12 h (OD_{600}=0.5) with 0.2–2 mM H_2O_2 for 1.5 h at 30 °C and 225 rpm. Catalase activity and cell viability were measured as described under *Materials and Methods*. Lines between the data points in panels D and E were added as a visualization aid.

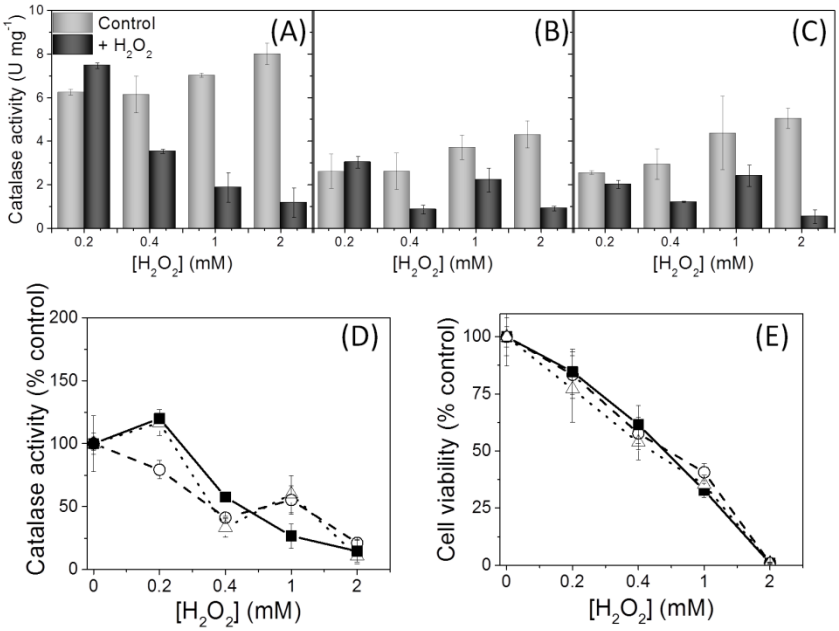

Fig. 5. 4 *H_2O_2 challenge in KPi impairs catalase activation in YPH250 cells.* Catalase activity before and after H_2O_2challenge relative to the control (no H_2O_2) of: (A) wild-type cells producing both Ctt1 and Cta1; (B) *cta1*Δ cells producing cytosolic Ctt1 only; and (C) *ctt1*Δ cells producing peroxisomal/mitochondrial Cta1 only. (D) Catalase activity and (E) cell viability following H_2O_2 exposure relative to the control (no H_2O_2) for wild-type (solid squares), *cta1*Δ (open circles) and *ctt1*Δ (open triangles) cells. Exponentially growing cells in YPD medium were washed twice after 12 h (OD_{600}=0.5), suspended to the same OD_{600} in KPi, and challenged with 0.2–2 mM H_2O_2 for 1.5 h at 30 °C and 225 rpm. Catalase activity and cell viability were measured as described under *Materials and Methods*. Lines between the data points in panels D and E were added as a visualization aid.

5.5.3) Wild-type cells become H_2O_2-adapted on pre-challenge with 0.2 mM H_2O_2 in YPD but not in KPi

Challenge of yeast cells with sublethal doses of a stressor activates stress-response signaling pathways to make cells more resistant to the stressor, a phenomenon known as

adaptation [38, 41, 46, 206]. Izawa *et al.* pre-challenged wild-type YPH250 cells in YPD with 0.2 mM H_2O_2, a sublethal concentration, and observed increased resistance to higher H_2O_2 levels [38]. This is consistent with the results in Fig. 5. 2A, which demonstrates that exposure of wild-type YPH250 cells to 0.2 mM H_2O_2 in YPD results in an 8-fold increase in catalase activity. However, catalase upregulation is negligible in KPi (Fig. 5. 4A) so pre-challenge with a low dose of H_2O_2 in YPD but not in KPi (Fig. 5. 4A) should protect cells against a subsequent challenge with a lethal H_2O_2 dose. To test this, wild-type cells were pre-adapted with 0.2 mM H_2O_2 in YPD or KPi and challenged with 2 mM H_2O_2 in KPi (Fig. 5. 1). Cells pre-adapted in YPD exhibited ~10-fold higher catalase activity and ~60-fold higher viability than non-adapted cells (Fig. 5. 5A,B). In contrast, pre-challenge in KPi abrogates the adaptive response to H_2O_2 and exposure of starving cells to 0.2 mM H_2O_2 prior to challenge with 2 mM H_2O_2 actually lowers their viability compared to challenge with a single high dose of H_2O_2 (Fig. 5. 5A). On the other hand, the dramatic increase in catalase activity and cell survival on pre-adaptation in YPD (Fig. 5. 5) further demonstrates that cell viability on H_2O_2 challenge is clearly linked to the stimulation of catalase activity. Izawa *et al.* [38] concluded that catalase is important in H_2O_2 adaptation but not in direct H_2O_2 challenge because of their experimental design. H_2O_2 challenge of non-adapted cells was performed in KPi so cells were unable to increase their catalase activity and respond to the stress [38, 71]. In contrast, cells were pre-adapted in YPD so the induced catalase activity protected cells against subsequent lethal H_2O_2 challenge [38]. Had they also pre-adapted the cells in KPi, the protective effects of catalase would have been lost (Fig. 5. 5). Notably, Wieser *et al.* observed that mild heat shock of cells in YPD induced H_2O_2 adaptation via increased *CTT1* expression, consistent with the reported protective effects of heat shock against oxidative stress [46].

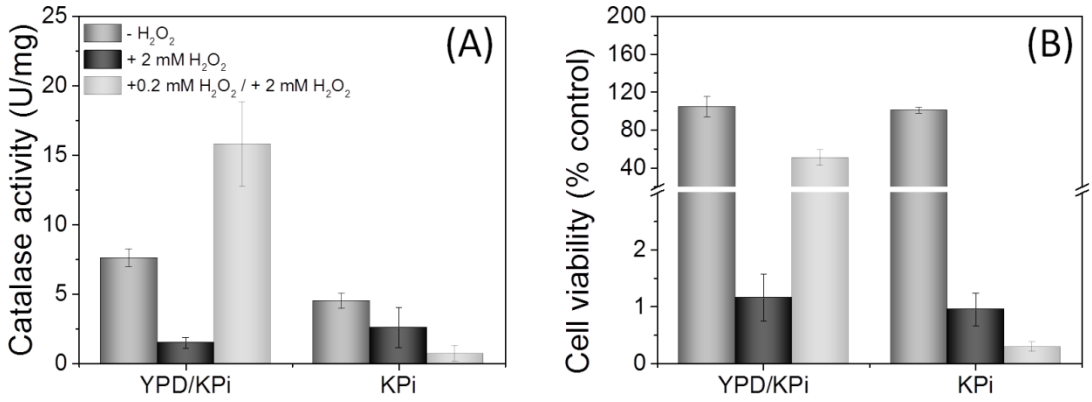

Fig. 5. 5 *Adaptation of wild-type YPH250 cells to H_2O_2 challenge requires nutrient-rich medium to stimulate catalase activity.* Catalase activity (A) and cell viability (B) without (control) and with pre-adaption of cells to H_2O_2 followed by challenge with a lethal H_2O_2 dose. Exponentially growing cells in YPD medium for 12 h (OD_{600}=0.5) were pre-challenged with 0.2 mM H_2O_2 for 1 h in YPD or in KPi (see Fig. 5. 1) followed by challenge with 2 mM H_2O_2 in KPi for 1.5 h (see Fig. 5. 1). Note that control cells were incubated for 1.5 h (YPD/KPi) and 2.5 h (KPi) in the absence of glucose and likely started to respire, which may explain their higher catalase activity relative to control cells in Fig. 5. 2A. Additionally, the switch of cells from YPD to KPi increases catalase activity of control cells as shown in Fig. 5. 3 vs Fig. 5. 4A. Cell viability and catalase activity were measured as described under *Materials and methods*.

5.6) Discussion

Here we demonstrate that cytosolic Ctt1 activity is induced on H_2O_2 challenge of yeast cells in nutrient-rich YPD medium (Fig. 5. 6). Catalase provides protection against H_2O_2 stress, consistent with its being a highly efficient H_2O_2 scavenger. Critically, H_2O_2 challenge of starving cells expressing the *CTT1* gene in KPi prevents upregulation of Ctt1 activity and masks the hypersensitivity of *ctt1*Δ cells to this ROS (Fig. 5. 6).

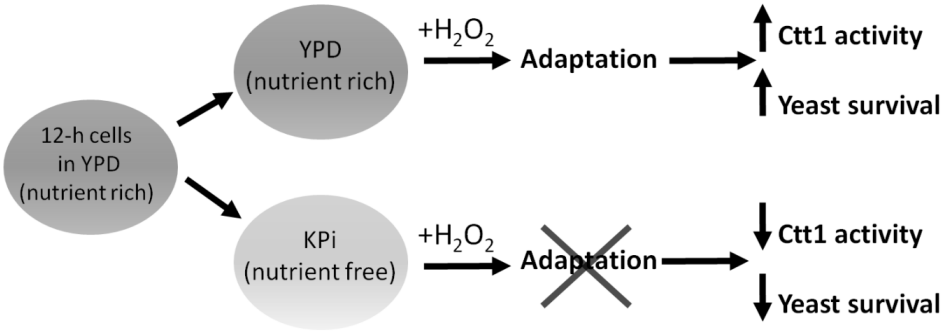

Fig. 5. 6 *Summary of nutrient-dependent catalase activation on challenge with exogenous H_2O_2.* When nutrients are present during H_2O_2 challenge (YPD) yeast cells adapt to the stress by increasing catalase activity, which results in higher survival rates. H_2O_2 challenge in nutrient-depleted media (KPi) prevents adaptation and catalase activation, which results in lower survival (published as graphical abstract in [171]).

Although catalases have been studied for many years, there are conflicting reports regarding their protective role on H_2O_2 challenge [38, 42, 71]. Yeast strains with different genetic backgrounds were examined but the nutrient status of the growth medium is likely the more critical parameter controlling the outcome of H_2O_2 challenge. For example, a dramatic H_2O_2-induced catalase upregulation was observed in cells challenged in SCD [42] but not in cells challenged in KPi [38]. H_2O_2 adaption experiments yielded more consistent results but cells were pre-challenged only in nutrient-rich media [38, 46]. Since catalases are synthesized *de novo* in response to endogenous or exogenous H_2O_2 challenge or pre-challenge [42, 46, 110], nutrients are necessary for their induction and few studies report on catalase activity pre- and post-H_2O_2 challenge [71].

Abundant antioxidants such as glutathione, protect yeast cells on H_2O_2 challenge even in nutrient-free medium [39]. However, glutathione levels can be as high as 10 mM in yeast cytosol [21]. Also, H_2O_2 challenge in nutrient-free medium may reveal the importance of highly abundant, constitutively produced antioxidant enzymes such as glutathione and thioredoxin

peroxidases, whereas information on H_2O_2-induced antioxidant defenses such as catalases is lost. Furthermore, some peroxidases perform roles in addition to H_2O_2 removal. For example, thioredoxin peroxidase 1 (Tsa1), the most abundant cytosolic peroxiredoxin in yeast, is converted to a dodecameric chaperone on H_2O_2 stress [87], and is likely critical in protecting other proteins against H_2O_2-induced misfolding. Therefore, the striking phenotype of H_2O_2 hypersensitivity and poor growth on *TSA1* deletion [30] may be due mainly to loss of its chaperone rather than H_2O_2-scavenging function. Deletion of glutathione peroxidase 3 (Gpx3), but not knockout of the Gpx1 and Gpx2 isoforms, results in a dramatic increase in H_2O_2 sensitivity [40]. This may be attributed to the non-redundant sensor function of Gpx3 [48, 49, 207] in activation of the Yap1-dependent oxidative stress response [48, 49]. In essence, the importance of highly abundant antioxidant enzymes, especially those with chaperone or signaling functions, may be apparent on challenge in nutrient-free medium whereas the contribution of less abundant, inducible enzymes such as catalases can be masked in starving cells due to the lack of *de novo* protein synthesis and/or repair.

We also observed that when the catalase activity drops below a threshold level of ~10 U per mg protein, YPH250 and BY4741 cells become sensitive to exogenous H_2O_2. Based on our results, H_2O_2 becomes lethal to *S. cerevisiae* when it overwhelms the cell's inducible Ctt1 activity as this leads to a significant loss of cell viability. For example, on challenge of YHP250 cells with ~2 mM H_2O_2 the catalase activity drops to the basal level and cell viability plummets (Fig. 5. 2A,B). BY4741 cells respond similar manner on challenge with only 0.8 mM H_2O_2 (Fig. 5. 2C,D). We speculate that turnover inactivation by excess H_2O_2 lowers catalase activity and induction of apoptosis-like death [99] may play a role in the resulting high cell death rates.

5.7) Conclusions

We identified Ctt1 as essential in protecting yeast cells against exogenous H_2O_2 and unmasked the H_2O_2-hypersensitive phenotype of *ctt1*Δ cells. More generally, our results reveal that investigations of the relative importance of an antioxidant enzyme should consider: (1) its relative abundance, (2) its inducible vs constitutive expression, (3) nutrient availability for triggering its induction, and (4) the stressor dose that causes its inactivation. Specifically, when analyzing the role of yeast catalases we found that it is critical to provide nutrients for the cell to respond to the H_2O_2 insult by *de novo* Ctt1 synthesis and likely enhanced NAPDH generation. Furthermore, catalase deletion by genetic intervention had to be complemented by activity measurements before and after H_2O_2 challenge to uncover the importance of Ctt1 activity in defending cells. Thus, our work emphasizes the necessity of *directly* measuring the enzyme activity of interest in wild-type and knockout cells before and after applying a stress. Equally important, inducible antioxidant defences should be examined in the presence of nutrients so cells can adapt to the challenge.

Chapter 6: Sod1 oxidation during aging of yeast

6.1) Preface

The work presented in this chapter corresponds to the following reference: Martins D, English AM (2014). **Sod1 oxidation and formation of soluble aggregates in yeast: Relevance to sporadic ALS development.** Redox Biology, 2, 632-639. The production and interpretation of all datasets, writing and revision of the manuscript were performed by me. Dr. Ann M. English contributed with the lab structure, equipment and reagents as well as the discussions, data analysis and revisions of the paper. The graphical abstract of the original paper was included in this chapter as Fig. 6. 6

6.2) Abstract of the manuscript

Misfolding and aggregation of copper-zinc superoxide dismutase (Sod1) are observed in neurodegenerative diseases such as amyotrophic lateral sclerosis (ALS). Mutations in Sod1 lead to familial ALS (FALS), which is a late-onset disease. Since oxidative damage to proteins increases with age it had been proposed that oxidation of Sod1 mutants may trigger their misfolding and aggregation in FALS. However, over 90% of ALS cases are sporadic (SALS) with no obvious genetic component. We hypothesized that oxidation could also trigger the misfolding and aggregation of wild-type Sod1 and sought to confirm this in a cellular environment. Using quiescent, stationary-phase yeast cells as a model for non-dividing motor neurons, we probed for post-translational modification (PTM) and aggregation of wild-type Sod1 extracted from these cells. By size-exclusion chromatography (SEC), we isolated two populations of Sod1 from yeast: a low-molecular weight (LMW) fraction that is catalytically active and a catalytically inactive, high-molecular weight (HMW) fraction. High-resolution mass

spectrometric analysis revealed that LMW Sod1 displays no PTMs but HMW Sod1 is oxidized at Cys146 and His71, two critical residues for the stability and folding of the enzyme. HMW Sod1 is also oxidized at His120, a copper ligand, which will promote loss of this catalytic metal cofactor essential for SOD activity. Monitoring the fluorescence of a Sod1-green-fluorescent-protein fusion (Sod1-GFP) extracted from yeast chromosomally expressing this fusion, we find that HMW Sod1-GFP levels increase up to 40-fold in old cells. Thus, we speculate that increased misfolding and inclusion into soluble aggregates is a consequence of elevated oxidative modifications of wild-type Sod1 as cells age. Our observations argue that oxidative damage to wild-type Sod1 initiates the protein misfolding mechanisms that give rise to SALS.

6.3) Introduction

Copper-zinc superoxide dismutase (Sod1) is an abundant, ubiquitous enzyme found in the cytosol [208], mitochondria [114, 208] and nucleus [208] of eukaryotic cells. It is critical in the detoxification of superoxide radicals produced during aerobic respiration and its deletion renders eukaryotes hypersensitive to oxygen [35]. The biophysical properties of Sod1 have been extensively studied since its misfolding and aggregation are associated with the development of late-onset neurodegenerative diseases such as Parkinson's, Alzheimer's and Amyotrophic Lateral Sclerosis (ALS) [10, 63]. Notably, close to 180 ALS-associated mutations have been reported in the human *SOD1* gene [6] and neurotoxicity is linked to their structural instability. The ALS mutant proteins appear more prone than wild-type Sod1 to aggregation into high molecular weight structures that form non-amyloid aggregates [10, 55, 56, 58], a hallmark of ALS [58, 209]. However, 90% of ALS cases are not linked to any known genetic mutation and are classified as sporadic ALS (SALS). The protein misfolding mechanisms underlying the development of SALS and FALS remain poorly understood. Human Sod1 was demonstrated to

have prion-like properties that can trigger its aggregation [210], but ALS may be distinct from other late-onset neurodegenerative diseases [10] in that non-amyloid aggregates contribute to its development [62, 211][212].

Oxidative damage is generally implicated in the misfolding of Sod1 mutants that cause FALS [62, 211][212] and oxidized proteins accumulate during cell aging [8, 64]. Paradoxically, its dismutase activity that forms H_2O_2 as a product may render Sod1 more susceptible to oxidative PTMs than other proteins [55, 58]. The redox-active catalytic Cu center of Sod1 displays pseudoperoxidase activity and exposure of the enzyme to excess H_2O_2 *in vitro* results in selective oxidation of Cu-coordinating residues with loss of catalytic activity and oligomerization [55, 58, 61, 213] by mechanisms that have not been fully elucidated [119, 214]. Cu is ligated to His46, His48, His120 and to His63, which bridges Cu to the Zn cofactor (Fig. 6. 1). Zn is also coordinated to His71, His80 and Asp83 (Fig. 6. 1), and plays an important structural role that stabilizes the Sod1 homodimer [58]. Additionally, Cys57 and Cys146 form an intrasubunit disulfide that facilitates coordination of the histidine residues to the metal cofactors and also stabilizes the enzyme [58]. Thus, oxidation of a Zn ligand with loss of the metal [62, 215] or disruption of the Cys57-Cys146 disulfide also destabilize the enzyme and promote its aggregation [215]. Since wild-type Sod1 is oxidized by H_2O_2 *in vitro* [61, 216], this could also occur *in vivo*. Increased oxidative stress has been associated with both FALS and SALS [10, 217], and increased protein oxidation has been detected by oxyblot in transgenic mouse models of ALS [10, 217, 218]. However, the oxidized Sod1 does not accumulate in the livers of aging rats [65], so despite strong links between oxidative stress and ALS, oxidative PTMs in Sod1 have not been correlated with pathogenicity.

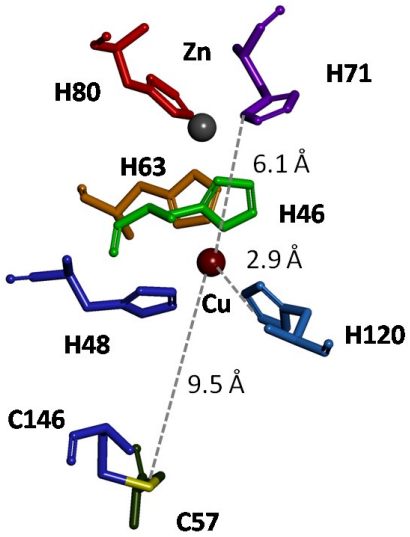

Fig. 6. 1 *Active-site residues in Sod1*. The catalytic Cu cofactor is coordinated to His46, His48, His120 and bridging His63. The structural Zn cofactor is coordinated to His63, His71 and His80 as well as aspartic acid Asp83 (not shown). The intrasubunit disulfide bridge between Cys57 and Cys146 is important in stabilizing the Sod1 homodimer [55, 58, 215]. The distances from Nε of His120 and His71, and the Cys57-Cys146 disulfide bridge to the catalytic Cu (2.1, 6.9 and 9.5 Å, respectively) were measured in the 1.15-Å resolution crystal structure of human Sod1 (PDB 2V0A).

Liver protein turnover is relatively rapid so modified protein accumulation in this organ may be less than in other tissues. Thus, in order to probe for specific sites of Sod1 oxidation in an aging cellular environment, we selected stationary-phase yeast. In this state, yeast cells are non-dividing [67] and in this respect resemble other quiescent cells such as motor neurons [68, 69, 174, 219]. However, yeast rapidly age [67], which allows protein modification to be examined over a cell's lifespan in a matter of weeks rather than years. Furthermore, yeast and human Sod1 share 70% homology and over 90% identity in their active-site residues.

We report here that distinct populations of Sod1 exist in stationary-phase yeast. A low molecular weight, catalytically active fraction with the mass (~32 kDa) of the native Sod1 dimer (LMW Sod1) and a soluble, high molecular weight, catalytically inactive fraction, with a mass over 300 kDa (HMW Sod1). High-resolution mass spectrometry (MS) revealed negligible

oxidation in LMW Sod1 but HMW Sod1 was oxidized at residues critical for SOD activity and enzyme stability, suggesting that oxidative damage may trigger Sod1 inclusion into soluble HMW aggregates. Furthermore, HMW Sod1-GFP levels increased dramatically in old yeast chromosomally expressing this fusion, pointing to increased Sod1 oxidation with age. The possible relevance of oxidative PTM of Sod1 in SALS development is discussed.

6.4) Materials and methods

6.4.1) Yeast strains, media, and growth conditions

The BY4741 *Saccharomyces cerevisiae* strains used in this study are listed in Table 6. 1. Wild-type BY4741 was purchased from the European *Saccharomyces cerevisiae* Archive for Functional Analysis (EUROSCARF, Frankfurt, Germany). The BY4741 strain expressing chromosomal *SOD1* C-terminally tagged with green fluorescent protein was kindly provided by Prof. Christopher Brett (Department of Biology, Concordia University). The two strains were grown in YPD liquid medium (1% yeast extract, 2% peptone and 2% glucose) at a flask-to-medium volume ratio of 1:5. The cultures at an initial OD_{600}=0.01 were incubated at 30 °C with shaking at 225 rpm. The spent YPD medium was replaced with 0.85% NaCl solution (w/v) after 72 h to transform cells into stationary phase, a quiescent, non-dividing state [68, 69, 174].

Table 6. 1 *S. cerevisiae* strains used in this study

Strain	Description	Reference
wild-type BY4741	*MATa his3Δ1 leu2Δ0 met15Δ0 ura3Δ0*	EUROSCARF
Sod1-GFP expressing strain	BY4741 cells with *SOD1-GFP*	This work

6.4.2) Preparation of soluble protein extracts

These were prepared as previously described [83]. Cells were collected at 2000xg, washed twice with 20 mM KPi (pH 7.0) containing 0.1 mM PMSF, the pellets were suspended in the same buffer ±0.1 M iodoacetamide, and mixed with an equal volume of acid-washed glass beads. Cell suspensions were vortexed (4x15 s cycles), cell debris was removed by centrifugation at 13000xg for 10 min at 4 ºC, and the total protein concentration in the supernatants (*i.e.*, the soluble protein extracts) was determined by the Bradford assay with bovine serum albumin as a standard [104].

6.4.3) Fractionation of soluble protein extracts by size-exclusion chromatography (SEC)

Extracts from wild-type and Sod1-GFP-producing yeast strains were fractionated by SEC on a Superose 12 HR 10/30 column (Amersham; total volume 25 mL; void volume 7 mL; fractionation range 1–300 kDa) coupled to an ÄKTApurifier 10. The SEC column was equilibrated with 20 mM KPi/300 mM NaCl (pH 7.0), 1 mL of extract (0.1–0.4 mg total protein) in 20 mM KPi (pH 7.0) was loaded on the column. Proteins were eluted with the equilibration buffer at a flow rate of 0.3 mL/min, and detected spectrophotometrically at 280 nm. SEC fractions of 1 mL were collected and probed for Sod1 by SOD activity assay and immunodot blotting. Extracts containing Sod1-GFP were analyzed using the same Superose 12 HR column attached to an Agilent 1100 HPLC with a fluorescence detector to monitor GFP in the eluate (ex/em 470/520 nm).

6.4.4) In-gel SOD activity assay

SOD activity in the SEC fractions was assayed in native polyacrylamide gels to separately measure the activity of the Sod1 and Sod2 isoforms present in yeast [106]. The

unfractionated soluble protein extracts and the SEC fractions containing 1–5 μg total protein were electrophoresed in 12% resolving gels at 50 mA for 2 h at 4 ºC. The gels were incubated for 30 min at 20 ºC in the dark with a staining solution (0.17 mM NBT, 6.7 mM TEMED and 0.3 mM riboflavin in 100 mM KPi, pH 7.2), rinsed twice with distilled water and exposed to white light from a 60-W mercury lamp for 60 min, and scanned on an AlphaImager (AlphaInnotec) to quantify the optical densities of the negative bands containing SOD activity by ImageJ software.

6.4.5) Immunodetection of Sod1 in the SEC fractions

These fractions were probed for the Sod1 protein by immunodot blot. Briefly, a 10 μL drop of the unfractionated soluble protein extract or of a SEC fraction containing 5–20 μg protein was spotted onto a methanol-soaked PVDF membrane and allowed to dry for 10 min at room temperature. The membrane was blocked for 1 h in TBST (50 mM Tris, 150 mM NaCl and 0.05% Tween 20 v/v, pH 7.6) containing 5% skimmed milk (wt/v), and incubated with rabbit anti-human Sod1 antibody (Stressgen; dilution 1:1,000) in 1% milk/TBST for 3 h at room temperature. After washing with TBST, the membrane was incubated for 1 h with goat anti-rabbit HRP-conjugated secondary antibody (BioRad; dilution 1:10,000) diluted in 1% milk/TBST. Sod1-containing peaks were detected by chemiluminescence using an ECL kit (Thermo Fisher) and the membrane was scanned on the AlphaImager.

6.4.6) SDS-PAGE and trypsin digestion of SEC fractions

The SEC fractions containing Sod1 protein were decomplexified by 1D SDS-PAGE under reducing conditions on 6% stacking and 12% resolving gels. After 1 h electrophoresis at 120 V, the gels were Coomassie stained and 4 slices 1-cm wide were excised between the 10 and 25-kDa MW markers that bracket the mass of the Sod1 monomer (16 kDa). In this mass range, we selected for aggregates stablized by non-covalent bonds (disulfides were reduced) to

maximize sequence coverage by mass spectrometry as discussed below. Following destaining with 5% acetonitrile in 50 mM aqueous ammonium bicarbonate (pH 7.5), proteins in the gel slices were reduced with 10 mM DTT for 30 min at 60 °C, and alkylated with 55 mM iodoacetamide for 30 min at room temperature. The gel slices were separately incubated overnight with trypsin at 37 °C and the peptides were extracted from the gel slices with 60% acetonitrile in 50 mM aqueous ammonium bicarbonate (pH 7.5) for analysis by LC-MS.

6.4.7) LC-MS screening for oxidative PTMs in Sod1

Tryptic peptides (5 µL/injection) were separated on a home-made reversed-phase C18 column (0.75 µm ID x7.5 cm) attached to an Easy NanoLC 1000 (Thermo Scientific) using a 2–94% acetonitrile gradient in 0.1% aqueous formic acid at a flow rate of 200 nL/min. The nanoLC output was directed into the ESI source of a LTQ Orbitrap Velos mass spectrometer (Thermo Scientific) and analyzed in full-scan mode using the Orbitrap high resolution mass analyzer (m/z range 350–3,000; resolution 60,000 at m/z 400). Other MS parameters were electrospray voltage 3 kV, CID collision energy 30 V and heated capillary temperature 200 ºC. Precursor ions of the Sod1 peptides were selected using a mass exclusion threshold of 10 ppm and subjected to MS/MS in the Velos linear ion trap mass analyzer using a mass tolerance of 0.8 u for the fragment ions. MS/MS fragments with an intensity count of 20 or greater were analyzed using Proteome Discoverer 1.3.0 (Thermo Scientific) and the Sequest search engine with mass filters for oxidation (+16, +32, +48 u) of Met, Cys, Trp, Tyr; and Cys alkylation by iodoacetamide (+57 u) or acrylamide (+71 u). Sequest correlated the MS/MS spectra with peptide sequences in the yeast proteome database downloaded from the NCBI website (ftp://ftp.ncbi.nlm.nih.gov/). For confident identification of Sod1, the following Sequest filters were implemented: Score >30, XCorr ≥2, False Discovery Rate <0.01 and a minimum of two

unique peptides. The Score is the probability that the identified protein is a correct match based on a comparison of its experimental and theoretical MS/MS spectra. XCorr is the cross-correlation between the theoretical and experimental MS/MS spectra of the sequenced peptides. Unique peptides are those present in Sod1 only and absent from all other proteins in the yeast database. Table S6 1 lists the precursors ion analyzed by MS/MS and Table S6 2, Table S6 3, and Table S6 4 (Supplementary information) summarize the *b* and *y* sequence used to assign the PTMs.

6.5) Results

6.5.1) Catalytically inactive Sod1 is present in HMW fractions from the SEC column

SEC fractionation of the soluble protein extract from 7-day yeast cells yielded four resolved chromatographic peaks (P1–P4, Fig. 6. 2A) and shoulders appear on P3 and P4. Peak P1 elutes within the void volume of the column (7 mL) and hence contains soluble protein complexes or aggregates >300 kDa, the upper limit of the fractionation range of the Superose column. P2, P3 and P4 elute at 12, 18 and 20 mL, respectively, and contain increasingly smaller soluble proteins. SOD activity was detected only in the extract and P3 (Fig. 6. 2B, upper panel) but the immunodot blot reveals the presence of Sod1 protein in the extract, P1, P1′ (7 and 7.5 mL, respectively) and P3 (Fig. 6. 2B, lower panel). Hence, stationary-phase yeast cells contain HMW catalytically inactive populations of soluble Sod1 in addition to the expected LMW catalytically active enzyme.

6.5.2) HMW Sod1 is oxidized at Cys146, His120 and His71

To determine if PTMs are present in HMW Sod1, we examined aliquots of P1 by LC-MS with high mass resolution (R=60,000) and high mass accuracy (<10 ppm). The P1 and P1'

fractions in the immunodot blot (Fig. 6. 2B, lower panel) both come from the single unresolved SEC peak, P1 (Fig. 6. 2) and were combined for further analysis. The SEC peak P1 was subjected to 1D SDS-PAGE under reducing conditions (0.7 M 2-mercaptoethanol) (Fig. 6. 3), slices were excised from the gel, and following in-gel protein digestion, the tryptic peptide mixtures were extracted and analyzed by LC-MS/MS. The LMW Sod1 SEC fraction (P3) was treated in the same manner and a representative SDS-PAGE gel in shown in Fig. 3. Sod1 identification by LC-MS of its tryptic peptides gave high confidence Scores and ≥77% sequence coverage (Table 6. 2).

Sod1 peptides were present in two gel slices cut from lane P1 close to the expected MW of the Sod1 monomer (16 kDa) (Fig. 6. 3A). This suggests that treatment with SDS detergent converts HMW Sod1 into LMW species under reducing conditions. Nonetheless, a fraction of HMW Sod exhibits aberrant migration in SDS-PAGE since peptides from LMW Sod1 were detected only in the gel slice cut from lane P3 below the 15 kDa MW marker (Fig. 6. 3A). As expected, LMW Sod1 migrates within the mass range (14–17 kDa) reported for the native yeast Sod1 monomer in SDS-PAGE gels [220]. Notably, no Sod1 peptides were reliably detected in gel slices containing proteins with an apparent MW >30 kDa (data not shown).

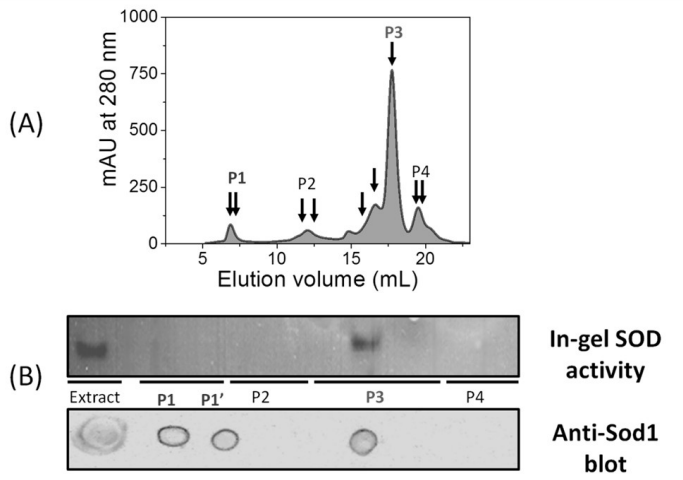

Fig. 6. 2 *SEC reveals presence of HMW and LMW Sod1 populations in the soluble protein extract from 7-day stationary-phase yeast cells.* (A) Size exclusion chromatogram of the extract. A 100-µL aliquot of extract containing 0.4 mg of protein was diluted to 1 mL with of 20 mM KPi (pH 7.0) and loaded on a Superose 12 HR 10/30 column (1.0 cm x 30 cm) equilibrated with 20 mM KPi/300 mM NaCl (pH 7.0) and connected to the ÄKTApurifier. Proteins were eluted with the equilibration buffer at a flow rate of 0.3 mL/min and detected at 280 nm. The arrows indicate the fractions that were tested for immunoreactivity and SOD activity. (B) Upper panel: in-gel Sod1 activity following native PAGE of the extract and the SEC fractions each containing 1 µg of total protein. Bands were stained with riboflavin as superoxide generator and NBT, which is reduced to formazan in presence of superoxide [106]. (B) Lower panel: Sod1 protein was detected by immunodot blot in the extract, two fractions of the SEC void volume P1 (7 mL) and P1′ (7.5 mL), and in P3 (18 mL). Samples containing 10 µg of protein were dotted onto PVDF membranes and probed with rabbit anti-human Sod1 antibody. See MATERIALS AND METHODS for additional information. Sod1 that was eluted in P1, P1′ and in P3 is referred to in the text as HMW Sod1 and LMW Sod1, respectively. P1 and P1′ were combined and treated as a single P1 fraction for LC-MS analysis. Proteins were extracted from three independent cultures and representative results are presented here.

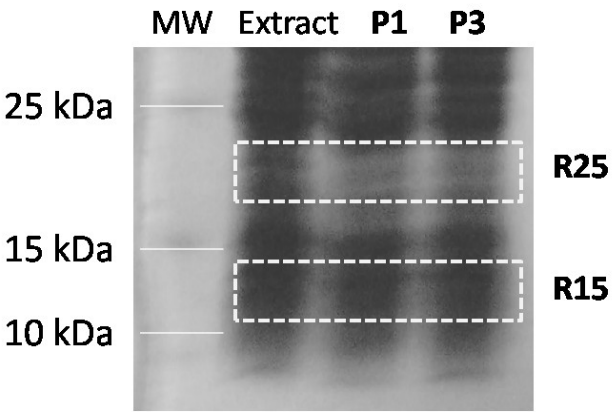

Fig. 6. 3 *Decomplexation of Sod1-containing SEC fractions by SDS-PAGE.* Aliquots (~25 µL) of the P1 and P3 SEC fractions from Fig. 6. 2A containing 20 µg of protein were analyzed by reducing SDS-PAGE. Bands were excised from lanes P1 and P3 of the gel and subjected to in-gel tryptic digestion. Digests from regions R15 and R25 (denoted by the white boxes) gave the highest score and sequence coverage so Table 6. 2 and Table 6. 3 summarize the LC-MS/MS results for these regions. Extracts from three independent cultures were analyzed and this gel is representative of the three (n=3). A white line indicates the center of each marker in lane MW since the molecular weight markers are poorly visible in the scanned gel (lane MW).

Table 6. 2 *LC-MS analysis of Sod1 peptides in P1 and P3* [a]

Sample	P1 (R15)	P1 (R25)	P3 (R15)
Score [b]	171	85	96
% Sequence coverage [c]	77	84	94
Unique peptides [d]	11/15	12/15	13/15

[a] The soluble proteins were extracted from three independent cultures, fractionated by SEC (Fig. 6. 2A) and SDS-PAGE (Fig. 6. 3), in-gel digested with trypsin and analyzed LC-MS (data not shown). P1 and P3 refer to the Sod1-containing SEC peaks in Fig. 6. 2A; R15 and R25 refer to regions of the SDS-PAGE gel in Fig. 6. 3. This table provides representative results from the three cultures.

[b] The Score calculated by the Proteome Discoverer software is the probability that the identified protein is a correct match based on a comparison of its experimental and theoretical MS/MS spectra. Scores were in the range of 65–171 for the three independent experiments.

[c] The % Sequence coverage corresponds to the number of residues in all the Sod1 peptides detected by MS divided by 154 residues in yeast Sod1. Sequence coverage was in the range of 68-94% for the three independent experiments.

[d] Unique peptides are those present in Sod1 only and absent from all other proteins in the NCBI yeast database (ftp://ftp.ncbi.nlm.nih.gov).

We next examined the Sod1 tryptic peptides for PTMs. LMW Sod1 peptides were alkylated at cysteine residues by the added iodoacetamide and by trace acrylamide in the gel. They were also oxidized at methionine residues but this likely occurs during sample processing since we frequently find oxidized methionine in peptides and in intact proteins analyzed by LC-MS. Importantly, no peptide derivatives were found in LMW Sod1 that we could attribute to PTM. Thus, we assume that LMW Sod1 was not oxidized *in vivo,* consistent with its retention of SOD activity (Fig. 6. 2B). In contrast, Cys146 is oxidized to the sulfonic acid in HMW Sod1 (Fig. 6. 4A) that migrates below the 15 kDa marker in SDS-PAGE (Fig. 6. 3). Although Cys146 and Cys57 form an intrasubunit disulfide bond, we did not detect oxidative modification of Cys57 in the samples analyzed. Cys146 was also oxidized in HMW Sod1 from the iodoacetamide-treated lysates (Table 6. 3) but alkylated in the corresponding LMW Sod1 sample. Hence, we conclude that Cys146 oxidation is a Sod1 PTM that occurs in intact cells and is not an artifact of sample preparation.

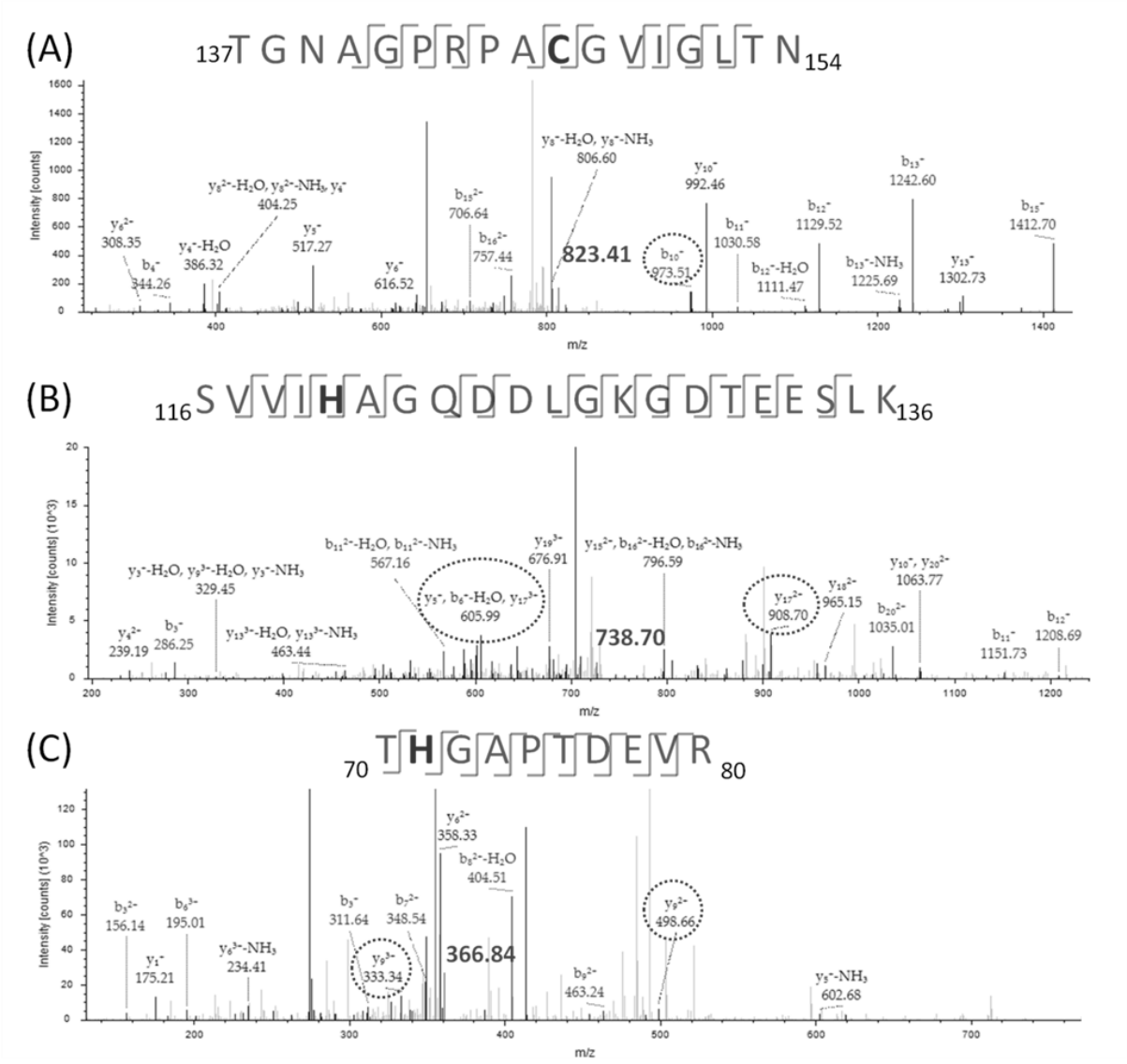

Fig. 6. 4 *HMW Sod1 is oxidized at Cys146, His71 and His120.* MS/MS spectrum of the: (A) $(M+2H)^{2+}$ ion at m/z 823.41 of the C-terminal peptide containing Cys146-SO_3H; (B) $(M+3H)^{3+}$ ion at m/z 738.70 of the oxo-His120 peptide; and (C) $(M+3H)^{3+}$ ion at m/z 366.84 of the oxo-His71 peptide. The peptide (precursor) ions (bold) (see Table S1 and sequence above spectra) were fragmented by CID (30 V) to give *b* (red) and *y* sequence ions (blue). The smallest visible *b* or *y* ion bearing the modified residue (See Tables S2-S4) is circled in each spectrum. The peptide ion match (number of *y*+*b* ions identified in the MS/MS spectrum divided by the theoretical number of *y*+*b* ions generated by CID) is (A) 18/32, (B) 22/80, and (C) 13/36. The XCorr values are (A) 2.5, (B) 2.0 and (C) 2.0. The MS operating parameters are given under *Materials and Methods.*

Table 6. 3 *Summary of oxidative modifications found in HMW Sod1 from 7-day yeast cells* [a]

	SDS-PAGE R15 region	SDS-PAGE R15 Region +IA	SDS-PAGE R25 Region	SDS-PAGE R25 Region +IA
% Sequence coverage [b]	77	78	84	74
Cys146 [c]	SO_3H	SO_3H	P [d]	A/P [d]
His120 [c]	none	none	Oxo-His	Oxo-His
His71 [c]	none	none	Oxo-His	Oxo-His

[a],[b] See footnotes a,c of Table 6. 2.

[c] PTMs at these residues detected in the MS/MS spectra of tryptic peptides (Fig. 6. 4) from HMW Sod1 present in region R15 or R25 of the SDS-PAGE gel (Fig. 6. 3). MS/MS spectra were recorded only for precursor ions found in LC-MS spectra (data not shown) that resulted in >70% sequence coverage.

[d] A/P, acetamide and propionamide adducts formed on reaction of cysteine sulfhydryl with iodoacetamide (IA) when added before cell lysis or with free acrylamide present in the gels during SDS-PAGE.

Aberrantly migrating HMW Sod1 cut from lane P1 of the gel above the 15 kDa marker (Fig. 6. 3), was also found to be oxidized. However, in this fraction, the targets are His120 and His71 rather than cysteine. In fact, the Cu ligand His120 is 100% oxidized to oxo-histidine (Fig. 6. 4B), which would explain the lack of SOD activity in P1 (Fig. 6. 2B, upper panel) since H_2O_2 exposure of purified Sod1 in solution results in oxidation of the Cu ligands His46, His48 and His120, and loss of SOD activity [61, 213, 216]. The Zn ligand, His71, is additionally 100% oxidized to oxo-histidine in this fraction (Fig. 6. 4C). Critycally, loss of Zn destabilizes the homodimer interface of Sod1 and results in monomer aggregation *in vitro* [215]. Hence, His71 oxidation *in vivo* could promote the aggregation that generated the soluble HMW Sod1 fractions in P1 (Fig. 6. 2A). We conclude that there are differential mechanisms of Sod1 oxidation in

stationary-phase yeast that result in its oxidation at Cys146, His120 or His71. These PTMs result in loss of catalytic activity and in the formation of soluble HMW Sod1-containing aggregates that are disrupted by detergent under reducing conditions. 6.5.3) HMW Sod1 content increases as yeast cells age

Since ALS and other neurodegenerative diseases are late-onset [10, 55, 58], we questioned if HMW Sod1 accumulation increased during yeast aging. Thus, we monitored Sod1-GFP fluorescence in SEC fractions from stationary-phase yeast cells expressing this fusion protein over several weeks. HMW Sod1-GFP fluorescence in P1 corresponds to 0.2% of the total Sod1-GFP fluorescence in the SEC fractions cells as cell begin to enter stationary phase (day 3, Fig. 6. 5A). However, this value climbs to 8%, a 40-fold increase, in 30-day cells before dropping significantly in 40- and 52-day cells (Fig. 6. 5B). Thus, Sod1-GFP aggregation increases as cell age but HMW Sod1-GFP may be converted in very old cells into insoluble aggregates that would be pelleted prior to SEC fractionation.

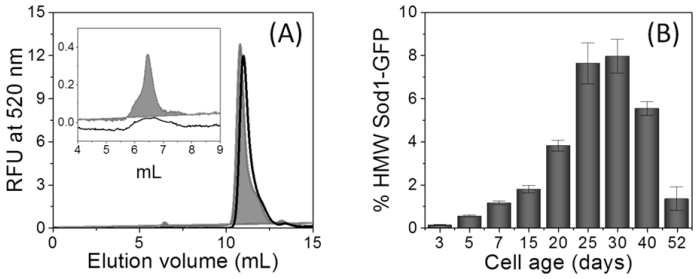

Fig. 6. 5 *HMW Sod1-GFP accumulates as yeast age but declines in very old cells.* Soluble protein extracts from cells chromosomally expressing Sod1-GFP were fractionated by SEC as described in the legend of Fig. 6. 2 except that the Superose column was coupled to an Agilent 1100 HPLC with a fluorescence detector, and GFP fluorescence was monitored with ex/em 470/520 nm. (A) Size-exclusion chromatogram of extracts from 3- (black line) and 7-day (grey line) cells. LMW Sod1-GFP is present in the intense peaks centered at ~11 mL and the inset shows a 100-fold expansion of the HMW Sod1-GFP fractions at 6.5 mL. (B) Variation with cell age of HMW Sod1-GFP as a percentage of the total peak area.

6.6) Discussion

A fraction of Sod1 is present in HMW aggregates and possesses oxidative PTMs in 7-day, stationary-phase yeast cells (Fig. 6. 4; Table 6. 3). Within these aggregates Sod1 is catalytically inactive and oxidized at Cys146, His71 or His120 (Fig. 6. 4). These three residues are critical for the folding and stability of the Sod1 homodimer, and their oxidation likely triggers formation of HMW Sod1 that is readily isolated from the soluble protein extracts by SEC (Fig. 6. 2). We summarized these observations in Fig. 6. 6.

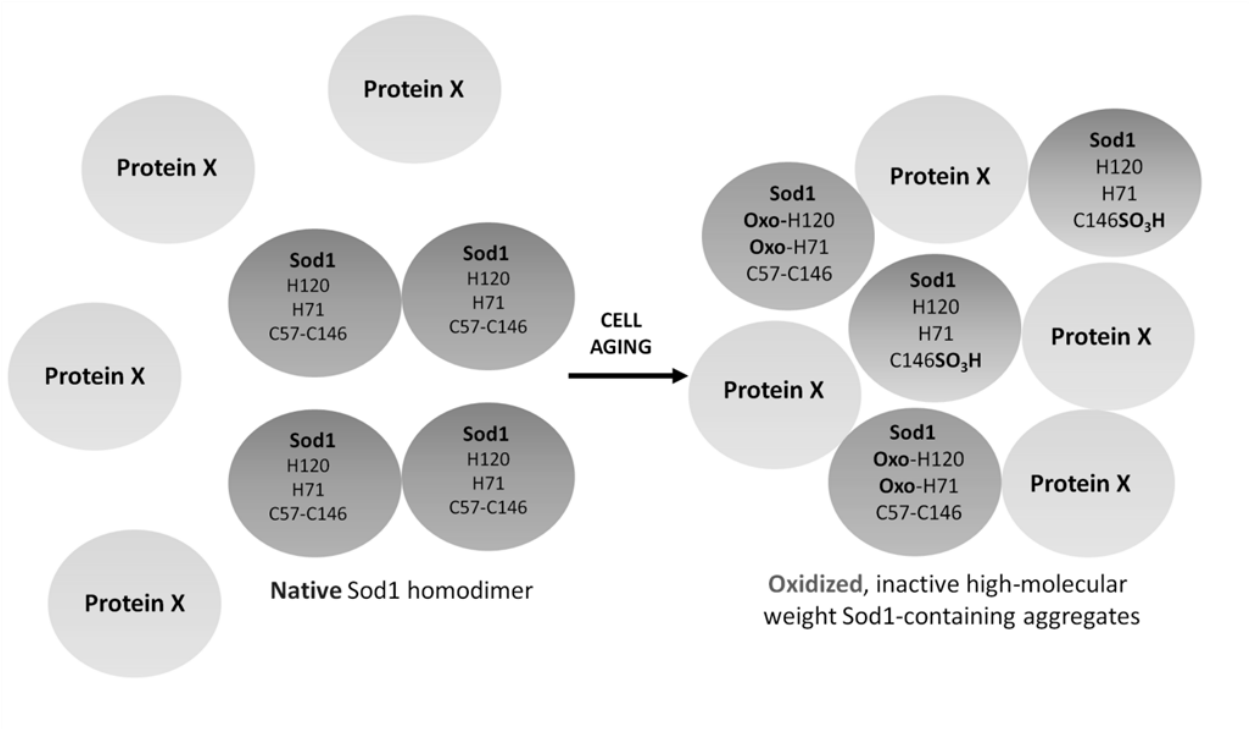

Fig. 6. 6 *Residues oxidized in catalytically inactive Sod1 present in HMW aggregates isolated from 7-day, stationary phase, yeast cells.* Sod1 oxidized at Cys146 or His120 and His71 elutes in HMW fractions of SEC, and may be associated with other proteins (?). This figure is the graphical abstract of the original manuscript (see Preface).

The intrasubunit Cys147-Cys57 disulfide (Fig. 6. 1) is essential in stabilizing the active site of Sod1 by orienting the coordinating ligands towards the Cu and Zn cofactors [221]. Notably, Cys146-SO_3H (human Sod1 numbering) was isolated from Parkinson's and

Alzheimer's brains [63], and inactive Sod1 from the airway epithelia of asthmatic patients displays disruption of Cys146-Cys57 disulfide [222]. Since disulfides are more resistant to oxidation than thiols, Cys146 may undergo oxidation in immature Sod1 prior to Cys146-Cys57 disulfide formation. In addition to destabilizing the dimer, such oxidation would decrease the SOD activity of cells since the ALS Sod1 C146R variant has <10% of wild-type activity [58]. Curiously, we did not detect oxidized Cys57, the disulfide partner of Cys146, although both cysteines are mutated in FALS [56].

Oxidation of the histidines that bind Sod1's metal cofactors (Fig. 6. 1) will labilize the metals. Three of the four copper ligands, His46, His48 and His120 (Fig. 6. 1) that are mutated in FALS [56] are found to be oxidized in H_2O_2-treated Sod *in vitro* [216]. Curiously, His120 is the only Cu ligand we find oxidized in our soluble HMW Sod1 fraction isolated from yeast (Fig. 6. 4B). Although no Zn ligands were found be oxidized by H_2O_2 *in vitro* [216], we discovered that His71, which is not a reported mutation site in FALS [6], is a target of oxidative modification in yeast (Fig. 6. 4C). Hence, oxidative PTMs could labilize both metal cofactors in Sod1 and promote its aggregation since Cu loss during acid denaturation decreases the enzyme's kinetic stability [223] and Zn loss promotes subunit aggregation *in vitro* [215].

A copper-bound hydroxyl radical formed during the pseudoperoxidase activity of Sod1 may mediate oxidation of a copper ligand such as His120 [17]. In contrast, a diffusible oxidant such as copper released from the oxidized enzyme or a carbonate radical formed by the pseudoperoxidase activity [119, 214] in presence of physiological CO_2 levels likely oxidizes His71 at 6.1 Å from copper (Fig. 6. 1). Notably, we find that both His120 and His71 are present as oxo-histidine in the same HMW Sod1 fraction, suggesting that these oxidations are somehow coupled. However, Cys146 oxidation is observed in a different HMW Sod1 fraction, which we

proposed above may arise from immature metal-free Sod1. Although we identified three sites of oxidative PTMs in Sod1 from aged yeast, it is important to emphasize that the protein may undergo more PTMs. Our current methodology is selective for soluble aggregates stabilized by non-covalent interactions (Fig. 6. 2A, Fig. 6. 3). Additional oxidative PTMs may trigger the formation of aggregates stabilized by covalent interactions that would migrate slowly during SDS-PAGE or of insoluble aggregates that would be pelleted with cell debris.

Neurotoxicity has been associated with borderline stability that results in the conversion of Sod1variants into non-amyloid aggregates [10]. However, a FALS-causing human Sod1 mutant with wild-type stability has recently been identified [57], suggesting that additional genetic and/or environmental factors are responsible for SALS induction. Clearly, HMW Sod1-GFP sharply increases during the chronological aging of yeast (Fig. 6. 5B), which may reflect increased oxidative damage to the protein as anticipated in old cells [64]. But if Sod1 oxidation occurs during normal cell aging, what triggers soluble HMW Sod1 aggregates to become toxic to motor neurons? This may involve accumulation of the aggregates in mitochondria followed by respiratory dysfunction [10, 224], co-aggregation of Sod1 with transcription factors necessary for neuronal survival [10] or membrane disruption [10]. A cell's capacity to degrade misfolded Sod1 or to immobilize soluble aggregates into insoluble forms may additionally control the accumulation of toxic species.

The mechanisms underlying the development of SALS remain unclear but are likely multiple and heterogeneous [55, 58]. Of the three sites of oxidative PTMs that we identify in Sod1 from stationary-phase yeast, only a Cys146 FALS mutant (C146R) has been described [56, 58]. Also, oxidation of His71 by H_2O_2 has not been reported *in vitro*. Thus, our work has identified an unexpected oxidative PTM in Sod1 from yeast and has additionally suggested two

possible independent mechanisms of Sod1 aggregation involving Cys146 oxidation in the immature protein, and His71 plus His120 oxidation of the metal-loaded protein.

Although disulfide cleavage and metal cofactor release [7, 8] are associated with human Sod1 aggregation and ALS, it is critical to establish if the PTMs observed here are relevant to disease development. Sod1 has a highly conserved active site, but human and yeast Sod1 possess only 70% sequence identity. Thus, we will examine PTMs in human Sod1 from yeast expressing this protein. Another critical issue is to distinguish between normal and pathological Sod1 aggregation with age as well as the sequestering of other essential proteins by Sod1 aggregates. To this end we will express aggressive Sod1 FALS mutants in yeast and examine their PTMs and their aggregates over time. Stationary-phase yeast cells are in a quiescent, non-dividing state like neurons [68] and exhibit the protein misfolding seen in neurodegenerative diseases such as ALS [225] and Parkinson's disease [226]. Also, the genetic modification of yeast to accelerate or decelerate the aging process is well documented, including strains we characterized that vary in their production of reactive oxygen species (ROS) [20, 97]. We will use these strains to examine how variation in oxidative stress affects Sod1 modification as cells age. Such studies can be easily performed since yeast cells rapidly age and data can be collected at numerous time points from independent cultures. Additionally, to establish if strains expressing Sod1-GFP can be used as indicators of Sod1 aggregation with age (Fig. 6. 5), we will compare aggregation of wild-type protein with its GFP fusion to determine how the tag influences this process.

6.7) Conclusions

PTMs associated with protein misfolding have not been systematically investigated in the cellular environment. By combining SEC with high-performance LC-MS/MS, we discovered that oxidation of residues critical for folding and activity leads to HMW Sod1 formation in stationary-phase yeast. Further detailed characterization of oxidized Sod1 and its aggregation in yeast will provide important insights into protein misfolding mechanisms driven by oxidative stress in aging cells.

6.8) Supplementary information

Table S6 1 *Modified peptide ions selected as precursor ions for MS/MS analyses* [a]

Peptide sequence (modified residue)	***Obs*** **m/z (z)**	***Obs*** **mass**	***Calc*** **mass** [b]	**Error (ppm)**[c]
TGNAGPRPA**C**GVIGLTN (Cys146)	823.40955 (2+)	1644.819	1644.804	9.2
SVVI**H**AGQDDLGKGDTEESLK (His120)	738.70239 (3+)	2213.107	2213.103	1.8
T**H**GAPTDEVR (His71)	366.84491 (3+)	1097.535	1097.532	0.003

[a] Precursor ions used for MS/MS analyses were filtered using a mass exclusion threshold of 10 ppm.

[b] Masses calculated with Proteome Discoverer and Cys oxidized to cysteic acid ($-SO_3H$) and His to oxo-histidine.

[c] Error in ppm = 10^6 (*Obs* mass–*Calc* mass)/*Calc* mass

Table S6 2 *Assignment of sequence ions in the MS/MS spectrum of the Cys146-modified peptide*[a]

Peak m/z [a]	Assignment [b]	Sequence [c]	Error (*Obs*−*Calc*) u [d]
234.11	y_2	NT	-0.08
404.21	y_4	NTLG	-0.03
517.30	y_5	NTLGI	0.02
616.37 / 308.69	y_6 / y_6^{2+}	NTLGIV	-0.15 / 0.15
673.39	y_7	NTLGIVG	-0.13
412.69	y_8^{2+}	NTLGIVG**C**	0.08
992.47 / 496.74	y_{10} / y_{10}^{2+}	NTLGIVG**C**AP	-0.01 / -0.48
574.79	y_{11}^{2+}	NTLGIVG**C**APR	0.01
1245.63 / 623.32	y_{10} / y_{10}^{2+}	NTLGIVG**C**APRP	-0.05 / 0.24
1302.65 / 651.83	y_{13} / y_{13}^{2+}	NTLGIVG**C**APRPG	-0.08 / -0.41
1373.68	y_{14}	NTLGIVG**C**APRPGA	-0.18
273.112	b_3	TGN	0.14
344.16	b_4	TGNA	-0.11
401.185	b_5	TGNAG	-0.20
498.23	b_6	TGNAGP	0.06
654.33	b_7	TGNAGPR	0.04
751.38	b_8	TGNAGPRP	0.32
822.42 / 411.71	b_9 / b_9^{2+}	TGNAGPRPA	0.26 / 0.23
973.42 / 487.21	b_{10} / b_{10}^{2+}	TGNAGPRPA**C**	-0.09 / 0.08
1030.44 / 515.72	b_{11} / b_{11}^{2+}	TGNAGPRPA**C**G	0.14 / 0.04
1129.51 / 565.26	b_{12} / b_{12}^{2+}	TGNAGPRPA**C**GV	0.01 / 0.01
1242.59 / 621.80	b_{13} / b_{13}^{2+}	TGNAGPRPA**C**GVI	0.01 / 0.29
1299.61 / 650.31	b_{14} / b_{14}^{2+}	TGNAGPRPA**C**GVIGL	0.02 / 0.10
1412.70 / 706.85	b_{15} / b_{15}^{2+}	TGNAGPRPA**C**GVIGLT	0.01 / 0.05
1513.74 / 757.38	b_{16} / b_{16}^{2+}	TGNAGPRPA**C**GVIGLTN	0.03 / 0.06

[a] Observed b_n and y_n sequence ions in Spectrum A of Fig. 6. 4 for peptide TGNAGPRPA**C**GVIGLTN. Note that for clarity sequence ions of low abundance are not mass labelled in the spectra in Fig. 6. 4.

[b] The charge on the y_n and b_n sequence ions is 1+ unless otherwise indicated.

[c] The sequence assignment is based on residue masses at 0.8 u mass tolerance.

[d] Errors (*Obs* mass−*Calc* mass, u) were calculated based on the monoisotopic masses of the residues plus the mass of H_3O^+ to account for the addition of water to the C-terminal residue.

Table S6 3 *Assignment of sequence ions in the MS/MS spectrum of the His120-modified peptide*[a]

Peak m/z [a]	Assignment [b]	Sequence [c]	Error (*Obs–Calc*) u [d]
260.20	y_2	KL	0.21
347.23	y_3	KLS	0.07
476.27 /238.64	y_4 / y_4^{2+}	KLSE	0.32 / -0.55
605.31	y_5	KLSEE	-0.67
706.36 / 353.68	y_6 / y_6^{2+}	KLSEET	0.32 / 0.01
821.39 / 411.20	y_7 / y_7^{2+}	KLSEETD	-0.54 / -0.03
878.41	y_8	KLSEETDG	-0.25
1006.51 / 503.76 / 336.17	y_9 / y_9^{2+} / y_9^{3+}	KLSEETDGK	0.67 / -0.42 / 0.01
1063.53 / 532.27	y_{10} / y_{10}^{2+}	KLSEETDGKG	-0.24 / -0.09
588.81 / 392.87	y_{11}^{2+} / y_{11}^{3+}	KLSEETDGKGL	0.36 / 0.29
646.32	y_{12}^{2+}	KLSEETDGKGLD	-0.43
703.84	y_{13}^{2+}	KLSEETDGKGLDD	-0.15
767.87 / 512.25	y_{14}^{2+} / y_{14}^{3+}	KLSEETDGKGLDDQ	-0.62 / -0.01
796.38 / 531.25	y_{15}^{2+} / y_{15}^{3+}	KLSEETDGKGLDDQG	-0.02 / 0.35
831.89 / 554.93	y_{16}^{2+} / y_{16}^{3+}	KLSEETDGKGLDDQGA	0.24 / -0.45
908.42 / 605.95	y_{17}^{2+} / y_{17}^{3+}	KLSEETDGKGLDDQGA**H**	-0.28 / -0.04
964.96 / 643.65	y_{18}^{2+} / y_{18}^{3+}	KLSEETDGKGLDDQGA**H**I	-0.19 / -0.13
1014.50 / 676.67	y_{19}^{2+} / y_{19}^{3+}	KLSEETDGKGLDDQGA**H**IV	0.19 / -0.25
1064.03 / 709.69	y_{20}^{2+} / y_{20}^{3+}	KLSEETDGKGLDDQGA**H**IVV	-0.08 / -0.28
286.18	b_3	SVV	-0.07
399.26	b_4	SVVI	-0.09
552.31 / 276.66	b_5 / b_5^{2+}	SVVI**H**	-0.28 / -0.28
623.35 / 312.18	b_6 / b_6^{2+}	SVVI**H**A	-0.14 / -0.09
680.37 / 340.69	b_7 / b_7^{2+}	SVVI**H**AG	-0.47 / -0.71
923.46 / 462.23 / 308.49	b_9 / b_9^{2+} / b_9^{3+}	SVVI**H**AGQD	0.01 / 0.29 / -0.71
1038.49 / 346.83	b_{10} / b_{10}^{3+}	SVVI**H**AGQDD	-0.18 / -0.33
1151.57 / 576.29 / 384.53	b_{11} / b_{11}^{2+} / b_{11}^{3+}	SVVI**H**AGQDDL	-0.16 / -0.79 / -0.11
1208.59	b_{12}	SVVI**H**AGQDDLG	-0.10
446.23	b_{13}^{3+}	SVVI**H**AGQDDLGK	-0.21
697.36 / 465.24	b_{14}^{2+} / b_{14}^{3+}	SVVI**H**AGQDDLGKG	0.38 / -0.11
754.87 / 503.58	b_{15}^{2+} / b_{15}^{3+}	SVVI**H**AGQDDLGKGD	-0.60 / -0.59
805.39 / 537.26	b_{16}^{2+} / b_{16}^{3+}	SVVI**H**AGQDDLGKGDT	0.44 / -0.02
580.28	b_{17}^{3+}	SVVI**H**AGQDDLGKGDTE	0.69
623.29	b_{18}^{3+}	SVVI**H**AGQDDLGKGDTEE	-0.19
977.95 / 652.30	b_{19}^{2+} / b_{19}^{3+}	SVVI**H**AGQDDLGKGDTEES	-0.43 / -0.35
1034.50 / 690.00	b_{20}^{2+} / b_{20}^{3+}	SVVI**H**AGQDDLGKGDTEESL	-0.51 / -0.21

[a] Observed b_n and y_n sequence ions in Spectrum B of Fig. 6. 4 for peptide SVVI**H**AGQDDLGKGDTEESLK.

[b,c,d] See footnotes b,c,d of Table S6 2

Table S6 4 *Assignment of sequence ions in the MS/MS spectrum of the His71-modified peptide* [a]

Peak m/z [a]	Assignment [b]	Sequence [c]	Error (*Obs–Calc*) u [d]
175.12	y_1	R	-0.09
274.19	y_2	RV	-0.01
619.30 /310.16	y_5 / y_5^{2+}	RVEDT	0.01 / -0.77
716.36 / 358.68 / 239.46	y_6 / y_6^{2+} / y_6^{3+}	RVEDTP	-0.20 / 0.28 /-0.04
263.14	y_7^{3+}	RVEDTPA	0.24
282.14	y_8^{3+}	RVEDTPAG	0.46
499.24 / 333.16	y_9^{2+} / y_9^{3+}	RVEDTPAG**H**	0.51 / -0.18
312.13 / 156.57	b_3 / b_3^{2+}	T**H**G	0.25 / 0.17
383.17 / 128.39	b_4 / b_4^{3+}	T**H**GA	0.16 / -0.59
291.14 / 194.43	b_6^{2+} / b_6^{3+}	T**H**GAPT	0.31 / -0.55
696.29 / 348.65	b_7 / b_7^{2+}	T**H**GAPTD	0.02 / 0.11
825.34 / 413.17 / 257.78	b_8 / b_8^{2+} / b_8^{3+}	T**H**GAPTDE	-0.02 / -0.15 / 0.16
462.71 / 308.81	b_9^{2+} / b_9^{3+}	T**H**GAPTDEV	-0.39 / 0.20

[a] Observed b_n and y_n sequence ions in Spectrum C of Fig. 6. 4 for peptide T**H**GAPTDEVR.

[b,c,d] See footnotes b,c,d of Table S6 2.

Chapter 7: General conclusions

Overall, my work provides new insights into the roles of ROS and antioxidant enzymes in redox signaling, stress response [171] and cell aging [20, 97]. In Chapter 2, Ccp1 was uncovered as a novel sensor of mitochondrial H_2O_2 [20]. As discussed previously, several examples of thiol-mediated H_2O_2 sensing in the cytosol and mitochondria have been reported [48, 49, 70, 207, 227, 228] but no example of direct H_2O_2 sensing has been described for a heme protein. This work uncovers the first heme-based H_2O_2 sensor that modulates intracellular ROS levels and antioxidant defenses when H_2O_2 is endogenously generated during aging or exogenously added as a bolus. Interestingly, intensified Ccp1 sensing (*ccp1*^{W191F} mutant) lowers endogenous H_2O_2 levels by increasing Cta1 activity, which depresses the H_2O_2-mediated stress response and Sod2 activity. However, Ccp1 sensing is critical to protect yeast cells against exogenous H_2O_2 by increasing catalase and peroxiredoxin activities. These findings corroborate reports that the outcome of H_2O_2 signaling depends on its site of generation (endogenous vs exogenous), compartmentalization (mitochondrial vs cytosolic), its concentration, and dynamics of the activation/deactivation of its sensors.

The mechanisms underlying the distinct responses to endogenous vs exogenous H_2O_2 by Ccp1 sensing are unclear, and we speculate that endogenous H_2O_2 triggers heme transfer from Ccp1 to Cta1 (see Future Work), whereas exogenous H_2O_2 activates a Ccp1-dependent Yap1/Skn7-mediated stress response. Nevertheless, these distinct responses likely have critical implications for parasitic cells that are exposed to exogenous H_2O_2 produced by the host defenses. This is supported by the high level of Ccp- and catalase-based H_2O_2 scavenging activity exhibited by parasitic bacteria [229] and fungi [230]. As shown in Chapter 3, Ccp1 sensing also increases cell resistance to ONOO(H), an inorganic peroxide involved in host

defense [96]. After challenge with the ONOO(H) generator SIN-1, Ccp1 sensing augments catalase and peroxiredoxin activities, enzymes that display both H_2O_2 and ONOO(H) reductase activity [148, 149]. Although the role of Ccp1-mediated ONOO(H) sensing in yeast aging was not fully investigated in this thesis, the results on challenge with SIN-1 suggest that cells possess common mechanisms of sensing and responding to low-molecular-weight peroxides, which is controlled by their cross-reactivity with peroxidases and catalases. Clearly, this is the case for H_2O_2 and ONOO(H) in yeast since both peroxides exhibit high reactivity with Ccp1, catalases and peroxiredoxins.

By uncovering the sensing role of Ccp1 and how its manipulation alters endogenous ROS levels and antioxidant enzyme activities, it was possible to clarify the relative contribution of $O_2^{\bullet-}$, H_2O_2 and $^{\bullet}OH$ on cell lifespan [97]. My work also demonstrates the critical role of mitochondrial integrity in controlling lifespan, since increased protein oxidation in these organelles tracks lifespan depression. The results from Chapter 4 explain at the chemical level the dual role of ROS in shortening lifespan, as proposed by the free radical theory of aging [6, 7], or extending longevity as proposed by the mitohormesis theory [15, 16]. Basal levels of H_2O_2 are necessary to trigger mitohormesis [15-19, 97], since intensified H_2O_2 sensing and signaling depress the endogenous H_2O_2 stress response and Sod2 activity [20], increase $O_2^{\bullet-}$, $^{\bullet}OH$ levels and mitochondrial damage, and shortens yeast lifespan [97]. Thus, the cell signaling triggered by endogenous H_2O_2 synchronizes the activity of antioxidant enzymes to prevent the accumulation of $O_2^{\bullet-}$ and $^{\bullet}OH$ radicals. Importantly, my results clearly demonstrate that the role of a given ROS in accelerating or delaying aging depends on its concentration and chemical nature.

Chapter 5 readresses the importance of catalases in protecting yeast cells against exogenous H_2O_2. The roles of catalases in yeast have been misunderstood for almost two

decades. While increased protein levels of Ctt1 were detected on H_2O_2 challenge [42], its deletion appeared not to increase H_2O_2 sensitivity [38]. These somewhat contradictory findings could be explained by compensation for the loss of H_2O_2-scavenging activity by the upregulation of abundant enzymes such as peroxiredoxins. However, my work reveals that the confusion is due to the nutrient depletion status of the medium, which diminishes catalase activity even in wild-type cells, whereas in nutrient-rich medium, Ctt1 activity is induced on H_2O_2 challenge and it is critical for adaptation and response to this stress. More generally, a critical finding is that the role of inducible antioxidant defenses on stress response must be analyzed under conditions that allow cells to respond to the stress by increasing *de novo* protein synthesis.

Chapter 6 provides insight into how the antioxidant enzyme Sod1 is post-translationally modified during the lifespan of eukaryotic cells. These findings implicate oxidative PTMs as a driving force for protein misfolding and inactivation during the aging mechanism, and advance a non-genetic component in the development of late-onset diseases. In particular, the gain of toxic function by Sod1 in neurodegenerative diseases such as ALS is associated with its misfolding [10, 55, 58, 231]. PTM-driven Sod1 misfolding deserves further investigation since it may provide an explanation for the development of sporadic ALS, which corresponds to 90% of all ALS but to date has no clear etiology [55, 58].

In sum, the findings of my thesis uncover the different strategies and synchronization of antioxidant defenses to prevent damage caused by exogenous and endogenous ROS. Rapidly mounting a strong antioxidant defense by cell signaling and induction of antioxidant enzymes is the critical step in overcoming an acute, exogenous stress, as shown in Chapters 2, 3 and 5. Chapters 4 and 6 divulge that the response to chronic oxidative stress during cell aging depends on the synchronization of antioxidant enzymes to balance the H_2O_2-mediated stress response.

This opposes the accumulation of more toxic species such as $O_2^{\bullet-}$ and $^{\bullet}OH$, which can promote damage and misfolding of metabolic and antioxidant enzymes specially in the mitochondrion. Although high concentrations of any ROS are unquestionably toxic [4], the severity of their effects *in vivo* depends on how cells synchronize their antioxidant defenses to circumvent both acute and chronic challenge.

Chapter 8: Future work

1) My work opened up a series of avenues for future investigation. The redox sensing function of Ccp1 is critical in modulating Cta1 activity [20], which then controls H_2O_2 levels and prevents activation of H_2O_2-dependent stress response [20] and limits lifespan [97]. The next logical step is to elucidate how Ccp1 controls Cta1 activity. The first possibility is that the redox signal transduced by Ccp1 increases Cta1 protein levels, and Western blotting investigation of how Cta1 protein expression varies in wild-type Ccp1 and its mutants is of interest. On the other hand, Ccp1 may modulate the heme-status of Cta1 by acting as a redox-sensitive heme chaperone or heme donor. We have preliminary evidence that H_2O_2 induces heme transfer from Ccp1 to apomyoglobin [Kathiresan *et al.,* manuscript in preparation]. An interesting experiment to be performed is to pull down Cta1 using immunoprecipitation or affinity tags and measure the relative heme-loading of this protein in cells expressing wild-type Ccp1, $Ccp1^{W191F}$ or in the *CCP1*-null strain. This should give direct evidence as to whether Ccp1 is a player in intracellular heme trafficking. Once Ccp1's signaling mechanism is elucidated, it will be interesting to identify the residues that are important for Ccp1 signaling but not catalysis.
2) Regarding yeast catalases, it remains unclear whether Ctt1 is inactivated or its synthesis is inhibited when cells are exposed to lethal H_2O_2 concentrations in KPi. Previous work suggests that Ctt1 protein levels are induced on H_2O_2 challenge in SCD medium [42]. Thus, measuring Ctt1 protein levels after H_2O_2 challenge in KPi by Western blotting would reveal whether or not *de novo* protein synthesis of Ctt1 took place.
3) The lack of nutrients in KPi must also contribute to thie inhibition by H_2O_2 of any pre-existing catalase activity. Thus, a possibility is that intracellular NADPH, which serves as

stabilizing co-factor for Ctt1 [205, 232], becomes limiting on H_2O_2 challenge in KPi media. Thus, the levels of intracellular NADPH/$NADP^+$ should be determined when cells are challenged with H_2O_2 in KPi.

4) H_2O_2 may additionally induce post-translational modifications in Ctt1 that deplete its activity in KPi. Hence, mass spectrometric analysis of Ctt1 isolated from cells exposed to H_2O_2 in KPi is another topic of interest for future investigation.
5) The literature suggests that deletion of yeast catalases does not result in hypersensitivity to H_2O_2 due to compensation by other antioxidant defenses such as the abundant Tsa1 and GSH [39, 40, 233]. Although this is not unreasonable, these conclusions were drawn from experiments where cells were challenged with H_2O_2 in nutrient-free medium where no Ctt1 induction takes place. Thus, cells may be simply dealing with the stress with pre-existing, constitutive antioxidant defenses. Evaluation of the H_2O_2 senstivity of the Ctt1 knockout combined with depletion of GSH or deletion of Tsa1 would address if these latter abundant antioxidant defenses do compensate for the lack of Ctt1 activity or if other constitutive, pre-existing antioxidant enzymes allow cells (*e.g.,* Tsa1 and GSH) to cope with the stress when catalases are not induced or not present at all.
6) Several questions arise from our observations on Sod1 aggregation. A key question is how heterogeneous are the HMW Sod1 aggregates. Subfractionation of the HMW species should be performed on a SEC column with a fractionation range greater than 300 kDa. The goal is to determine if other proteins co-aggregate with Sod1 since the toxicity of ALS Sod1 variants has been attributed in part to the sequestration of transcription factors important for cell survival [10].

7) The amyloid vs non-amyloid of the Sod1-containing aggregates should be characterized by Congo Red staining, a dye that displays highly protein environment-dependent absorbance and fluorescence spectra [234]. This method should reveal if oxidized Sod1 aggregates display ALS-like properties, since this disease is characterized by formation of non-amyloid Sod1 aggregates [10, 212].

8) An exciting future direction is to quantitate the formation of these high molecular weight species in yeast strains with shortened or extended lifespans. This should reveal if there is a toxic threshold above which these species promote loss of viability. The strains expressing wild-type Ccp1, its Ccp1^{W191F} variant and the *ccp1*Δ mutant are a suitable platform of study since their ROS levels change differently during aging (Chapter 2) and they have different lifespans (Chapter 4).

9) A complementary approach would be to co-express aggressive ALS Sod1 variants such as A4V in yeast and monitor their oxidation and aggregation during aging. Ultimately, *post-mortem* tissues from ALS brains should be examined to establish if they contain Sod1 with the PTMs identified in Chapter 6.

Appendices

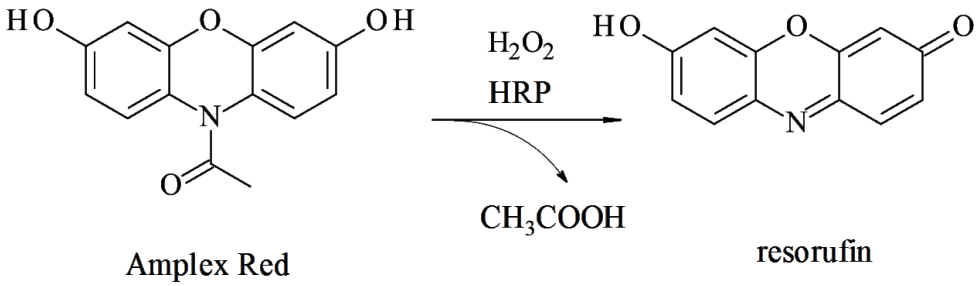

Appendix 2. 1 *Structures of the profluorescent dye Amplex Red and its fluorescent, oxidized form resorufin.* This membrane-impervious probe lacks an ester moiety to promote its cell uptake. Amplex Red is disposed to oxidation by H_2O_2 in presence of horseradish peroxidase (HRP) as catalyst.

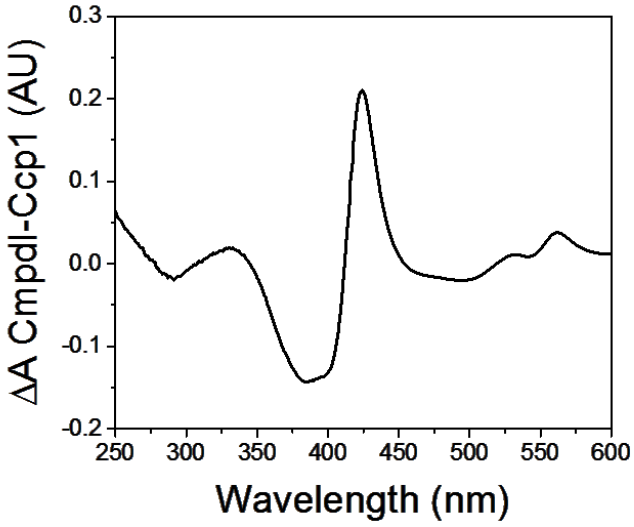

Appendix 3. 1 *ONOO(H)-oxidized Ccp1 is converted to Compound I (CmpdI).* 4 μM Ccp1 was oxidized with 8 μM ONOO(H) and its UV-vis spectra was subtracted from the spectra of 4 μM resting Ccp. The resulting spectra displays a maximum absorbance at 424 nm, which is characteristic of CmpdI.

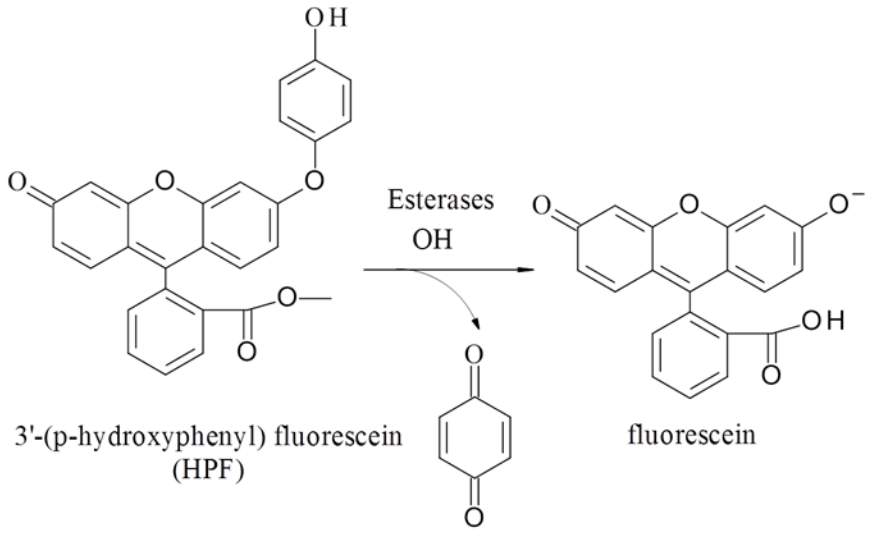

Appendix 4. 1 *Structures of the profluorescent dye 3'-(p-hydroxyphenyl) fluorescein (HPF) and its fluorescent, oxidized form fluorescein.* The probe is susceptible to oxidation by $^{\bullet}OH$ but not by H_2O_2 and $O_2^{\bullet-}$.

References

[1] Nohl, H.; Staniek, K.; Gille, L. Imbalance of oxygen activation and energy metabolism as a consequence or mediator of aging. *Exp Gerontol***32:**485-500; 1997.

[2] Tuena Gomez-Puyou, M. T.; Martins, O. B.; Gomez-Puyou, A. Synthesis and hydrolysis of ATP by the mitochondrial ATP synthase. *Biochem Cell Biol***66:**677-82; 1988.

[3] Azzi, Z. Oxidative stress: A dead end or a laboratory hypothesis? *Biochem Biophys Res Commun***362:**262-232; 2007.

[4] Miwa, S.; Muller, F. L.; Beckman, K. B. *The basics of oxidative biochemistry.* Humana Press; 2008.

[5] Loschen, G.; Azzi, A.; Richter, C.; Flohe, L. Superoxide radicals as precursors of mitochondrial hydrogen peroxide. *FEBS Lett***42:**68-72; 1974.

[6] Harman, D. Aging: A theory based on free radical and radiation chemistry. *J Gerontol***11:**298-300; 1956.

[7] Harman, D. The biologic clock: The mitochondria? *J Am Geriatr Soc***20:**145-147; 1972.

[8] Berlett, B. S.; Stadtman, E. R. Protein oxidation in aging, disease, and oxidative stress. *J Biol Chem***272:**20313-20316; 1997.

[9] Wells, P. G.; McCallum, G. P.; Chen, C. S.; Henderson, J. T.; Lee, C. J.; Perstin, J.; Preston, T. J.; Wiley, M. J.; Wong, A. W. Oxidative stress in developmental origins of disease: Teratogenesis, neurodevelopmental deficits, and cancer. *Toxicol Sci***108:**4-18; 2009.

[10] Mulligan, V. K.; Chakrabartty, A. Protein misfolding in the late-onset neurodegenerative diseases: Common themes and the unique case of amyotrophic lateral sclerosis. *Proteins***81:**1285-1303; 2013.

[11] Ogusucu, R.; Rettori, D.; Netto, L. E.; Augusto, O. Superoxide dismutase 1-mediated production of ethanol- and DNA-derived radicals in yeasts challenged with hydrogen peroxide: Molecular insights into the genome instability of peroxiredoxin-null strains. *J Biol Chem***284:**5546-5556; 2009.

[12] Romano, A. D.; Serviddio, G.; Matthaeis, A. d.; Bellanti, F.; Vendemiale, G. Oxidative stress and aging. *J Nephrol***15:**S29-36; 2010.

[13] Klaunig, J. E.; Kamendulis, L. M.; Hocevar, B. A. Oxidative stress and oxidative damage in carcinogenesis. *Toxicol Pathol***38:**96-109; 2010.

[14] Giacco, F.; Brownlee, M. Oxidative stress and diabetic complications. *Circ Res***107:**1058-1070; 2010.

[15] Ristow, M.; Zarse, K. How increased oxidative stress promotes longevity and metabolic health: The concept of mitochondrial hormesis (mitohormesis). *Exp Gerontol***45:**410-418; 2010.

[16] Ristow, M.; Schmeisser, S. Extending life span by increasing oxidative stress. *Free Radic Biol Med***51:**327-336; 2011.

[17] Schulz, T. J.; Zarse, K.; Voigt, A.; Urban, N.; Birringer, M.; Ristow, M. Glucose restriction extends caenorhabditis elegans life span by inducing mitochondrial respiration and increasing oxidative stress. *Cell Metab***6:**280-293; 2007.

[18] Goldberg, A. A.; Bourque, S. D.; Kyryakov, P.; Gregg, C.; Boukh-Viner, T.; Beach, A.; Burstein, M. T.; Machkalyan, G.; V, R.; Rampersad, S.; Cyr, D.; Milijevic, S.; Titorenko, V. I. Effect of calorie restriction on the metabolic history of chronologically aging yeast. *Exp Gerontol***44:**555-571; 2009.

[19] Mesquita, A.; Weinberger, M.; Silva, A.; Marques, B. S.; Almeida, B.; Leao, C.; V, C.; Rodrigues, F.; Burhans, W. C.; Ludovico, P. Caloric restriction or catalase inactivation extends yeast chronological lifespan by inducing H2O2 and superoxide dismutase activity. *Proc Natl Acad Sci USA***107:**15123-15128; 2010.

[20] Martins, D.; Kathiresan, M.; English, A. M. Cytochrome c peroxidase is a mitochondrial heme-based H2O2 sensor that modulates antioxidant defense. *Free Radic Biol Med***65:**541-551; 2013.

[21] Penninckx, M. J. An overview on glutathione in saccharomyces versus non-conventional yeasts. *FEMS Yeast Res***2:**295-305; 2002.

[22] Yadav, A.; Mishra, P. C. Modeling the activity of glutathione as a hydroxyl radical scavenger considering its neutral non-zwitterionic form. *J Mol Model***19:**767-777; 2013.

[23] Zheng, S. X.; Newton, G. L.; Ward, J. F.; Fahey, R. C. Aerobic radioprotection of pBR322 by thiols - effect of thiol net charge upon scavenging of hydroxyl radicals and repair of DNA radicals. *Radiat Res***130:**183-193; 1992.

[24] Fridovich, I. Superoxide radical and superoxide dismutases. *Annu Rev Biochem***64:**97-112; 1995.

[25] Fridovich, I. Superoxide radical: An endogenous toxicant. *Annu Rev Pharmacol Toxicol***23:**239-257; 1983.

[26] English, A. M.; Tsaprailis, G. Catalytic structure-function relationships in heme peroxidases. In: Anonymous *Adv Inorg Chem, volume Volume 43*Academic Press; 1995: 79-125.

[27] Switala, J.; Loewen, P. C. Diversity of properties among catalases. *Arch Biochem Biophys***401:**145-154; 2002.

[28] Chelikani, P.; Fita, I.; Loewen, P. C. Diversity of structures and properties among catalases. *Cell Mol Life Sci***61:**192-208; 2004.

[29] Nicholls, P.; Fita, I.; Loewen, P. C. Enzymology and structure of catalases. In: Anonymous *Adv Inorg Chem, volume Volume 51*Academic Press; 2000: 51-106.

[30] Munhoz, D. C.; Netto, L. E. Cytosolic thioredoxin peroxidase I and II are important defenses of yeast against organic hydroperoxide insult: Catalases and peroxiredoxins cooperate in the decomposition of H2O2 by yeast. *J Biol Chem***279:**35219-35227; 2004.

[31] Rhee, S. G.; Woo, H. A. Multiple functions of peroxiredoxins: Peroxidases, sensors and regulators of the intracellular messenger H2O2, and protein chaperones. *Antioxid Redox Signal***15:**781-794; 2011.

[32] Rhee, S. G.; Woo, H. A.; Kil, I. S.; Bae, S. H. Peroxiredoxin functions as a peroxidase and a regulator and sensor of local peroxides. *J Biol Chem***287:**4403-4410; 2012.

[33] Brigelius-Flohé, R.; Maiorino, M. Glutathione peroxidases. *Biochim Biophys Acta***1830:**3289-3303; 2013.

[34] Beetlestone, J. The oxidation of cytochrome c by cytochrome c peroxidase. *Arch Biochem Biophys***89:**35-40; 1960.

[35] Longo, V. D.; Gralla, E. B.; Valentine, J. S. Superoxide dismutase activity is essential for stationary phase survival in saccharomyces cerevisiae. mitochondrial production of toxic oxygen species in vivo. *J Biol Chem***271:**12275-12280; 1996.

[36] Longo, V. D.; Liou, L. L.; Valentine, J. S.; Gralla, E. B. Mitochondrial superoxide decreases yeast survival in stationary phase. *Arch Biochem Biophys***365:**131-142; 1999.

[37] Longo, V. D.; Mitteldorf, J.; Skulachev, V. P. Programmed and altruistic ageing. *Nature Rev Genet***6:**866-872; 2005.

[38] Izawa, S.; Inoue, Y.; Kimura, A. Importance of catalase in the adaptive response to hydrogen peroxide: Analysis of acatalasaemic saccharomyces cerevisiae. *Biochem J***320:**61-67; 1996.

[39] Izawa, S.; Inoue, Y.; Kimura, A. Oxidative stress-response in yeast - effect of glutathione on adaptation to hydrogen-peroxide stress in saccharomyces-cerevisiae. *FEBS Lett***368:**73-76; 1995.

[40] Inoue, Y.; Matsuda, T.; Sugiyama, K.; Izawa, S.; Kimura, A. Genetic analysis of glutathione peroxidase in oxidative stress response of saccharomyces cerevisiae. *J Biol Chem***274:**27002-27009; 1999.

[41] Davies, J. M. S.; Lowry, C. V.; Davies, K. J. A. Transient adaptation to oxidative stress in yeast. *Arch Biochem Biophys***327:**1-6; 1995.

[42] Godon, C.; Lagniel, G.; Lee, J.; Buhler, J. M.; Kieffer, S.; Perroti, M.; Boucheriei, H.; Toledano, M. B.; Labarre, J. The H2O2 stimulon in saccharomyces cerevisiae. *J Biol Chem***273:**22480-22489; 1998.

[43] Lee, J.; Godon, C.; Lagnie, G.; Spector, D.; Garini, G.; Labarre, J.; Toledano, M. B. Yap1 and Skn7 control two specialized oxidative stress response regulons in yeast. *J Biol Chem***274:**16040-16046; 1999.

[44] Jang, H. H.; Lee, K. O.; Chi, Y. H.; Jung, B. G.; Park, S. K.; Park, J. H.; Lee, J. R.; Lee, S. S.; Moon, J. C.; Yun, J. W.; Choi, Y. O.; Kim, W. Y.; Kang, J. S.; Cheong, G. W.; Yun, D. J.; Rhee, S. G.;

Cho, M. J.; Lee, S. Y. Two enzymes in one: Two yeast peroxiredoxins display oxidative stress-dependent switching from a peroxidase to a molecular chaperone function. *Cell***117:**625-635; 2004.

[45] Kho, C. W.; Lee, P. Y.; Bae, K. H.; Kang, S.; Cho, S.; do, H. L.; Sun, C. H.; Yi, G. S.; Park, B. C.; Park, S. G. Gpx3-dependent responses against oxidative stress in saccharomyces cerevisiae. *J Microbiol Biotechnol***18:**270-282; 2008.

[46] Wieser, R.; Adam, G.; Wagner, A.; Schuller, C.; Marchler, G.; Ruis, H.; Krawiec, Z.; Bilinski, T. Heat shock factor-independent heat control of transcription of the CTT1 gene encoding the cytosolic catalase T of saccharomyces cerevisiae. *J Biol Chem***266:**12406-12411; 1991.

[47] Harris, N.; MacLean, M.; Hatzianthis, K.; Panaretou, B.; Piper, P. Increasing saccharomyces cerevisiae stress resistance, through the overactivation of the heat shock response resulting from defects in the Hsp90 chaperone, does not extend replicative life span but can be associated with slower chronological ageing of nondividing cells. *Molecular Genetics and Genomics***265:**258-263; 2001.

[48] Delaunay, A.; Pflieger, D.; Barrault, M. B.; Vinh, J.; Toledano, M. B. A thiol peroxidase is an H2O2 receptor and redox-transducer in gene activation. *Cell***111:**471-481; 2002.

[49] Paulsen, C. E.; Carroll, K. S. Chemical dissection of an essential redox switch in yeast. *Chem Biol***16:**217-225; 2009.

[50] Muller, F. L.; Lustgarten, M. S.; Jang, Y.; Richardson, A.; H, H. V. R. Trends in oxidative aging theories. *Free Radic Biol Med***43:**447-503; 2007.

[51] Sohal, R. S.; Agarwal, A.; Agarwal, S.; Orr, W. C. Simultaneous overexpression of copper-containing and zinc-containing superoxide-dismutase and catalase retards age-related oxidative

damage and increases metabolic potential in drosophila-melanogaster. *J Biol Chem***270:**15671-15674; 1995.

[52] Schriner, S. E.; Linford, N. J.; Martin, G. M.; Treuting, P.; Ogburn, C. E.; Emond, M.; Coskun, P. E.; Ladiges, W.; Wolf, N.; Remmen, H. V.; Wallace, D. C.; Rabinovitch, P. S. Extension of murine life span by overexpression of catalase targeted to mitochondria. *Science***308:**1909-1911; 2005.

[53] Van-Raamsdonk, J. M.; Hekimi, S. Superoxide dismutase is dispensable for normal animal lifespan. *Proc Natl Acad Sci USA***109:**5785-5790; 2012.

[54] Li, Y. B.; Huang, T. T.; Carlson, E. J.; Melov, S.; Ursell, P. C.; Olson, T. L.; Noble, L. J.; Yoshimura, M. P.; Berger, C.; Chan, P. H.; Wallace, D. C.; Epstein, C. J. Dilated cardiomyopathy and neonatal lethality in mutant mice lacking manganese superoxide-dismutase. *Nat Genet***11:**376-381; 1995.

[55] Valentine, J. S.; Hart, P. J. Misfolded CuZnSOD and amyotrophic lateral sclerosis. *Proceedings of the National Academy of Sciences of the United States of America***100:**3617-3622; 2003.

[56] Abel, O.; Powell, J. F.; Andersen, P. M.; Al-Chalabi, A. ALSoD: A user-friendly online bioinformatics tool for amyotrophic lateral sclerosis genetics. *Hum Mutat***33:**1345-1351; 2012.

[57] Synofzik, M.; Ronchi, D.; Keskin, I.; Basak, A. N.; Wilhelm, C.; Gobbi, C.; Birve, A.; Biskup, S.; Zecca, C.; Fernandez-Santiago, R.; Kaugesaar, T.; Schoels, L.; Marklund, S. L.; Andersen, P. M. Mutant superoxide dismutase-1 indistinguishable from wild-type causes ALS. *Hum Mol Genet***21:**3568-3574; 2012.

[58] Valentine, J. S.; Doucette, P. A.; Potter, S. Z. Copper-zinc superoxide dismutase and amyotrophic lateral sclerosis. *Annual Review of Biochemistry***74:**563-593; 2005.

[59] Harris, N.; Costa, V.; MacLean, M.; Mollapour, M.; Moradas-Ferreira, P.; Piper, P. W. Mnsod overexpression extends the yeast chronological (G(0)) life span but acts independently of Sir2p histone deacetylase to shorten the replicative life span of dividing cells. *Free Radic Biol Med***34:**1599-1606; 2003.

[60] Cozzolino, M.; Pesaresi, M. G.; Amori, I.; Crosio, C.; Ferri, A.; Nencini, M.; Carri, M. T. Oligomerization of mutant SOD1 in mitochondria of motoneuronal cells drives mitochondrial damage and cell toxicity. *Antioxid Redox Signal***11:**1547-U3; 2009.

[61] Uchida, K.; S Kawakishi, S. Identification of oxidized histidine generated at the active site of cu,zn-superoxide dismutase exposed to H2O2. selective generation of 2-oxo-histidine at the histidine 118. *J Biol Chem***269:**2405-2410; 1994.

[62] Rakhit, R.; Cunningham, P.; Furtos-Matei, A.; Dahan, S.; Qi, X. F.; Crow, J. P.; Cashman, N. R.; Kondejewski, L. H.; Chakrabartty, A. Oxidation-induced misfolding and aggregation of superoxide dismutase and its implications for amyotrophic lateral sclerosis. *J Biol Chem***277:**47551-47556; 2002.

[63] Choi, J.; Rees, H. D.; Weintraub, S. T.; Levey, A. I.; Chin, L. S.; Li, L. Oxidative modifications and aggregation of cu,zn-superoxide dismutase associated with alzheimer and parkinson diseases. *J Biol Chem***280:**11648-11655; 2005.

[64] Brandes, N.; Tienson, H.; Lindemann, A.; Vitvitsky, V.; Reichmann, D.; Banerjee, R.; Jakob, U. Time line of redox events in aging postmitotic cells. *Elife***2:**e00306; 2013.

[65] Ghezzo-Schoneich, E.; Esch, S. W.; Sharov, V. S.; Schoneich, C. Biological aging does not lead to the accumulation of oxidized cu,zn-superoxide dismutase in the liver of F344 rats. *Free Radic Biol Med***30:**858-864; 2001.

[66] Herrero, E.; Ros, J.; Belli, G.; Cabiscol, E. Redox control and oxidative stress in yeast cells. *Biochim Biophys Acta***1780:**1217-1235; 2008.

[67] Barros, M. H.; Cunha, F. M. d.; Oliveira, G. A.; Tahara, E. B.; Kowaltowski, A. J. Yeast as a model to study mitochondrial mechanisms in ageing. *Mech Ageing Dev***131:**494-502; 2010.

[68] Piper, P. W. Long-lived yeast as a model for ageing research. *Yeast***23:**215-226; 2006.

[69] Fabrizio, P.; Longo, V. D. The chronological life span of saccharomyces cerevisiae. *Aging Cell***2:**73-81; 2003.

[70] Veal, E. A.; Day, A. M.; Morgan, B. A. Hydrogen peroxide sensing and signaling. *Mol Cell***26:**1-14; 2007.

[71] Bayliak, M.; Semchyshyn, H.; Lushchak, V. Effect of hydrogen peroxide on antioxidant enzyme activities in saccharomyces cerevisiae is strain-specific. *Biochemistry (Mosc)***71:**1013-1020; 2006.

[72] Banci, L.; Bertini, I.; Boca, M.; Girotto, S.; Martinelli, M.; Valentine, J. S.; Vieru, M. SOD1 and amyotrophic lateral sclerosis: Mutations and oligomerization. *PLoS One***3:**e1677; 2008.

[73] Winterbourn, C. C. The biological chemistry of hydrogen peroxide. *Methods Enzymol***528:**3-25; 2013.

[74] Kuge, S. Regulation of yAP-1 nuclear localization in response to oxidative stress. *EMBO J***16:**1710-1720; 1997.

[75] Boveris, A. Mitochondrial production of hydrogen peroxide in saccharomyces cerevisiae. *Acta Physiol Lat Am***26:**303-309; 1976.

[76] Marada, A.; Allu, P. K.; Murari, A.; Pullareddy, B.; Tammineni, P.; Thiriveedi, V. R.; Danduprolu, J.; Sepuri, N. B. Mge1, a nucleotide exchange factor of Hsp70, acts as an oxidative sensor to regulate mitochondrial Hsp70 function. *Mol Biol Cell***24:**692-703; 2013.

[77] Chandel, N. S.; Schumacker, P. T. Cellular oxygen sensing by mitochondria: Old questions, new insight. *J Appl Physiol***88:**1880-1889; 2000.

[78] Waypa, G. B.; Schumacker, P. T. Hypoxia-induced changes in pulmonary and systemic vascular resistance: Where is the O2 sensor? *Respir Physiol Neurobiol***174:**201-211; 2010.

[79] Forman, H. J.; Maiorino, M.; Ursini, F. Signaling functions of reactive oxygen species. *Biochemistry***49:**835-842; 2010.

[80] Yonetani, T.; Ray, G. S. Studies on cytochrome c peroxidase: I. purification and some properties. *J Biol Chem***240:**4503-4508; 1965.

[81] Yonetani, T.; Ohnishi, T. Cytochrome c peroxidase, a mitochondrial enzyme of yeast. *J Biol Chem***241:**2983-2984; 1966.

[82] Kwon, M.; Chong, S.; S, S. H.; Kim, K. Oxidative stresses elevate the expression of cytochrome c peroxidase in saccharomyces cerevisiae. *Biochim Biophys Acta***1623:**1-5; 2003.

[83] Jiang, H.; English, A. M. Phenotypic analysis of the ccp1Delta and ccp1Delta-ccp1W191F mutant strains of saccharomyces cerevisiae indicates that cytochrome c peroxidase functions in oxidative-stress signaling. *J Inorg Biochem***100:**1996-2008; 2006.

[84] Suppanz, I. E.; Wurm, C. A.; Wenzel, D.; Jakobs, S. The m-AAA protease processes cytochrome c peroxidase preferentially at the inner boundary membrane of mitochondria. *Mol Biol Cell***20:**572-580; 2009.

[85] Miller, M. A.; Vitello, L.; Erman, J. E. Regulation of interprotein electron transfer by trp 191 of cytochrome c peroxidase. *Biochemistry***34:**12048-12058; 1995.

[86] Charizanis, C.; Juhnke, H.; Krems, B.; Entian, K. D. The mitochondrial cytochrome cperoxidase Ccp1 of saccharomyces cerevisiae is involved in conveying an oxidative stress signal to the transcription factor Pos9 (Skn7). *Mol Gen Genet***262:**437-447; 1999.

[87] Trotter, E. W.; Rand, J. D.; Vickerstaff, J.; Grant, C. M. The yeast Tsa1 peroxiredoxin is a ribosome-associated antioxidant. *Biochem J***412:**73-80; 2008.

[88] Lim, J. C.; Choi, H. I.; Park, Y. S.; Nam, H. W.; Woo, H. A.; Kwon, K. S.; Kim, Y. S.; Rhee, S. G.; Kim, K.; Chae, H. Z. Irreversible oxidation of the active-site cysteine of peroxiredoxin to cysteine sulfonic acid for enhanced molecular chaperone activity. *J Biol Chem***283:**28873-28880; 2008.

[89] Balny, C.; Anni, H.; Yonetani, T. A stopped-flow study of the reaction of cytochrome c peroxidase with hydroperoxides. *FEBS Lett***221:**349-354; 1987.

[90] Tachibana, T.; Okazaki, S.; Murayama, A.; Naganuma, A.; Nomoto, A.; Kuge, S. A major peroxiredoxin-induced activation of Yap1 transcription factor is mediated by reduction-sensitive disulfide bonds and reveals a low level of transcriptional activation. *J Biol Chem***284:**4464-4472; 2009.

[91] Brachmann, C. B.; Davies, A.; Cost, G. J.; Caputo, E.; Li, J.; Hieter, P.; Boeke, J. D. Designer deletion strains derived from saccharomyces cerevisiae S288C: A useful set of strains and plasmids for PCR-mediated gene disruption and other applications. *Yeast***14:**115-132; 1998.

[92] Ito, H.; Funkuda, Y.; Murata, K.; Kimura, A. Transformation of intact cells treated with alkali cations. *J Bacteriol***153:**163-168; 1983.

[93] Sikorski, R. S.; Boeke, J. D. In vitro mutagenesis and plasmid shuffling: From cloned gene to mutant yeast. *Methods Enzymol***194:**302-318; 1991.

[94] Burtner, C. R.; Murakami, C. J.; Kennedy, B. K.; Kaeberlein, M. A molecular mechanism of chronological aging in yeast. *Cell Cycle***5:** 2009.

[95] Kalyanaraman, B.; Darley-Usmar, V.; Davies, K. J.; Dennery, P. A.; Forman, H. J.; Grisham, M. B.; Mann, G. E.; Moore, K.; Roberts, L. J.,2nd; Ischiropoulos, H. Measuring reactive oxygen and nitrogen species with fluorescent probes: Challenges and limitations. *Free Radic Biol Med***52:**1-6; 2012.

[96] Ferrer-Sueta, G.; Radi, R. Chemical biology of peroxynitrite: Kinetics, diffusion, and radicals. *ACS Chem Biol***4:**161-177; 2009.

[97] Martins, D.; Titorenko, V. I.; English, A. M. Cells with impaired mitochondrial H2O2 sensing generate less *OH radicals and live longer. *Antioxid Redox Signal***in press:** 2014.

[98] Longo, V. D.; Viola, K. L.; Klein, W. L.; Finch, C. E. Reversible inactivation of superoxide-sensitive aconitase in Abeta1-42-treated neuronal cell lines. *J Neurochem***75:**1977-1985; 2000.

[99] Madeo, F.; Frohlich, E.; Ligr, M.; Grey, M.; Sigrist, S. J.; Wolf, D. H.; Frohlich, K. U. Oxygen stress: A regulator of apoptosis in yeast. *J Cell Biol***145:**757-767; 1999.

[100] Kundu, K.; Knight, S. F.; Lee, S.; Taylor, W. R.; Murthy, N. A significant improvement of the efficacy of radical oxidant probes by the kinetic isotope effect. *Angew Chem Int Ed Engl***49:**6134-6138; 2010.

[101] Sikorski, R. S.; Hieter, P. A system of shuttle vectors and yeast host strains designed for efficient manipulation of DNA in saccharomyces cerevisiae. *Genetics***122:**19-27; 1989.

[102] Yeung, B. K.; Wang, X.; Sigman, J. A.; Petillo, P. A.; Lu, Y. Construction and characterization of a manganese-binding site in cytochrome c peroxidase: Towards a novel manganese peroxidase. *Chem Biol***4:**215-221; 1997.

[103] Meisinger, C.; Pfanner, N.; Truscott, K. N. Isolation of yeast mitochondria. *Methods Mol Biol***313:**33-39; 2006.

[104] Bradford, M. M. Rapid and sensitive method for the quantitation of microgram quantities of protein utilizing the principle of protein-dye binding. *Anal Biochem***72:**248-254; 1976.

[105] Beers, R. F.; Sizer, I. W. A spectrophotometric method for measuring the breakdown of hydrogen peroxide by catalase. *J Biol Chem***195:**133-140; 1952.

[106] Weydert, C. J.; Cullen, J. J. Measurement of superoxide dismutase, catalase and glutathione peroxidase in cultured cells and tissue. *Nat Protoc***5:**51-66; 2010.

[107] Jara, M.; Vivancos, A. P.; Calvo, I. A.; Moldon, A.; Sanso, M.; Hidalgo, E. The peroxiredoxin Tpx1 is essential as a H2O2 scavenger during aerobic growth in fission yeast. *Mol Biol Cell***18:**2288-2295; 2007.

[108] Rocher, C.; Lalanne, J. L.; Chaudiere, J. Purification and properties of a recombinant sulfur analog of murine selenium-glutathione peroxidase. *Eur J Biochem***205:**955-960; 1992.

[109] Welinder, C.; Ekblad, L. Coomassie staining as loading control in western blot analysis. *J Proteome Res***10:**1416-1419; 2011.

[110] Bissinger, P. H.; Wieser, R.; Hamilton, B.; Ruis, H. Control of saccharomyces cerevisiae catalase T gene (CTT1) expression by nutrient supply via the RAS-cyclic AMP pathway. *Mol Cell Biol***9:**1309-1315; 1989.

[111] Thieringer, R.; Shio, H.; Han, Y. S.; Cohen, G.; Lazarow, P. B. Peroxisomes in saccharomyces cerevisiae: Immunofluorescence analysis and import of catalase A into isolated peroxisomes. *Mol Cell Biol***11:**510-522; 1991.

[112] Petrova, V. Y.; Drescher, D.; Kujumdzieva, A. V.; Schmitt, M. J. Dual targeting of yeast catalase A to peroxisomes and mitochondria. *Biochem J***380:**393-400; 2004.

[113] Petrova, V. Y.; Rasheva, T. V.; Kujumdzieva, A. V. Catalase enzyme in mitochondria of saccharomyces cerevisiae. *Electron J Biotechnol***5:** 2002.

[114] Sturtz, L. A.; Diekert, K.; Jensen, L. T.; Lill, R.; Culotta, V. C. A fraction of yeast cu,zn-superoxide dismutase and its metallochaperone, CCS, localize to the intermembrane space of mitochondria. A physiological role for SOD1 in guarding against mitochondrial oxidative damage. *J Biol Chem***276:**38084-38089; 2001.

[115] Ravindranath, S. D.; Fridovich, I. Isolation and characterization of a manganese-containing superoxide dismutase from yeast. *J Biol Chem***250:**6107-6112; 1975.

[116] Ghaemmaghami, S.; Huh, W. K.; Bower, K.; Howson, R. W.; Belle, A.; Dephoure, N.; O'Shea, E. K.; Weissman, J. S. Global analysis of protein expression in yeast. *Nature***425:**737-741; 2003.

[117] Veal, E. A.; Ross, S. J.; Malakasi, P.; Peacock, E.; Morgan, B. A. Ybp1 is required for the hydrogen peroxide-induced oxidation of the Yap1 transcription factor. *J Biol Chem***278:**30896-30904; 2003.

[118] Okazaki, S.; Naganuma, A.; Kuge, S. Peroxiredoxin-mediated redox regulation of the nuclear localization of Yap1, a transcription factor in budding yeast. *Antioxid Redox Signal***7:**327-334; 2005.

[119] Ramirez, D. C.; Mejiba, S. E. G.; Mason, R. P. Mechanism of hydrogen peroxide-induced cu,zn-superoxide dismutase-centered radical formation as explored by immuno-spin trapping: The role of copper- and carbonate radical anion-mediated oxidations. *Free Radic Biol Med***38:**201-214; 2005.

[120] Yim, M. B.; Chock, P. B.; Stadtman, E. R. Copper, zinc superoxide dismutase catalyzes hydroxyl radical production from hydrogen peroxide. *Proc Natl Acad Sci USA***87:**5006-5010; 1990.

[121] Ward, J. P. Oxygen sensors in context. *Biochim Biophys Acta***1777:**1-14; 2008.

[122] Pinkham, J. L.; Wang, Z.; Alsina, J. Heme regulates SOD2 transcription by activation and repression in saccharomyces cerevisiae. *Curr Genet***31:**281-297; 1997.

[123] Wong, C. M.; Ching, Y. P.; Zhou, Y.; Kung, H. F.; Jin, D. Y. Transcriptional regulation of yeast peroxiredoxin gene TSA2 through Hap1p, Rox1p, and Hap2/3/5p. *Free Radic Biol Med***34:**585-597; 2003.

[124] Zhang, L.; Hach, A. Molecular mechanism of heme signaling in yeast: The transcriptional activator Hap1 serves as the key mediator. *Cell Mol Life Sci***56:**415-426; 1999.

[125] Sels, A. A.; Cocriamont, C. Induced conversion of a protein precursor into cytochrome c peroxidase during adaptation of yeast to oxygen. *Biochem Biophys Res Commun***32:**192-198; 1968.

[126] Woloszczuk, W.; Sprinson, D. B.; Ruis, H. The relation of heme to catalase apoprotein synthesis in yeast. *J Biol Chem***255:**2624-2627; 1980.

[127] Zimniak, P.; Hartter, E.; Woloszczuk, W.; Ruis, H. Catalase biosynthesis in yeast: Formation of catalase A and catalase T during oxygen adaptation of saccharomyces cerevisiae. *Eur J Biochem***71:**393-398; 1976.

[128] Larsen, F. J.; Schiffer, T. A.; Weitzberg, E.; Lundberg, J. O. Regulation of mitochondrial function and energetics by reactive nitrogen oxides. *Free Radic. Biol. Med.***53:**1919-1928; 2012.

[129] Rees, D. D.; Palmer, R. M. J.; Moncada, S. Role of endothelium-derived nitric-oxide in the regulation of blood-pressure. *Proc. Natl. Acad. Sci. U. S. A.***86:**3375-3378; 1989.

[130] MacMicking, J.; Xie, Q. W.; Nathan, C. Nitric oxide and macrophage function. *Annu. Rev. Immunol.***15:**323-350; 1997.

[131] Furlong, B.; Henderson, A. H.; Lewis, M. J.; Smith, J. A. Endothelium-derived relaxing factor inhibits invitro platelet-aggregation. *Br. J. Pharmacol.***90:**687-692; 1987.

[132] Hogan, J. C.; Lewis, M. J.; Henderson, A. H. Invivo edrf activity influences platelet-function. *Br. J. Pharmacol.***94:**1020-1022; 1988.

[133] Bolanos, J. P.; Peuchen, S.; Heales, S. J. R.; Land, J. M.; Clark, J. B. Nitric oxide-mediated inhibition of the mitochondrial respiratory-chain in cultured astrocytes. *J. Neurochem.***63:**910-916; 1994.

[134] Burney, S.; Tamir, S.; Gal, A.; Tannenbaum, S. R. A mechanistic analysis of nitric oxide-induced cellular toxicity. *Nitric Oxide.***1:**130-144; 1997.

[135] Nomura, Y. A transient brain ischemia- and bacterial endotoxin-induced glial iNOS expression and NO-induced neuronal apoptosis. *Toxicol. Lett.***102-103:**65-69; 1998.

[136] Carballal, S.; Bartesaghi, S.; Radi, R. Kinetic and mechanistic considerations to assess the biological fate of peroxynitrite. *Biochim. Biophys. Acta.***in press:** 2013.

[137] Radi, R.; Cassina, A.; Hodara, R. Nitric oxide and peroxynitrite interactions with mitochondria. *Biol. Chem.***383:**401-409; 2002.

[138] Maller, C.; Schroeder, E.; Eaton, P. Glyceraldehyde 3-phosphate dehydrogenase is unlikely to mediate hydrogen peroxide signaling: Studies with a novel anti-dimedone sulfenic acid antibody. *Antioxid. Redox Signal.***14:**49-60; 2011.

[139] Han, D.; Canali, R.; Garcia, J.; Aguilera, R.; Gallaher, T. K.; Cadenas, E. Sites and mechanisms of aconitase inactivation by peroxynitrite: Modulation by citrate and glutathione. *Biochemistry***44:**11986-11996; 2005.

[140] Guingab-Cagmat, J. D.; Stevens, S. M.,Jr.; Ratliff, M. V.; Zhang, Z.; Gold, M. S.; Anagli, J.; Wang, K. K. W.; Kobeissy, F. H. Identification of tyrosine nitration in UCH-L1 and GAPDH. *Electrophoresis***32:**1692-1705; 2011.

[141] Yamakura, F.; Taka, H.; Fujimura, T.; Murayama, K. Inactivation of human manganese-superoxide dismutase by peroxynitrite is caused by exclusive nitration of tyrosine 34 to 3-nitrotyrosine. *J. Biol. Chem.***273:**14085-14089; 1998.

[142] Drechsel, D. A.; Estevez, A. G.; Barbeito, L.; Beckman, J. S. Nitric oxide-mediated oxidative damage and the progressive demise of motor neurons in ALS. *Neurotox. Res.***22:**251-264; 2012.

[143] Szabo, C. Role of nitrosative stress in the pathogenesis of diabetic vascular dysfunction. *Br. J. Pharmacol.***156:**713-727; 2009.

[144] Malinski, T. Nitric oxide and nitroxidative stress in alzheimer's disease. *J. Alzheimers Dis.***11:**207-218; 2007.

[145] Peluffo, G.; Radi, R. Biochemistry of protein tyrosine nitration in cardiovascular pathology. *Cardiovasc. Res.***75:**291-302; 2007.

[146] Floris, R.; Piersma, S. R.; Yang, G.; Jones, P.; Wever, R. Interaction of myeloperoxidase with peroxynitrite - a comparison with lactoperoxidase, horseradish-peroxidase and catalase. *Eur. J. Biochem.***215:**767-775; 1993.

[147] Brennan, M. L.; Wu, W. J.; Fu, X. M.; Shen, Z. Z.; Song, W.; Frost, H.; Vadseth, C.; Narine, L.; Lenkiewicz, E.; Borchers, M. T.; Lusis, A. J.; Lee, J. J.; Lee, N. A.; Abu-Soud, H. M.; Ischiropoulos, H.; Hazen, S. L. A tale of two controversies - defining both the role of peroxidases in nitrotyrosine formation in vivo using eosinophil peroxidase and myeloperoxidase-deficient mice, and the nature of peroxidase-generated reactive nitrogen species. *J. Biol. Chem.***277:**17415-17427; 2002.

[148] Dubuisson, M.; Stricht, D. V.; Clippe, A.; Etienne, F.; Nauser, T.; Kissner, R.; Koppenol, W. H.; Rees, J. F.; Knoops, B. Human peroxiredoxin 5 is a peroxynitrite reductase. *FEBS Lett.***571:**161-165; 2004.

[149] Gebicka, L.; Didik, J. Catalytic scavenging of peroxynitrite by catalase. *J. Inorg. Biochem.***103:**1375-1379; 2009.

[150] Masumoto, H.; Sies, H. The reaction of ebselen with peroxynitrite. *Chem. Res. Toxicol.***9:**262-267; 1996.

[151] Loo, S.; Erman, J. E. A kinetic study of the reaction between cytochrome c peroxidase and hydrogen peroxide. dependence on pH and ionic strength. *Biochemistry***14:**3467-3470; 1975.

[152] Hahm, S.; Miller, M. A.; Geren, L.; Kraut, J.; Durham, B.; Millett, F. Reaction of horse cytochrome c with the radical and the oxyferryl heme in cytochrome c peroxidase compound I. *Biochemistry***33:**1473-1480; 1994.

[153] Erman, J. E.; Yonetani, T. The oxidation of cytochrome c peroxidase by hydrogen peroxide. characterization of products. *Biochem Biophys Acta***393:**343-349; 1975.

[154] Trujillo, M.; Ferrer-Sueta, G.; Radi, R. Kinetic studies on peroxynitrite reduction by peroxiredoxins. *Nitric Oxide.***441:**173-196; 2008.

[155] Pryor, W. A.; Cueto, R.; Jin, X.; Koppenol, W. H.; Nguschwemlein, M.; Squadrito, G. L.; Uppu, P. L.; Uppu, R. M. A practical method for preparing peroxynitrite solutions of low ionic-strength and free of hydrogen-peroxide. *Free Radic Biol Med***18:**75-83; 1995.

[156] Yonetani, T.; Chance, B.; Kajiwara, S. Crystalline cytochrome c peroxidase and complex ES. *J. Biol. Chem.***241:**2981-2; 1966.

[157] Yonetani, T.; Anni, H. Yeast cytochrome-C peroxidase - coordination and spin states of heme prosthetic group. *J. Biol. Chem.***262:**9547-9554; 1987.

[158] Vitello, L. B.; Huang, M.; Erman, J. E. Ph-dependent spectral and kinetic-properties of cytochrome-C peroxidase - comparison of freshly isolated and stored enzyme. *Biochemistry (N. Y.)***29:**4283-4288; 1990.

[159] Margoliash, E.; Frohwirt, N.; Wiener, E. A study of the cytochrome c haemochromogen. *Biochem. J.***71:**559-70; 1959.

[160] Bradford, M. M. A rapid and sensitive method for the quantitation of microgram quantities of protein utilizing the principle of protein dye binding. *Anal. Biochem.***72:**248-254; 1976.

[161] Yonetani, T. Studies on cytochrome c peroxidase. II. stoichiometry between enzyme, H2O2, and ferrocytochrome c and enzymic determination of extinction coefficients of cytochrome c. *J Biol Chem***240:**4509-14; 1965.

[162] Ho, P. S.; Hoffman, B. M.; Kang, C. H.; Margoliash, E. Control of the transfer of oxidizing equivalents between heme iron and free radical site in yeast cytochrome c peroxidase. *J Biol Chem***258:**4356-4363; 1983.

[163] Burner, U.; Furtmuller, P. G.; Kettle, A. J.; Koppenol, W. H.; Obinger, C. Mechanism of reaction of myeloperoxidase with nitrite. *J Biol Chem***275:**20597-20601; 2000.

[164] Briviba, K.; Kissner, R.; Koppenol, W. H.; Sies, H. Kinetic study of the reaction of glutathione peroxidase with peroxynitrite. *Chem. Res. Toxicol.***11:**1398-1401; 1998.

[165] Erman, J. E.; Vitello, L. B.; Miller, M. A.; Shaw, A.; Brown, K. A.; Kraut, J. Histidine-52 is a critical residue for rapid formation of cytochrome-C peroxidase compound-i. *Biochemistry (N. Y.)***32:**9798-9806; 1993.

[166] Smith, B. C.; Marletta, M. A. Mechanisms of S-nitrosothiol formation and selectivity in nitric oxide signaling. *Curr. Opin. Chem. Biol.***16:**498-506; 2012.

[167] Martin-Romero, F. J.; Gutierrez-Martin, Y.; Henao, F.; Gutierrez-Merino, C. Fluorescence measurements of steady state peroxynitrite production upon SIN-1 decomposition: NADH versus dihydrodichlorofluorescein and dihydrorhodamine 123. *J. Fluoresc.***14:**17-23; 2004.

[168] Radi, R. Protein tyrosine nitration: Biochemical mechanisms and structural basis of functional effects. *Acc. Chem. Res.***46:**550-559; 2013.

[169] Brown, A. S.; Moro, M. A.; Masse, J. M.; Cramer, E. M.; Radomski, M.; Darley-Usmar', V. Nitric oxide-dependent and independent effects on human platelets treated with peroxynitrite. *Cardiovasc. Res.***40:**380-388; 1998.

[170] Lushchak, O. V.; Inoue, Y.; Lushchak, V. I. Regulatory protein Yap1 is involved in response of yeast saccharomyces cerevisiae to nitrosative stress. *Biochemistry (Mosc)***75:**629-635; 2010.

[171] Martins, D.; English, A. M. Catalase activity is stimulated by H_2O_2 in rich culture medium and is required for H_2O_2 resistance and adaptation in yeast
. *Redox Biol***2:**308-313; 2014.

[172] Kelm, M. Nitric oxide metabolism and breakdown. *Biochem Biophys Acta***1411:**273-289; 1999.

[173] Ristow, M.; Zarse, K.; Oberbach, A.; Kloting, N.; Birringer, M.; Kiehntopf, M.; Stumvoll, M.; Kahn, C. R.; Bluher, M. Antioxidants prevent health-promoting effects of physical exercise in humans. *Proc Natl Acad Sci USA***106:**8665-8670; 2009.

[174] Longo, V. D.; Shadel, G. S.; Kaeberlein, M.; Kennedy, B. Replicative and chronological aging in saccharomyces cerevisiae. *Cell Metab***16:**18-31; 2012.

[175] Hausladen, A.; Fridovich, I. Superoxide and peroxynitrite inactivate aconitases, but nitric oxide does not. *J Biol Chem***269:**29405-29408; 1994.

[176] Murakami, K.; Yoshino, M. Inactivation of aconitase in yeast exposed to oxidative stress. *Biochem Mol Biol Int***41:**481-486; 1997.

[177] Perry, J. J.; Shin, D. S.; Getzoff, E. D.; Tainer, J. A. The structural biochemistry of the superoxide dismutases. *Biochem Biophys Acta***1804:**245-262; 2010.

[178] Roux, A. E.; Chartrand, P.; Ferbeyre, G.; Rokeach, L. A. Fission yeast and other yeasts as emergent models to unravel cellular aging in eukaryotes. *J Gerontol A Biol Sci Med Sci***65:**1-8; 2010.

[179] Braun, R. J.; Westermann, B. Mitochondrial dynamics in yeast cell death and aging. *Biochem Soc Trans***39:**1520-1526; 2011.

[180] Gardner, P. R.; Nguyen, D. D.; White, C. W. Aconitase is a sensitive and critical target of oxygen poisoning in cultured mammalian cells and in rat lungs. *Proc Natl Acad Sci USA***91:**12248-12252; 1994.

[181] Setsukinai, K.; Urano, Y.; Kakinuma, K.; Majima, H. J.; Nagano, T. Development of novel fluorescence probes that can reliably detect reactive oxygen species and distinguish specific species. *J Biol Chem***278:**3170-3175; 2003.

[182] Delori, F. C.; Dorey, C. K. In vivo technique for autofluorescent lipopigments. *Methods Mol Biol***108:**229-243; 1998.

[183] Stookey LL. Ferrozine - a new spectrophotometric reagent for iron. Anal Chem 1970(7):779-781.

[184] Badia, A.; Huy Thai, N. H.; English, A. M.; Mikkelsen, S. R.; Patterson, R. T. Determination of ferrocene iron in protein matrices. *Anal Chim Acta***262:**87-90; 1992.

[185] Reznick, A. Z.; Packer, L. Oxidative damage to proteins: Spectrophotometric method for carbonyl assay. *Methods Enzymol***233:** 1994.

[186] Matsumoto, S.; Teshigawara, M.; Tsuboi, S.; Ohmori, S. Determination of glutathione and glutathione disulfide in biological samples using acrylonitrile as a thiol-blocking reagent. *Anal Sci***12:**91-95; 1996.

[187] Akerboom, T. P.; Sies, H. Assay of glutathione, glutathione disulfide, and glutathione mixed disulfides in biological samples. *Methods Enzymol***77:**373-382; 1981.

[188] Srinivasan, C.; Liba, A.; Imlay, J. A.; Valentine, J. S.; Gralla, E. B. Yeast lacking superoxide dismutase(s) show elevated levels of "free iron" as measured by whole cell electron paramagnetic resonance. *J Biol Chem***275:**29187-29192; 2000.

[189] Yazgan, O.; Krebs, J. E. Mitochondrial and nuclear genomic integrity after oxidative damage in saccharomyces cerevisiae. *Front Biosci***17:**1079-1093; 2012.

[190] Miao, R.; Kim, H.; Koppolu, U. M.; Ellis, E. A.; Scott, R. A.; Lindahl, P. A. Biophysical characterization of the iron in mitochondria from Atm1p-depleted saccharomyces cerevisiae. *Biochemistry***48:**9556-9568; 2009.

[191] Koppenol, W. H. The haber-weiss cycle - 70 years later. *Redox Report***6:**229-234; 2001.

[192] Scialo, F.; Mallikarjun, V.; Stefanatos, R.; Sanz, A. Regulation of lifespan by the mitochondrial electron transport chain: Reactive oxygen species-dependent and reactive oxygen species-independent mechanisms. *Antioxid. Redox Signal.* 2012.

[193] Kirby, K.; Hu, J. G.; Hilliker, A. J.; Phillips, J. P. RNA interference-mediated silencing of Sod2 in drosophila leads to early adult-onset mortality and elevated endogenous oxidative stress. *Proc Natl Acad Sci USA***99:**16162-16167; 2002.

[194] Reveillaud, I.; Phillips, J.; Duyf, B.; Hilliker, A.; Kongpachith, A.; Fleming, J. E. Phenotypic rescue by a bovine transgene in a Cu/Zn superoxide dismutase-null mutant of drosophila-melanogaster. *Mol Cell Biol***14:**1302-1307; 1994.

[195] Sun, J. T.; Molitor, J.; Tower, J. Effects of simultaneous over-expression of Cu/ZnSOD and MnSOD on drosophila melanogaster life span. *Mech Ageing Dev***125:**341-349; 2004.

[196] Van Remmen, H.; Ikeno, Y.; Hamilton, M.; Pahlavani, M.; Wolf, N.; Thorpe, S. R.; Alderson, N. L.; Baynes, J. W.; Epstein, C. J.; Huang, T. T.; Nelson, J.; Strong, R.; Richardson, A. Life-long reduction in MnSOD activity results in increased DNA damage and higher incidence of cancer but does not accelerate aging. *Physiol Genomics***16:**29-37; 2003.

[197] Elchuri, S.; Oberley, T. D.; Qi, W. B.; Eisenstein, R. S.; Roberts, L. J.; Van Remmen, H.; Jepstein, C. J.; Huang, T. T. CuZnSOD deficiency leads to persistent and widespread oxidative damage and hepatocarcinogenesis later in life. *Oncogene***24:**367-380; 2005.

[198] Perez, V. I.; Bokov, A.; Van Remmen, H.; Mele, J.; Ran, Q.; Ikeno, Y.; Richardson, A. Is the oxidative stress theory of aging dead? *Biochim Biophys Acta***1790:**1005-1014; 2009.

[199] Yang, W.; Hekimi, S. A mitochondrial superoxide signal triggers increased longevity in caenorhabditis elegans. *PLoS Biol***8:**e1000556; 2010.

[200] Zheng, J.; Edelman, S. W.; Tharmarajah, G.; Walker, D. W.; Pletcher, S. D.; Seroude, L. Differential patterns of apoptosis in response to aging in drosophila. *Proc Natl Acad Sci USA***102:**12083-12088; 2005.

[201] Butow, R. A.; Avadhani, N. G. Mitochondrial signaling: The retrograde response. *Mol Cell***14:**1-15; 2004.

[202] Kuhajda, F. P. Fatty acid synthase and cancer: New application of an old pathway. *Cancer Res***66:**5977-5980; 2006.

[203] Vander Heiden, M. G.; Cantley, L. C.; Thompson, C. B. Understanding the warburg effect: The metabolic requirements of cell proliferation. *Science***324:**1029-1033; 2009.

[204] Mager, W. H.; Dekruijff, A. J. J. Stress-induced transcriptional activation. *Microbiol Rev***59:**506-&; 1995.

[205] Kirkman, H. N.; Gaetani, G. F. Catalase: A tetrameric enzyme with four tightly bound molecules of NADPH. *Proc Natl Acad Sci USA***81:**4343-4347; 1984.

[206] Bilinski, T.; Kwolek, M.; Sas, E.; Krynicka, M.; Koziol, S.; Owsiak-Teleon, A.; Krzepilko, A.; Bartosz, G. A novel test for identifying genes involved in aldehyde detoxification in the yeast. increased sensitivity of superoxide-deficient yeast to aldehydes and their metabolic precursors. *Biofactors***24:**59-65; 2005.

[207] D'Autreaux, B.; Toledano, M. B. ROS as signalling molecules: Mechanisms that generate specificity in ROS homeostasis. *Nat Rev Mol Cell Biol***8:**813-824; 2007.

[208] Kawamata, H.; Manfredi, G. Import, maturation, and function of SOD1 and its copper chaperone CCS in the mitochondrial intermembrane space. *Antioxid Redox Signal***13:**1375-1384; 2010.

[209] Stieber, A.; Gonatas, J. O.; Gonatas, N. K. Aggregates of mutant protein appear progressively in dendrites, in periaxonal processes of oligodendrocytes, and in neuronal and astrocytic perikarya of mice expressing the SOD1(G93A) mutation of familial amyotrophic lateral sclerosis. *J Neurol Sci***177:**114-123; 2000.

[210] Grad, L. I.; Guest, W. C.; Yanai, A.; Pokrishevsky, E.; O'Neill, M. A.; Gibbs, E.; Semenchenko, V.; Yousefi, M.; Wishart, D. S.; Plotkin, S. S.; Cashman, N. R. Intermolecular transmission of superoxide dismutase 1 misfolding in living cells. *Proc Natl Acad Sci USA***108:**16398-16403; 2011.

[211] Rakhit, R.; Crow, J. P.; Lepock, J. R.; Kondejewski, L. H.; Cashman, N. R.; Chakrabartty, A. Monomeric cu,zn-superoxide dismutase is a common misfolding intermediate in the oxidation models of sporadic and familial amyotrophic lateral sclerosis. *J. Biol. Chem.***279:**15499-15504; 2004.

[212] Kerman, A.; Liu, H.; Croul, S.; Bilbao, J.; Rogaeva, E.; Zinman, L.; Robertson, J.; Chakrabartty, A. Amyotrophic lateral sclerosis is a non-amyloid disease in which extensive misfolding of SOD1 is unique to the familial form. *Acta Neuropathol***119:**335-344; 2010.

[213] Gottfredsen, R. H.; Larsen, U. G.; Enghild, J. J.; Petersen, S. V. Hydrogen peroxide induce modifications of human extracellular superoxide dismutase that results in enzyme inhibition. *Redox Biol***1:**24-31; 2013.

[214] Ranguelova, K.; Ganini, D.; Bonini, M. G.; London, R. E.; Mason, R. P. Kinetics of the oxidation of reduced cu,zn-superoxide dismutase by peroxymonocarbonate. *Free Radic Biol Med***53:**589-594; 2012.

[215] Roberts, B. R.; Tainer, J. A.; Getzoff, E. D.; Malencik, D. A.; Anderson, S. R.; Bomben, V. C.; Meyers, K. R.; Karplus, P. A.; Beckman, J. S. Structural characterization of zinc-deficient human superoxide dismutase and implications for ALS. *J Mol Biol***373:**877-890; 2007.

[216] Kurahashi, T.; Miyazaki, A.; Suwan, S.; Isobe, M. Extensive investigations on oxidized amino acid residues in H2O2-treated cu,zn-SOD protein with LC-ESI-Q-TOF-MS, MS/MS for the determination of the copper-binding site. *J Am Chem Soc***123:**9268-9278; 2001.

[217] Barber, S. C.; Shaw, P. J. Oxidative stress in ALS: Key role in motor neuron injury and therapeutic target. *Free Radic Biol Med***48:**629-641; 2010.

[218] Linares, E.; Seixas, L. V.; dos Prazeres, J. N.; Ladd, F. V. L.; Ladd, A. A. B. L.; Coppi, A. A.; Augusto, O. Tempol moderately extends survival in a hSOD1(G93A) ALS rat model by inhibiting neuronal cell loss, oxidative damage and levels of non-native hSOD1(G93A) forms. *Plos One***8:**e55868; 2013.

[219] Khurana, V.; Lindquist, S. Modelling neurodegeneration in saccharomyces cerevisiae: Why cook with baker's yeast? *Nat Rev Neurosci***11:**436-449; 2010.

[220] Tiwari, A.; Hayward, L. J. Familial amyotrophic lateral sclerosis mutants of copper/zinc superoxide dismutase are susceptible to disulfide reduction. *J Biol Chem***278:**5984-5992; 2003.

[221] Lindberg, M. J.; Normark, J.; Holmgren, A.; Oliveberg, M. Folding of human superoxide dismutase: Disulfide reduction prevents dimerization and produces marginally stable monomers. *Proc Natl Acad Sci USA***101:**15893-15898; 2004.

[222] Ghosh, S.; Willard, B.; Comhair, S. A.; Dibello, P.; Xu, W.; Shiva, S.; Aulak, K. S.; Kinter, M.; Erzurum, S. C. Disulfide bond as a switch for copper-zinc superoxide dismutase activity in asthma. *Antioxid Redox Signal***18:**412-423; 2012.

[223] Lynch, S. M.; Boswell, S. A.; Colon, W. Kinetic stability of Cu/Zn superoxide dismutase is dependent on its metal ligands: Implications for ALS. *Biochemistry***43:**16525-16531; 2004.

[224] Higgins, C. M. J.; Jung, C. W.; Xu, Z. S. ALS-associated mutant SOD1G93A causes mitochondrial vacuolation by expansion of the intermembrane space and by involvement of SOD1 aggregation and peroxisomes. *BMC Neurosci***4:**16-16; 2003.

[225] Bastow, E. L.; Gourlay, C. W.; Tuite, M. F. Using yeast models to probe the molecular basis of amyotrophic lateral sclerosis. *Biochem Soc Trans***39:**1482-1487; 2011.

[226] Tardiff, D. F.; Jui, N. T.; Khurana, V.; Tambe, M. A.; Thompson, M. L.; Chung, C. Y.; Kamadurai, H. B.; Kim, H. T.; Lancaster, A. K.; Caldwell, K. A.; Caldwell, G. A.; Rochet, J. C.; Buchwald, S. L.; Lindquist, S. Yeast reveal a "druggable" Rsp5/Nedd4 network that ameliorates alpha-synuclein toxicity in neurons. *Science***342:**979-983; 2013.

[227] Brown, J. D.; Day, A. M.; Taylor, S. R.; Tomalin, L. E.; Morgan, B. A.; Veal, E. A. A peroxiredoxin promotes H2O2 signaling and oxidative stress resistance by oxidizing a thioredoxin family protein. *Cell Rep***5:**1425-1435; 2013.

[228] Bozonet, S. M.; Findlay, V. J.; Day, A. M.; Cameron, J.; Veal, E. A.; Morgan, B. A. Oxidation of a eukaryotic 2-cys peroxiredoxin is a molecular switch controlling the transcriptional response to increasing levels of hydrogen peroxide. *J Biol Chem***280:**23319-23327; 2005.

[229] Eshghi, A.; Lourdault, K.; Murray, G. L.; Bartpho, T.; Sermswan, R. W.; Picardeau, M.; Adler, B.; Snarr, B.; Zuerner, R. L.; Cameron, C. E. Leptospira interrogans catalase is required for resistance to H2O2 and for virulence. *Infect Immun***80:**3892-3899; 2012.

[230] Dantas, A. S.; Andrade, R. V.; De Carvalho, M. J.; Felipe, M. S. S.; Campos, E. G. Oxidative stress response in paracoccidioides brasiliensis: Assessing catalase and cytochrome c peroxidase. *Mycol Res***112:**747-756; 2008.

[231] Elam, J. S.; Taylor, A. B.; Strange, R.; Antonyuk, S.; Doucette, P. A.; Rodriguez, J. A.; Hasnain, S. S.; Hayward, L. J.; Valentine, J. S.; Yeates, T. O.; Hart, P. J. Amyloid-like filaments and water-filled nanotubes formed by SOD1 mutant proteins linked to familial ALS. *Nat Struct Biol***10:**461-467; 2003.

[232] Hillar, A.; Nicholls, P.; Switala, J.; Loewen, P. C. NADPH binding and control of catalase compound II formation: Comparison of bovine, yeast, and escherichia coli enzymes. *Biochem J***300:**531-539; 1994.

[233] Grant, C. M.; Perrone, G.; Dawes, I. W. Glutathione and catalase provide overlapping defenses for protection against hydrogen peroxide in the yeast saccharomyces cerevisiae. *Biochem Biophys Acta***253:**893-898; 1998.

[234] Klunk, W. E.; Jacob, R. F.; Mason, R. P. Quantifying amyloid beta-peptide (A beta) aggregation using the congo red A beta (CR-A beta) spectrophotometric assay. *Anal Biochem***266:**66-76; 1999.